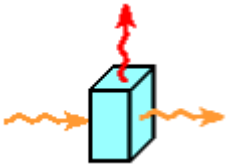

Optical Properties of Solids: Semiconductors

R. Boyn

Preface

The course is based on lectures I gave, at the Humboldt University in Berlin, for undergraduate and graduate students with a corresponding specialization. I am dealing with optical properties of *non-metallic solids* emphasizing effects that are important for semiconductors. I am concentrating on basic phenomena of *linear optics* , such as absorption, reflection, and (spontaneous) emission. For understanding the discussions, the reader should have basic knowledges of solid state physics, atomic physics , and quantum mechanics. I always endeavour to make clear the connection of the present treatments with the principles of solid state physics.

The lectures were running over many years, up to the end of the 90's. At this time the basic principles of most subjects treated here were clarified. This encouraged me to produce a written version of the course (originally in German, now translated into English).

The list of references mainly gives the sources of the figures presented. Further, some textbooks and monographs are quoted which may be useful for supplementing the discussions given here. It should be noted that since the time of writing (1998) better kinds of references may have appeared. I would be grateful for receiving remarks concerning this matter.

The present PDF version is intended to be used for printing. This should be done by means of a colour printer, because the figures cannot be understood in a black and white representation.

In addition to this paper edition, there is an electronic version written in HTML. I especially recommend to employ the latter version, because there you will find a presentation similar to the procedure met in the lecture room (see the preface of the electronic version for details). Of course, the two editions may be utilized in parallel. For easier work with the paper version, references to figures, equations, earlier or later discussions e. t. c. (see the Index) are given here in the same form as the corresponding links in the HTML version (e. g. Fig. 2.3, Bloch state and Supplement 4).

Table of Contents

Overview

We start with a survey of our subject by looking at a schematic optical absorption spectrum of a nonmetallic solid as given below.

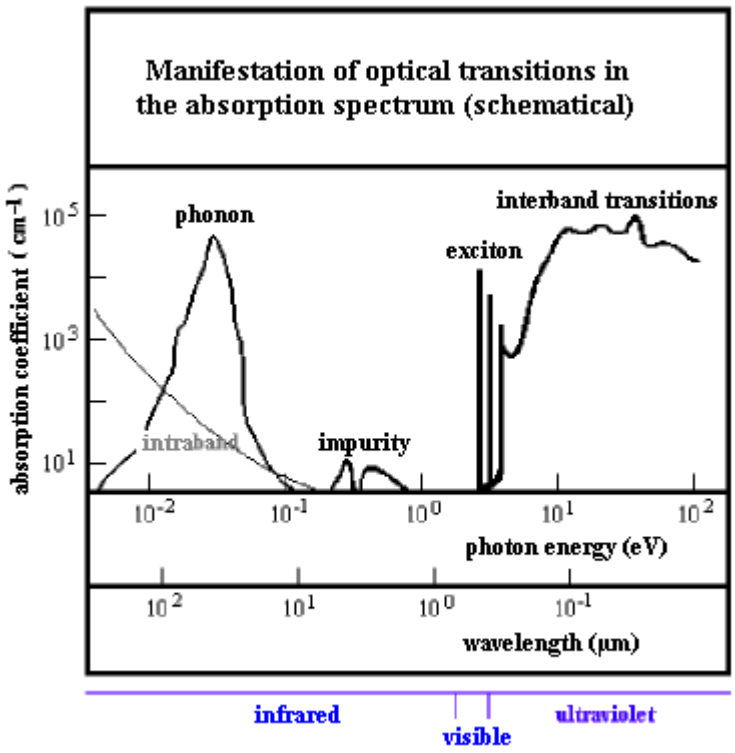

This diagram presents - on a double logarithmic scale - the absorption coefficient (a quantity describing the attenuation of light per unit length) as a function of photon energy and light wavelength. It should be noted that the presentation versus photon energy is the better choice, because it gives a more direct connection to the relevant optical transitions, and we shall mainly use this variant in the following.

In this section we shall give a first survey of the relevant processes, which are to be discussed in detail later, moving from high to low photon energies.

At the highest energies we see a range of continuous absorption, which is related to so-called **interband transitions**. These are processes in which a photon interacts with an electron in an occupied energy band (in particular, a valence band), transfers it to a higher non-occupied band (conduction band), and is thereby annihilated (absorbed). If we represent these transitions by arrows in the elementary band picture

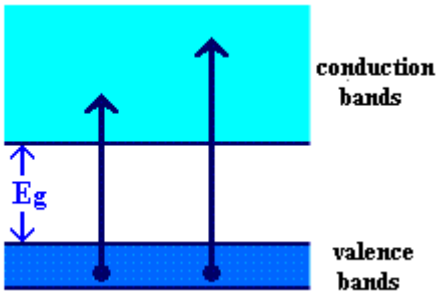

the lengths of the arrows correspond to the energies of the absorbed photons.It is obvious that we are concerned with a continuous spectrum, and that there is a minimum energy corresponding to the separation (E_g) between the lowest conduction band and the highest valence band. The second fact manifests itself in the appearance of a well-defined low-energy limit of the spectrum, which is called ***interband absorption edge***.

At photon energies above the region shown in the spectrum (X-ray region) one typically sees transitions between core bands (core levels) - lying below the valence bands - and the conduction bands.

In the low-energy part of the interband edge we observe, at sufficienly low temperatures, sharp lines which are due to so-called **exciton transitions**. Physically, we are dealing with the following process: In the case of interband transitions just discussed, an electron in a conduction band and a hole (defect electron) in a valence band (or a deeper band) are formed. These particles represent a negative and a positive charge, respectively, and are therefore subject to Coulomb attraction which may lead to a mutual binding of the two particles. Such bound states, referred to as excitons, can be visualized

as electron and hole rotating around a common center of gravity and, at the same time, performing a translational motion through the solid.

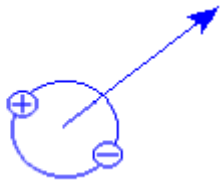

The lines appearing in the spectrum are related to the generation of excitons from a particle-free state due to the absorption of photons.The corresponding photon energies are somewhat lower than E_g, differing from E_g by the small binding energy (dissociation energy) of the two particles. So the lines are located at the lower limit of the interband range.

Proceeding to lower photon energies, we come to a spectral range in which generally no significant absorption is observed. Looking more carefully, weak absorption can be seen which is mainly due to **transitions at impurity centers**. More precisely, we are dealing with transitions beginning or ending on discrete levels in the gap between conduction and valence bands created by impurities. Examples are illustrated in the following:

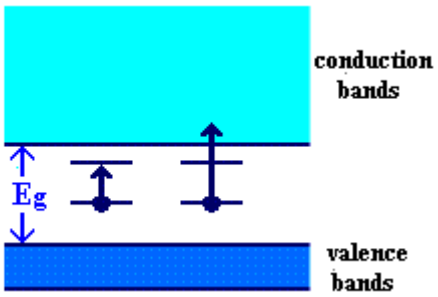

These processes can give rise to sharp lines or, alternatively, broad bands, the corresponding photon energies being obviously, in general, smaller than E_g. The strength of this contribution to the spectrum depends on the concentration of the impurities, e.g. absorption coefficients of typically about 1 to 10 cm^{-1} are to be expected for concentrations of 10^{16} active centers per cm^3.These values are by many orders of magnitude smaller than the contributions of interband and exciton transitions.

In the present lecture we shall not deal with impurity transitions.

Going further toward lower photon energies, i. e. to the middle and far infrared, we again find absorption regions of relatively high intensity. These are due to **phonon transitions**. The occurrence of these bands can be most simply explained in the case of materials consisting of several different types of atoms. In such materials the atoms ("ions") have positive and negative excess charges. (The intensity of the phonon bands shown in the Figure refers to this case.)

As illustrated in the following, the electric field of an incident electromagnetic wave (wavelength not drawn to scale) interacts with the charges, diverting positive and negative ions in opposite directions.

That means that - for a suitable magnitude of light frequency - the ions are excited to vibrations, whereby the light wave is (partly) absorbed. In the quantum physical particle-picture these processe are described as a transformation of photons into phonons.

In the infrared region one can also often detect so-called **intraband transitions**. These are processes in which an electron in a conduction band or a hole in a valence band receive energy by absorbing a photon.

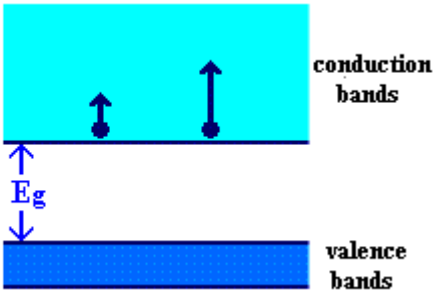

For the first case such a transition is shown above. Obviously such processes can only occur if there are actually electrons in the conduction band.It is well known that this requires, under normal conditions, the presence of suitable thermally ionized impurities (shallow donors; and not too low temperatures). Because the initial and final states have continuous distributions, the absorption spectrum also has continuous character. As shown by more detailed investigations, the absorption coefficient increases with decreasing photon energy.

The spectrum of intraband transitions is, in general, located in a range in which there are also phonon transitions. Consequently, this spectrum can be observed in pure form only outside the bands due to phonons.

It should be noted that in the case of metals, where the concentration of conduction electrons is extremely high, the intraband contribution is very large, governing the optical spectra together with the interband contribution.

Here we conclude our survey of the optical transitions. We shall see that processes of the kind discussed, as well as similar processes also manifest themselves in other types of optical spectra (e. g. reflection and luminescence spectra). In the following - after shortly compiling some basic concepts of solid state physics - the mentioned processes will be dealt with in detail.

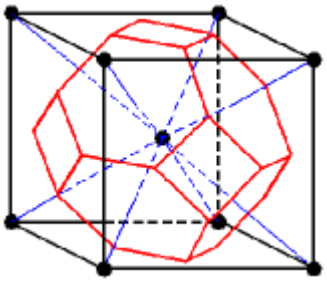

Chapter 1

Some Basic Concepts of Solid State Physics

In this chapter we repeat some basic concepts of theoretical solid-state physics. We think that this will enable many readers to get into our subject, without referring to corresponding textbooks. Our discussion is divided into four complexes:

- Crystal Structure
- Bloch States and Brillouin Zones
- Energy Band Structure
- Density of States

1.1 Crystal Structure

As our discussion will refer to *crystalline* solids we start with some crystallographic concepts.

An (ideal) ***crystal*** is characterized by the *periodic configuration of atoms*, as illustrated in Fig. 1.1

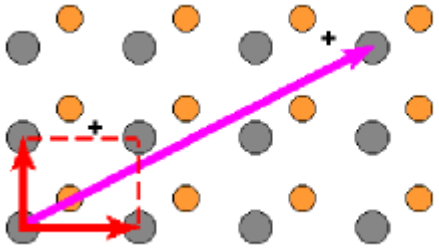

Fig. 1.1

for two constituting types of atoms, using a schematic two-dimensional picture.

Due to the periodic arrangement of the atoms, there are so-called ***equivalent points*** in the crystal. These are points from which an observer (located sufficiently far from the crystal surface) sees the same environment. In Fig. 1.1 two points of that kind are marked by **+**. Vectors connecting equivalent points are called ***lattice vectors*** (example in Fig. 1.1: ↗). A shift by a lattice vector transforms the crystal into itself (excluding regions near the surface). This property is called ***translation symmetry***.

The lattice vectors of minimum length (typically some 10^{-8} cm) are referred to as ***primitive lattice vectors*** . In Fig. 1.1 we characterize these by red arrows ↑ →.

In a three-dimensional crystal we are dealing with three primitive lattice vectors, which we shall designate as $\mathbf{a}_1$, $\mathbf{a}_2$ and $\mathbf{a}_3$. From these one can construct each general lattice vector($\mathbf{R}_n$) by forming linear combinations with integers (n_1,n_2,n_3) as coefficients:

(1.1) $\mathbf{R}_n = n_1\mathbf{a}_1 + n_2\mathbf{a}_2 + n_3\mathbf{a}_3$

Here n stands for n_1,n_2,n_3. The points generated by the vectors $\mathbf{R}_n$ are referred to as the ***lattice***.

The primitive lattice vectors span the ***unit cells***. In Fig. 1.1 we represent such a cell by – – – –. The unit cells are the smallest elements which can be thought of to build the crystal. In general there are several possibilities for defining the unit cell for a given crystal structure.

For discussing the electronic and vibrational states of crystals the concept of ***reciprocal lattice*** is required. The best way to introduce the reciprocal lattice is by means of corresponding primitive vectors:

(1.2) $\mathbf{b}_1 = (2\pi / V_0) (\mathbf{a}_2 \times \mathbf{a}_3),\quad \mathbf{b}_2 = (2\pi / V_0) (\mathbf{a}_3 \times \mathbf{a}_1),\quad \mathbf{b}_3 = (2\pi / V_0) (\mathbf{a}_1 \times \mathbf{a}_2)$

V_0 is the volume of the unit cell; ($\mathbf{a}_i \times \mathbf{a}_j$) are vector products.

The general ***vectors of the reciprocal lattice*** are defined in a way analogous to the lattice vectors introduced earlier:

(1.3) $\mathbf{G}_m = m_1\mathbf{b}_1 + m_2\mathbf{b}_2 + m_3\mathbf{b}_3$

m_1,m_2,m_3 are integers; m is an abbreviation of this triple.

1.2 Bloch States and Brillouin Zones

After these remarks on crystallography we go into the physical discussion. First we shall deal with the quantum mechanical states of electrons in a crystal. The Hamilton operator of an electron has the form

(1.4) $H = \mathbf{p}^2 / 2m_0 + U(\mathbf{r})$

Here **p** and **r** are the momentum and position vector,respectively, of the electron (operators), m_0 its rest mass. The two terms in H are the kinetic and potential energy of the electron. U(**r**) (shortly referred to as potential in the following) includes electronic contributions and contributions of the atomic nuclei.

We are interested in the solution of the corresponding Schrödinger equation

(1.5) $H\psi = E\psi$

(E, ψ energy eigenvalues and eigenstates, respectively).

The application of Equ. (1.4) and (1.5) implies using the so-called ***one-electron approximation***.

> Strictly speaking, in the case of a solid one is concerned with an extreme example of a many-electron problem: In a macroscopic crystal the are, to order of magnitude, 10^{22} to 10^{23} electrons. In our approximation, the effect of the other electrons in the crystal is described as a contribution to the potential U(**r**). This means that, simply speaking, only the time-averaged positions of the other electrons are taken into account. In most cases, results of calculations based on the one-electron approximation agree surprisingly well with experiment.

The fact that the potential is invariant with respect to a shift by lattice vectors $\mathbf{R}_n$,

(1.6) $U(\mathbf{r} + \mathbf{R}_n) = U(\mathbf{r})$

has important consequences (see Equ. (1.1))(***translation symmetry***, ***lattice periodicity***). Equ. (1.6) means that at equivalent points (**+** in Fig. 1.1) the electron feels the same potential, which is evident from the identity of the surrounding atomic configurations.

This property is conveyed to the total Hamilton operator:

(1.7) $H(\mathbf{r} + \mathbf{R}_n) = H(\mathbf{r})$

From Equ. (1.7) it follows, by simple considerations, that the wavefunctions ψ(**r**) have the form of ***Bloch functions*** (***Bloch states, Bloch waves***):

(1.8) $\psi_{\mathbf{k}\nu}(\mathbf{r}) = \exp(i\mathbf{kr})\, u_{\mathbf{k}\nu}(\mathbf{r})$

k and ν are referred to as ***propagation vector*** and ***band index***, respectively. $u_{\mathbf{k}\nu}(\mathbf{r})$ is the so-called ***Bloch factor***,which has lattice periodicity:

(1.9) $u_{\mathbf{k}\nu}(\mathbf{r} + \mathbf{R}_n) = u_{\mathbf{k}\nu}(\mathbf{r})$

Of course the energy eigenvalues E also depend on the quantities **k** and ν. The notation is

$E = E_\nu(\mathbf{k})$

If **k** is varied at a given ν, $E_\nu(\mathbf{k})$ will cover a certain range: We are concerned with a band type energy spectrum. The bands are numbered by the index ν.

On the one hand,the Bloch states $\psi_{\mathbf{k}\nu}(\mathbf{r})$ (see Equ. (1.8)) have wave character (wavelength $2\pi / |\mathbf{k}|$), due to the factor exp (i**kr**); on the other hand, in the vicinity of the atomic cores, they are similar to (strongly oscillating) atomic states, due to the effect of the Bloch factors $u_{\mathbf{k}\nu}(\mathbf{r})$. We visualize this (after[1]) in Fig. 1.2.

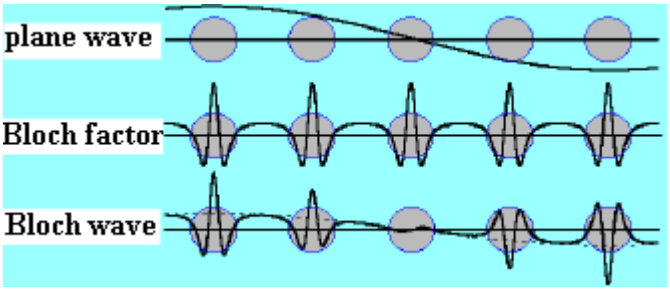

Fig. 1.2

Here the relevant functions (real parts) are plotted along a straight line passing a series of atoms of the same kind. Fig.1.2 shows that the motion of electrons in the crystal does not have much similarity with the motion of free particles (described by plane waves in quantum mechanics): the strong forces produced by the atoms have dramatic effects on the behaviour of the electrons in the atomic regions.

The dependence of the solutions on the (three-dimensional) vector **k** ist is periodic with respect to the reciprocal lattice vectors **G** (the index m has been omitted):

$$\psi_{\mathbf{k}+\mathbf{G},\nu}(\mathbf{r}) = \psi_{\mathbf{k}\nu}(\mathbf{r})$$

$$E_\nu(\mathbf{k}+\mathbf{G}) = E_\nu(\mathbf{k})$$

Note that both the vectors **k** and **G** (see the definitions (1.2) and (1.3)) have the dimension of a reciprocal length .

Due to this fact one can restrict oneself to a small part of **k** space (i. e. a kind of unit cell of the reciprocal lattice) when discussing **k** dependences. This "unit cell"is chosen symmetrically around the point **k** = 0 and is referred to as (first) Brillouin zone. Fig. 1.3 shows the Brillouin zone for the face-centered cubic (fcc) lattice (lattice for important crystal structures, e. g. diamond, zincblende, and rock-salt structure).

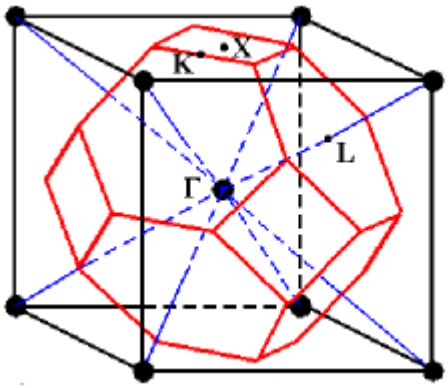

Fig. 1.3

The relevant points of the reciprocal lattice (body centered cubic (bcc) in the present case) are marked by ●. The point denoted by Γ corresponds to **k** = 0. Here the Brillouin zone (represented by red lines) is a truncated octahedron. This form of the Brillouin zone results from the following general principle:

Draw straight lines from the point **k** = 0 to all other reciprocal lattice points, and, in the centers of these pieces of lines, put up planes which are perpendicular to the line. The Brillouin zone is the smallest volume that is limited by such planes and contains **k**= 0 .

Obviously, the Brillouin zone in Fig. 1.3 is formed by two types of planes: the hexagons result from halving the lines to the cube corners, the squares come from the lines connecting **k** = 0 with the centers of the adjacent cubes.

1.3 Energy Band Structure

The set of functions $E_\nu(\mathbf{k})$ for a given crystalline solid is referred to as ***energy band structure***. This is one of the most important characteristics of the material. The energy band structure determines all properties based on electronic processes. According to our earlier remarks, we can restrict ourselves to the Brillouin zone in discussing the $E_\nu(\mathbf{k})$. Usually one considers the variation along certain straight lines in this zone. Fig. 1.4 shows a corresponding part of the band structure of GaAs [2]. (In this plot there are, altogether, nine bands; so the index ν assumes nine different values.) Since GaAs crystallizes in the zincblende structure, the Brillouin zone has the form just represented in Fig. 1.3. This zone is once more shown in Fig. 1.4, together with the lines (in violet) chosen for the $E_\nu(\mathbf{k})$ plots.

The symbols L_i, Γ_i and X_i characterize the symmetry properties of the Bloch states in the corresponding points of **k** space. The band structure in Fig. 1.4 is based on a combination of experimental and theoretical results (see section 2.5 for details on how such information is gained).

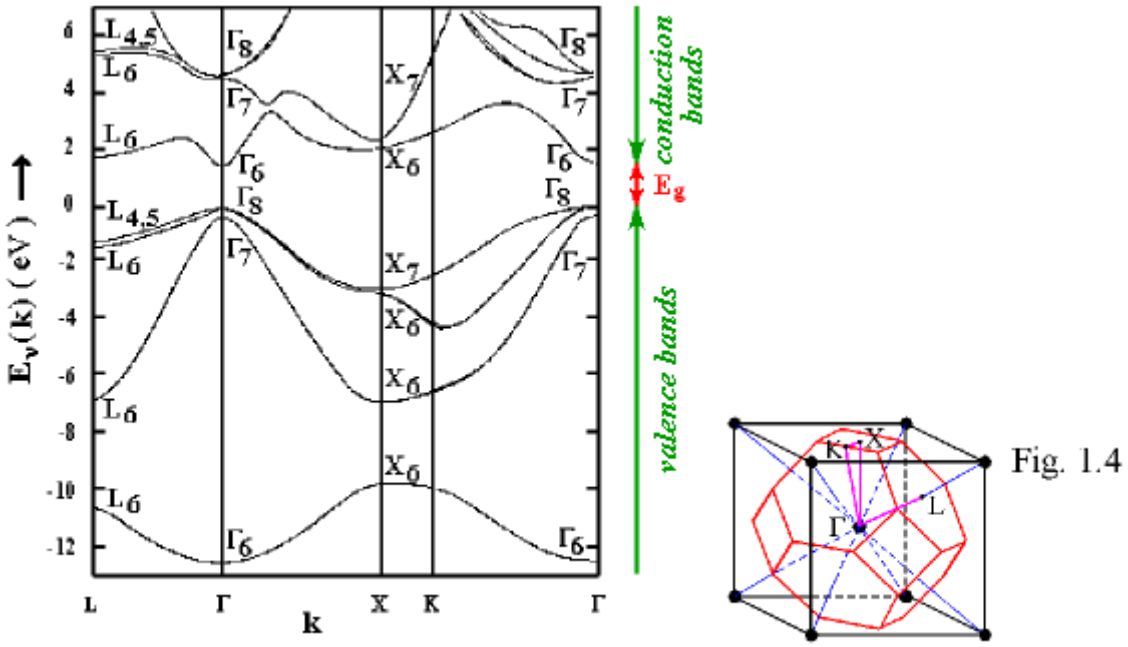

Fig. 1.4

The part of the band structure shown in Fig. 1.4 includes the lowest ***conduction bands*** and the highest ***valence bands***. Disregarding effects of impurities and of temperature one can state that the valence bands (and all deeper bands) are completely occupied with electrons, and all conduction bands are empty. In the case of GaAs there is an ***energy gap*** (***forbidden zone***, E_g in Fig. 1.4) between the lowest conduction band and the highest valence band. The E_g value of GaAs is about 1. 4 eV at room temperature and increases to somewhat above 1.5 eV on cooling to very low temperatures (see also Chapter 5). Obviously Fig. 1.4 specifies the well-known simple band picture in which only the limits of conduction and valence bands and the band gap are shown (see the pictures in the Overview Chapter).

A more detailed discussion of the occupation of energy bands with electrons is given in **Supplement 1**.

The band structure of GaAs shown in Fig. 1.4 has two features also found for many other materials:

- The maximum of the valence bands lies at the point Γ (**k** = 0). At this point two valence bands (Γ_8) are in contact, and a third band (Γ_7) closely approaches these two.
- The conduction band minimum is also located at **k** = 0.

The second property is found less frequently than the first one. (If both properties are present one is concerned with a so-called direct band structure, see Section 2.2.)

For describing the behaviour of electrons near the edges of conduction and valence bands one often uses the ***"effective mass"*** concept. The simplest way of introducing this concept is expanding $E_\nu(\mathbf{k})$ into a Taylor series around the corresponding extremal point. For the lowest conduction band (ν = c) this yields, in the case of Fig. 1.4:

$$(1.10)\quad E_c(\mathbf{k}) = E_c(0) + \sum_{i=1}^{3} \frac{1}{2} \left(\frac{\partial^2 E_c(\mathbf{k})}{\partial k_i^2} \right)_{k_i = 0} k_i^2 + \ldots .$$

Here k_i are the components of **k** in a Cartesian coordinate system. This is chosen in such a way that second-order terms of the type $k_i k_j$ (i different from j) do not occur, which can always be achieved by transformation to principal axes. There are no terms linear in **k** since the expansion is around the minimum. If we restrict ourselves to a small environment of **k** = 0, all terms of higher than second order can be neglected. Introducing new quantities $m_{c\,(i)}^*$ through the equations

$$(1.11)\quad \frac{1}{m_{c(i)}^*} = \frac{1}{\hbar^2} \left(\frac{\partial^2 E_c(\mathbf{k})}{\partial k_i^2} \right)_{k_i = 0}$$

we get

$$(1.12)\quad E_c(\mathbf{k}) \approx E_c(0) + \sum_{i=1}^{3} \frac{\hbar^2}{2\, m_{c(i)}^*}\, k_i^2$$

The $m_{c\,(i)}^*$ have the dimension of masses; they are called effective masses. Apart from a possible i-dependence, i. e. a possible anisotropy, Equ. (1.12) corresponds to the **k** dependence of the energy of free particles (with **k** = (1 / ħ) ×momentum of the particles).

Equ. (1.12) is the basis for describing the motion of electrons near the band edge as the motion of ***quasi-free*** particles, where only the real electronic mass is replaced by the effective mass (e. g. in discussions of electric conductivity). This description is justified as long as one restricts oneself to the range where Equ.(1.12) is valid, i. e. to a sufficiently small range near the band edge. As already mentioned in connection with Fig. 1.2 the motion of electrons in a solid is, in general, not very similar to a free-particle motion; this also manifests itself in the fact that the overall appearance of the $E_v(\mathbf{k})$ functions is rather complicated (Fig. 1.4).

In the GaAs case all three effective masses of the conduction band edge have the same value; this is a consequence of the cubic crystal-symmetry. One has

$$m_{c\,(1)}^* = m_{c\,(2)}^* = m_{c\,(3)}^* = 0.067\, m_0.$$

The magnitudes of the (negative) valence band masses are much larger, as is also the case for many other materials (typically some tenths of m_0); here the situation is more complex due to the contact of two bands.

1.4 Density of States

A concept often used in solid state physics is ***density of states***, more pricisely: ***density of states with respect to energy*** . To arrive at a definition, we first introduce an independent energy variable **E** and denote by g (**E**) d**E** the number of electronic states (band states) lying in the infinitesimal interval between **E** and **E** + d**E**. g (**E**) is the density of states. For GaAs we plot this function in Fig. 1.5 [2] together with the $E_v(\mathbf{k})$ diagram discussed in the last section , with coincident energy scales:

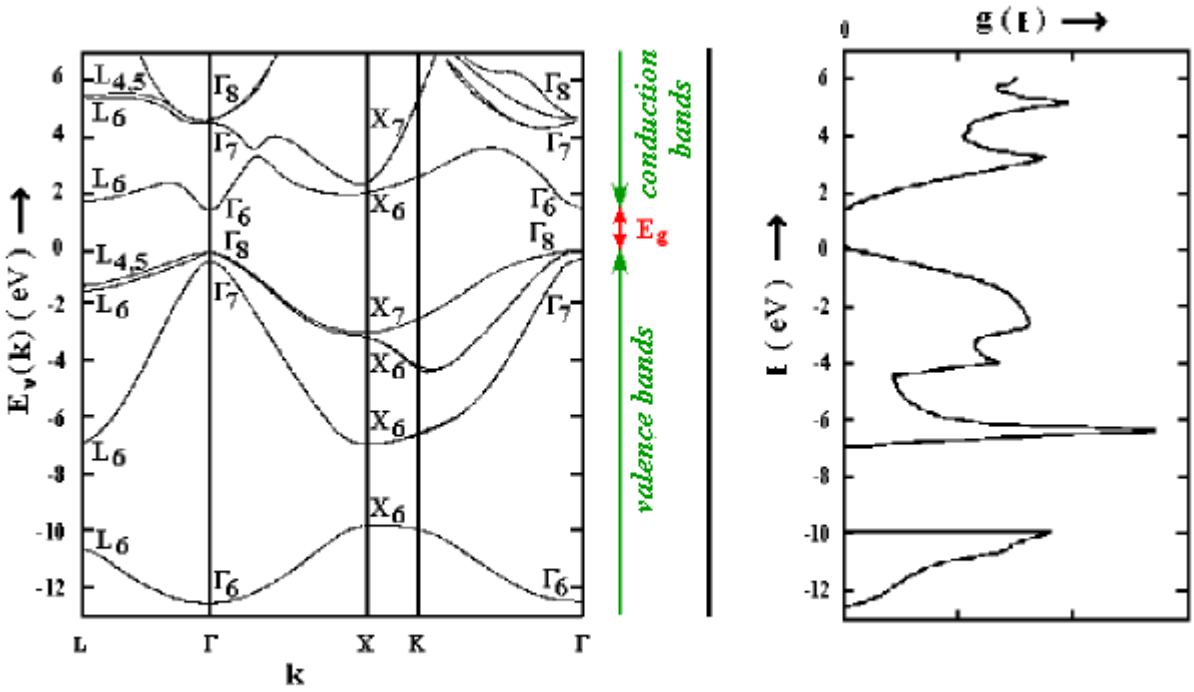

Fig. 1.5

The g (**E**) curve is obviously correlated with the $E_v(\mathbf{k})$ curve. There is the following connection between the two functions:

$$(1.13)\quad g(\mathbf{E}) = \sum_{\nu} g_{\nu}(\mathbf{E}) \qquad g_{\nu}(\mathbf{E}) = \frac{1}{4\pi^3} \int_{[E_{\nu}(\mathbf{k}) = \mathbf{E}]} \frac{d\sigma}{|\mathrm{grad}_{\mathbf{k}} E_{\nu}(\mathbf{k})|}$$

Here g (**E**) and g_{ν} (**E**) are related to unit volume. Integration is over ***surfaces of constant energy*** in **k** space. For a given energy (**E**) and a given band (ν) these are defined by the relation

$$(1.14)\quad E_{\nu}(\mathbf{k}) = \mathbf{E}$$

dσ is the surface element. Contributions to the sum in Equ. (1.13) are made by all bands containing the energy **E**, i. e. for which there is a **k** range in which Equ. (1.14) is fulfilled. Of course, such a band does not occur in the energy gaps, so the density of states is zero there (two such ranges can be seen in Fig. 1.5).

According to Equ. (1.13) g (**E**) is large (small) at given **E** if for the bands in question | $\mathrm{grad}_{\mathbf{k}} E_{\nu}$ (**k**)| has small (large) values. This correlation is due to the fact that in the case of flat (steep) E_{ν}(**k**) dependences there are many (few) states in a given interval d**E** (note the equidistance of the possible **k** values). In particular, the sharp peaks in g (**E**) correspond to extrema of the E_{ν} (**k**) curves (Fig. 1.5).

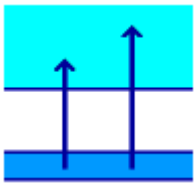

Chapter 2

Interband Transitions

2.1 Elementary Processes

Now we ask what are the conditions for an electron making a transition, under the influence of a radiation field, from a Bloch state in a band ν into a (nonoccupied) Bloch state in another band ν ' (a process manifesting itself, e. g., in the optical absorption spectrum):

(2.1) $\psi_{\mathbf{k}\nu}(\mathbf{r}) \rightarrow \psi_{\mathbf{k}'\nu'}(\mathbf{r})$

Let us illustrate this question using Fig. 2.1.

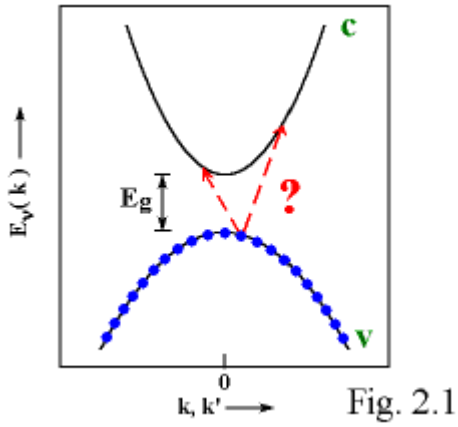

Fig. 2.1

In this Figure we only represent the highest valence band (**v**, completely occupied with electrons) and the lowest conduction band (**c**). (The extrema are assumed to lie at $\mathbf{k} = 0$, compare Section 1.3).

It is found that there are, generally, limitations for processes of type (2.1), i. e. *selection rules*. In the following we outline a way of proving that rule:

Let us describe the effect of an electromagnetic plane wave of frequency ω on the electron by means of the interaction operator [13]

(2.2) $W = -(e / m_0 c)\, \mathbf{A}\, \mathbf{p}, \quad \mathbf{A} = \mathbf{A}_0 e^{i(\mathbf{s}\mathbf{r} - \omega t)}$

Here **A** is the vector potential, $\mathbf{A}_0$ its amplitude, **s** the propagation vector of the light wave, and t the time. Combining all the t-independent factors in W:

(2.3) $W = W_0 e^{-i\omega t}, \quad W_0 = -(e / m_0 c)\, \mathbf{A}_0 e^{i\mathbf{s}\mathbf{r}}\, \mathbf{p}$

we obtain for the probability P of the transition (2.1), by specializing the corresponding general expression (" golden rule of quantum mechanics ")

(2.4) $P = (2\pi / \hbar)\, |\langle \mathbf{k}'\nu' | W_0 | \mathbf{k}\nu \rangle|^2\, \delta(E_{\nu'}(\mathbf{k}') - E_\nu(\mathbf{k}) - \hbar\omega)$

So, as usual, we are dealing essentially with a product of the squared matrix element of the interaction, taken between the final and initial states, and a δ - function with energy quantities in its argument.

By discussing the matrix element, one gets, making use of translation symmetry, that this is nonzero only under the restrictive condition

(2.5) $\mathbf{k}' = \mathbf{k} + \mathbf{s}$

(***k-selection rule***).

Arguments leading to this fundamental relation are given in Supplement 2.

Moreover, P is different from zero only if the argument of the δ function vanishes, i. e. if

(2.6) $E_{\nu'}(\mathbf{k}') = E_\nu(\mathbf{k}) + \hbar\omega$

We can interpret Equ. (2.5) and (2.6) using the *photon picture* for the radiation: First we note that in Equ. (2.5) after multiplication with ħ, we are concerned with quantities having the dimensions of momenta. That means that we can regard the optical transition as a collision of a photon with the electron, in which the photon disappears (is absorbed), its momentum ħs and energy ħω being transferred to the electron. Here the right- and left-hand sides of the two equations refer to the situation before and after the collision, respectively.

> This is a generalization of the classical collision concept,including the generation and annihilation of particles. Later we shall be often dealing with processes of that kind, especially processes with the participation of phonons.
>
> It should be noted that the quantities ħ**k** and ħ**k**' are, strictly speaking, not momenta of the electron. An electron in a Bloch state generally does not have a well-defined momentum in the sense of quantum mechanics (this is only the case for free particles, whose states are described by plane waves, see the comments related to Fig. 1.2). Those quantities should be referred to correctly as ***quasi-momenta***; however, we shall, as is usual, simply be speaking of momenta.

For discussing transitions at not too high photon energies (infrared, visible, and ultraviolet ranges) Equ. (2.5) can be further simplified, due to the fact that here the magnitude of **s** is much smaller than that of **k** and **k**'. Denoting the light wavelength by λ, we have in those spectral ranges, to order of magnitude,

$$|\mathbf{s}| = 2\pi / \lambda = 10^3 \ldots\ldots 10^6 \text{ cm}^{-1}.$$

We compare this with the size of the Brillouin zone, which is of the order 10^8 cm^{-1} (see the magnitude of the reciprocal lattice vectors taking into account the definition of the primitive lattice vectors). Thus the changes due to **s** can be safely ignored. Consequently, the simplified **k** selection rule is

(2.7) $\mathbf{k}' = \mathbf{k}$

and the modified energy balance

(2.8) $E_{\nu'}(\mathbf{k}) = E_{\nu}(\mathbf{k}) + \hbar\omega.$

Now we can answer our question of Fig. 2.1, see Fig. 2.2:

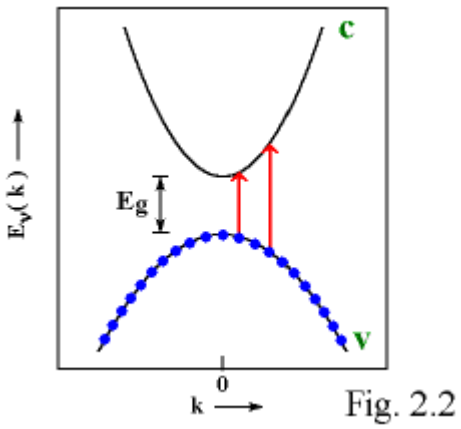

Fig. 2.2

As a consequence of Equ. (2.7) and (2.8) the allowed interband transitions are to be represented in $E_{\nu}(\mathbf{k})$ diagrams by vertical arrows of length ħω.

The conditions (2.7) und (2.8) also refer to transitions ↓ from a higher(ν ') into a lower (ν) band, as is evident from the derivation . Such transitions ("downward transitions") can be observed in the luminescence spectrum, provided that - after supplying energy from outside - there are electrons in a conduction band and free places in a valence band (Fig. 2.2) at the same **k**-vectors. In this way transitions are made possible accompanied by the emission of photons with energies ħω corresponding to Equ. (2.8). Such processes will be discussed in detail in Section 2.2.

The approximation (2.7) corresponds to the ***dipole approximation*** familiar from atomic physics. In both cases **s** is neglected, thus ignoring the spatial variation of the radiation field over the relevant range (atom, unit cell).

2.2 Transitions at Photon Energies Near E_g: Direct Band Structures

After these introductory remarks of mainly theoretical character, we shall now discuss the influence of the processes on experimental quantities, i. e. optical spectra. Usually we make a comparison with experiment by first considering what kind of spectra are to be *expected* from our previous theoretical analysis, and then discuss the reasons for possibl deviations.

Generally we are interested in manifestations of ***upward transitions*** (observable, e. g., in absorption spectra) and ***downward transitions*** (frequently visible in luminescence spectra). In the present section we shall deal wih these two types of spectra for photon energies close to E_g, and shall add, in each case, some remarks concerning simple experimental principles (see also Appendix 1).

In this section we refer to the spectra of so-called ***direct materials*** i. e. of substances for which the extrema of conduction band and valence band - as we have assumed in Fig. 2.1 and Fig. 2.2 - lie at the same **k** - vector. Later (in Section 2.3) we deal with the peculiarities found for ***indirect materials***, in which the extrema are displaced relative to each other in **k** - space.

Absorption Spectrum

The simplest way to determine absorption spectra is by a combination of transmission and reflection measurements; see Fig. 2.3:

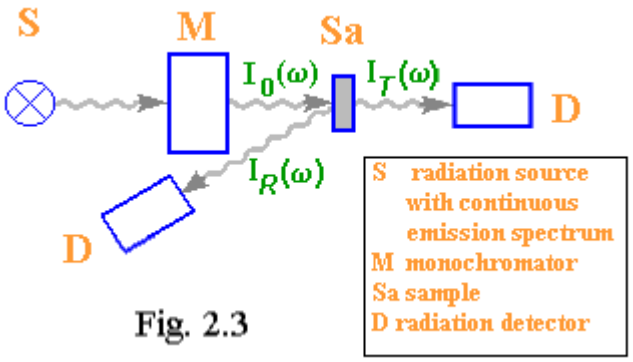

Fig. 2.3

For each frequency ω to which the monochromator is tuned one measures the intensities transmitted and reflected by the sample $I_T(\omega)$ and $I_R(\omega)$, respectively, and, in addition, by a "blank experiment", the incident intensity $I_0(\omega)$. Then one has, in simple cases (e. g. cubic symmetry, no interference effects)

(2.9) $$T(\omega) = (1 - R(\omega))^2 e^{-\alpha(\omega)d}$$

$T(\omega) = I_T(\omega) / I_0(\omega)$ and $R(\omega) = I_R(\omega) / I_0(\omega)$ are referred to as ***transmittivity*** and ***reflectivity***, respectively; d is the sample thickness, α is the ***absorption coefficient*** (dimension cm^{-1}), describing the attenuation of light per unit length.

$\alpha(\omega)$ is the dependence of interest to us, which can be obtained from the measured functions $I_T(\omega)$, $I_R(\omega)$ and $I_0(\omega)$ by correspondingly resolving Equ. (2.9).

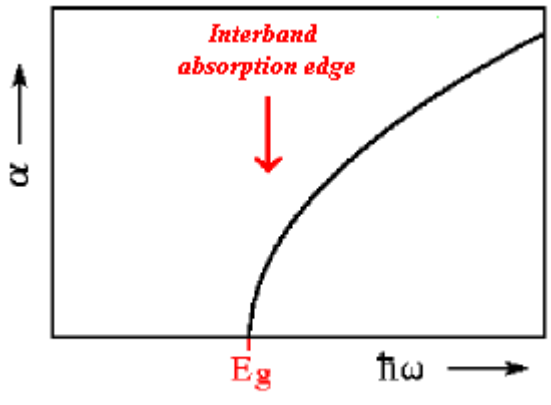

Fig. 2.4

From Fig. 2.2 we expect that $\alpha(\omega)$ *qualitatively* looks like the dependence shown in Fig. 2.4, i. e. α should be zero for

$\hbar\omega < E_g$ and steeply rise for $\hbar\omega \geq E_g$ (***interband absorption edge***). Roughly speaking, this expected behaviour is confirmed by experiment.

However, the *exact shape of the the interband edge* calculated on the basis of Section 2.1 generally does not agree very well with the measurements, mainly due to neglecting ***exciton effects***. Exciton effects often give rise to the appearance of absorption lines in the lower part of the edge (see the Overview Chapter and the detailed discussion in Chapter 5).

Further modifications arise from the ***electron-phonon interaction***, which has also been ignored in the previous analysis.

The discrepancies produced by those effects are much less pronounced at photon energies far above E_g, and usually can be disregarded in that range (Section 2.4).

Luminescence Spectrum

Radiative downward transitions are observed in luminescence spectra (called sometimes emission spectra or,rarely, fluorescence spectra). For the observation of luminescence some external supply of energy is required. Depending on the type of energy supply ("excitation"), one can distinguish photo-, cathodo-, electroluminescence e. t. c. First we deal here only with ***photoluminescence***, where excitation is by optical irradiation.The principle of an experimental arrangement is shown in Fig. 2.5.

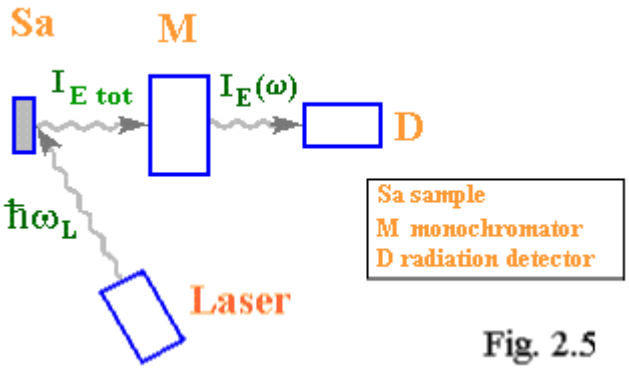

Fig. 2.5

Generally, the excitation leads to the emission of a whole spectrum of photon energies (total intensity I_{Etot}). Spectral decomposition is performed by passing through the monochromator (emerging intensities $I_E(\omega)$). The photon energy $\hbar\omega_L$ of the laser used for excitation is chosen larger than E_g in our case. We represent the relevant processes in the band structure diagram employed so far (see Fig. 2.2) in Fig. 2.6.

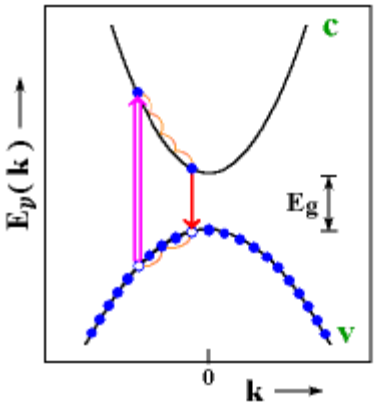

Fig. 2.6

In the absorption process of the laser photons ($\hbar\omega_L$), which is, of course, subject to the **k**-selection rule, electrons are transferred from the valence to the conduction band. Since thereby holes (defect electrons) are produced in the valence band, this process is referred to as the generation of ***electron-hole pairs***. Due to the high intensity of the laser radiation, the electron-hole pair generation rate is very large; we illustrate this by drawing a broad arrow ⇑.

What is of interest to us and can be observed in experiment, is the ***radiative recombination*** ↓ of electrons in the conduction band with holes in the valence band. However, before this process can occur to a significant degree, the two kinds of particles undergo ***relaxation*** (⟶) within the corresponding bands: By emitting phonons, i. e. in a nonradiative way, the electrons very rapidly (typically in 10^{-12} to 10^{-11} s) transfer energy to the crystal, thereby coming close to the

conduction band minimum. This process consists of many small steps. (Phonon energies usually are about some 10 meV, see Section 7.3.) Through analogous processes, the holes assemble near the valence band maximum. (Note that the upward motion of the holes actually involves a downward motion of the valence band electrons; consequently, one is dealing with a decrease of the energy of the electron system also in this respect.)

The probability of the radiative recombination transitions - which can occur only if the conduction band electron and the unoccupied valence band state are at the same **k**-vector - is relatively low compared with the relaxation probability (typical times larger than 10^{-9} s). This is why the recombination practically takes place *after* the relaxation, and starts from the band edges.

Consequently, we expect that the intensity spectrum $I_E(\omega)$ of the radiative electron-hole-pair recombination looks as shown in Fig. 2.7a.

That means we should be concerned with an emission band, whose low-energy limit (as that of the absorption spectrum $\alpha(\omega)$ reproduced from Fig. 2.4) is located at E_g, and which, due to the narrow energetic spread of the two kinds of particles before recombination,does not extend much to high photon energies.

Since the relaxation processes are fast, an equilibrium distribution similar to a Boltzmann distribution is established. Thus the emission bandwidth should be some $k_B T_{EHP}$, where k_B is the Boltzmann constant and T_{EHP} an effective temperature of the electron-hole-pair system. Frequently T_{EHP} is somewhat higher than the crystal temperature (as measured with a thermometer) which is determined by the phonon system (Section 7.3).

At any rate, the luminescence spectrum should extend less far to higher energies than the absorption spectrum, whose extension is determined by the width and location of the energy bands involved (Section 2.4).

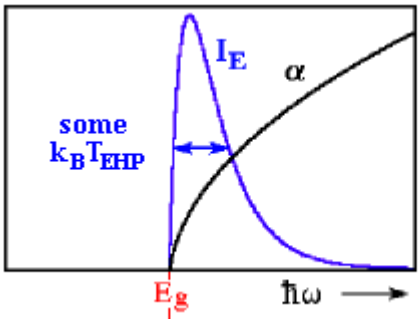

Fig. 2.7a

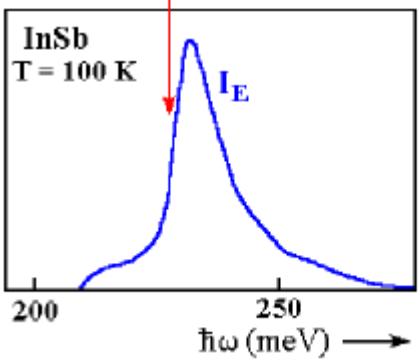

Fig. 2.7b

Experimental studies of the bands due to electron-hole-pair recombination are generally difficult,because the luminescence spectra at the low temperatures of interest are usually dominated by exciton effects (Section 5.4). Favourable conditions for observing such bands exist for materials for which those effects are weakly pronounced. As an example we show in Fig. 2.7b a luminescence spectrum of InSb in the relevant range [4]. This material has extreme properties in that respect (Section 5.5). The E_g value, which is about 227 meV is indicated. The band does not extend much to high energies, as we expect (halfwidth about 11 meV). The low plateau preceding the band at small energies is attributed to recombination processes in which a phonon is emitted in addition to the photon.

2.3 Transitions at Photon Energies Near E_g: Indirect Band Structures

The previous discussion of optical spectra referred to the case in which the extrema of conduction and valence band lie at **k** = 0 (Fig. 2.2). The results are valid for all materials with direct band structure, i. e. including cases where the two extrema are not located at **k** = 0, but both at the same point in the Brillouin zone.

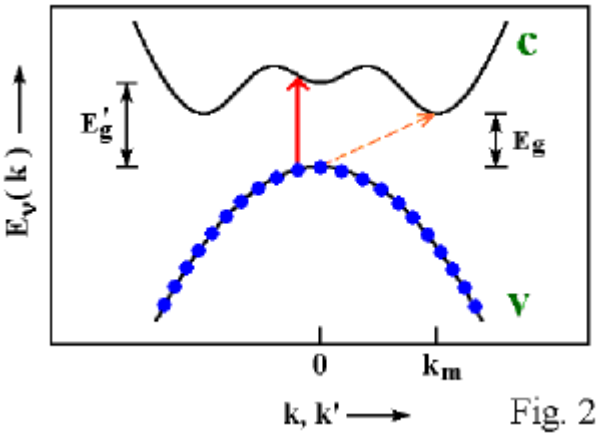

Fig. 2.8

However, there are several substances for which the extrema are displaced relative to each other (substances with ***indirect band structure***). Due to this fact their optical behaviour is different in some respect. This group of materials includes several important semiconductors, such as Si, Ge, and GaP. In these semiconductors the highest valence band maximum is still at $\mathbf{k} = 0$, while the conduction band possesses, in addition to the $\mathbf{k} = 0$ minimum, some deeper minima at different $\mathbf{k}$ vectors. In Fig. 2.8 we illustrate this situation. We shall refer to this Figure in the following.

Here we show the $E_\nu(\mathbf{k})$ dependence along a straight line in the Brillouin zone, passing through $\mathbf{k} = 0$ and two of the other conduction band minima. All minima excluding that at $\mathbf{k} = 0$ have the same depth and are situated symmetrically (in a star-shaped manner) in the Brillouin zone. For GaP there are, e. g., six minima of that kind. These are located close to the centers of the boundary squares, i. e. close to the X points (Fig. 1.3).

Let us first consider the spectrum of *upward transitions* (absorption spectrum). On the basis of the k selection rule (Equ. (2.7)) we expect that only vertical transitions can occur (↑), so that the low-energy limit of the absorption spectrum would be given by the *smallest vertical* distance between conduction and valence band E_g'(see Fig.2.4 ;replacing E_g by E_g'). According to our present knowledge, interband transitions should not be possible below E_g', although photon energies larger than the minimum band separation E_g would be sufficient for these processes. Such transitions, which are originally forbidden, would correspond to the oblique arrows in Fig. 2.8 - - - - →. Nevertheless, this type of transitions do occur, although with comparatively small probability. As discussed in the following, these processes take place with the participation of phonons, which provide the changes in momentum necessary in the case of the oblique transitions.

As dealt with in more detail in Chapter 7, phonons are characterized by

- a propagation vector $\mathbf{q}$, which is restricted to the Brillouin zone, or a quasi-momentum $\hbar\mathbf{q}$ (analogous to the electronic quantities $\mathbf{k}$ or $\hbar\mathbf{k}$, respectively),
- a band index j (analogous to the electronic band index ν) and
- the energy $\hbar\omega_j(\mathbf{q})$ (analogous to $E_\nu(\mathbf{k})$).

More details for the semiconductors which are of interest in our case are presented in Supplement 3.

For the interband transitions to be discussed it is important that electrons and phonons interact with each other. The elementary processes of this interaction can be described, in simple cases, in terms of collisions between electrons and phonons. Since we can regard the "normal" interband transitions as collisions between a photon and an electron (Section 2.1), the processes dealt with here may be considered as *three-particle collisions between a photon, an electron, and a phonon* . (In these processes photon and phonon only interact with the electron, not with each other.)

To begin with, we write - with some rearrangement of terms - the momentum balance, Equ. (2.5) and the energy balance, Equ. (2.6) for the simple electron-photon collision, specializing to the relevant bands ν = **v** and ν' = **c** and putting again $\mathbf{s} = 0$:

(2.10) $\mathbf{k}' - \mathbf{k} = 0$

(2.11) $E_c(\mathbf{k}') - E_v(\mathbf{k}) = \hbar\omega$

To describe the three-particle collision we add the contributions to momentum and energy, of the collision partner phonon:

(2.12) $\mathbf{k}' - \mathbf{k} \pm \mathbf{q} = 0$

(2.13) $E_c(\mathbf{k}') - E_v(\mathbf{k}) \pm \hbar\omega_j(\mathbf{q}) = \hbar\omega$

Here we have to distinguish, with respect to the phonons, two types of processes, i. e. processes involving the generation (*emission*, + sign) and processes involving the annihilation (*absorption*, - sign) of a phonon. So, in the case of Equ. (2.12) and (2.13) we are concerned, as a whole, with processes in which the electron absorbs a photon and *simultaneously* emits or absorbs a phonon. Here it should be noted that the phonon energies (typically some 10 meV) are always much smaller than the photon energies (between some tenths of an eV and some eV, corresponding to the separations of conduction and valence band).

*Consequently, transitions of electrons between the displaced extrema in Fig. 2.8 (- - - - →) are enabled by the fact that the collision partner phonon can supply the difference **k**'- **k** of the displaced extrema of the electronic propagation vectors: The electrons interact with phonons from the whole Brillouin zone, in particular with those whose **q**-vector is similar to the separation of the band extrema.*

Such processes, represented by oblique arrows, are referred to as ***indirect transitions***; the processes due to pure electron-photon interaction, represented by vertical arrows, are called, in this connection, ***direct transitions***. The terms direct / indirect are also used to characterize materials with coincident and displaced band extrema, respectively, since the two kinds of transitions determine the low-energy limit of the interband spectrum. In an analogous manner, one distinguishes ***direct*** and ***indirect energy band structures***.

Using Equ. (2.12) and (2.13) the qualitative shape of the absorption spectrum at photon energies in the vicinity of E_g can be established for indirect band structures (Fig. 2.8). In order to find this, we specialize to transitions exactly between two extreme points, putting $\mathbf{k} = 0$ and $\mathbf{k}' = \mathbf{k}_m$. Thus $\mathbf{q} = \pm\mathbf{k}_m$ is obtained from Equ.(2.12). Inserting this into Equ. (2.13) and considering that the phonon energies are even functions of **q** (see also Chapter 7) we get

(2.14) $E_c(\mathbf{k}_m) - E_v(0) \pm \hbar\omega_j(\mathbf{k}_m) = E_g \pm \hbar\omega_j(\mathbf{k}_m) = \hbar\omega$

From this equation we can find the photon energies $\hbar\omega$ at which transitions between the specified elctronic states can occur: We are dealing with processes for which the change of the electronic state is accompanied by the emission or absorption of type j phonons with propagation vectors $\mathbf{q} = \pm\mathbf{k}_m$ and energy $\hbar\omega_j(\mathbf{k}_m)$. Assuming for simplicity that there are only two important types of phonons (e. g. LA und LO) we obtain four $\hbar\omega$-values lying symmetrically around E_g. These are indicated in Fig. 2.9 by markings (|) on the energy axis.

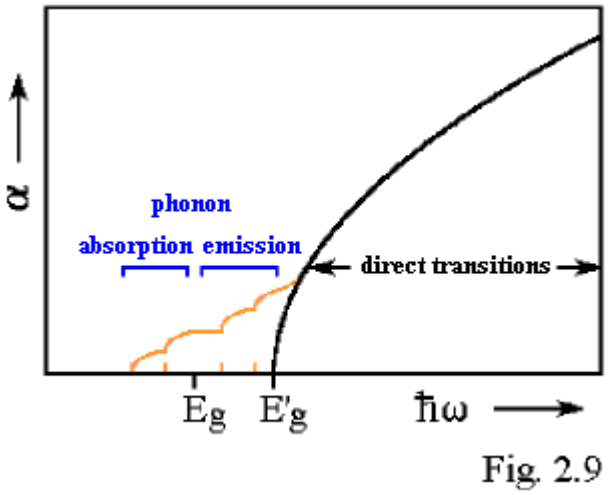

Fig. 2.9

Taking also into account the electronic transitions that connect **k**-and **k**'-vectors outside the extrema, each of the markings becomes a continuum which begins at the marking and extends to high energies. Superposition results in a spectrum with step-like structure (——); above E_g' this merges with the steeply rising spectrum of direct transitions. (Strictly speaking, exciton effects are important for the appearance of pronounced steps.)

The low intensity of the contribution of indirect transitions compared with that of direct transitions is a consequence of the smaller transition probability ("three-particle collisions are less probable than two-particle collisions").

The α-values in the range of the indirect transitions are temperature-dependent: On cooling there is a strong decrease in the range $\hbar\omega < E_g$ and a weak decrease in the range $\hbar\omega > E_g$. This is due to the fact that we are concerned with processes including phonon absorption in the low-energy part, and mainly processes including phonon emission in the high-energy part (Equ. (2.14), Fig. 2.9). The probability of the former processes is proportional to the number of phonons offered, i. e. phonons available, and therefore tends to zero when the temperature approaches absolute zero. As a matter of fact, the

probability of processes with phonon emission also somewhat depends on the number of phonons available (contribution of *stimulated* emission of phonons), but the cooling-induced decrease due to this effect is relatively small. This different temperature dependence can be used for identifying the step-shaped structure for unknown materials.

As an example, we now have a look, in **Fig. 2.10**, at an experimental absorption spectrum in the range of indirect transitions; this refers to GaP [5].

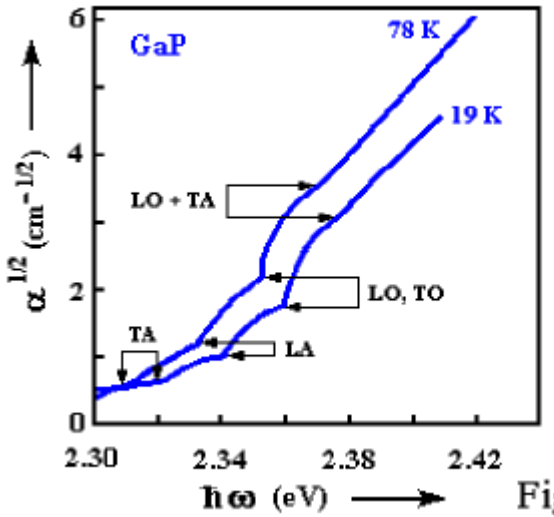

Fig. 2.10

Here we show $\alpha^{1/2}$ ($cm^{-1/2}$) plotted versus $\hbar\omega$ (eV) in the range of transitions with phonon emission for two temperatures. (It comes out from a theoretical treatment not reproduced here that the $\alpha^{1/2}$ representation is especially favourable.) We see the step-shaped structure to be expected. As the temperature decreases, there is an overall shift to higher energies but essentially no change in the band shape. The shift is due to a temperature dependence of E_g, whose origin will not be discussed here either. The types of phonons responsible for the individual steps (TA, LA, ...) are indicated, LO- and TO-phonons being not resolvable. The structure at the highest energy, characterized by LO + TA (not clearly visible on the scale employed) is based on a combination of LO- und TA-phonons. We are dealing here with processes that are described, instead of Equ. (2.14), by an Equ. with *two* phonon energies on the left-hand side (and thus can be declared as four-particle collisions, obviously having relatively high probability in this special case).

We finish this Section with some remarks concerning the *radiative recombination of electron-hole pairs* for indirect band structures. We again consider the case of photoluminescence (Fig. 2.5). Referring to **Fig. 2.11** we represent the relevant processes in our $E_v(\mathbf{k})$ diagram (compare Fig. 2.8).

The electrons in the conduction band and holes in the valence band generated by the laser photons (⇑) are subject, as the particles in earlier cases, to relaxation, accumulating in the deepest conduction band minima and highest valence band maximum, respectively, before recombining. Consequently, the radiative recombination also can only occur through indirect (oblique) transitions ⇐ - - - - i. e. with the participation of phonons (essentially the same types of phonons as in the case of the upward processes).

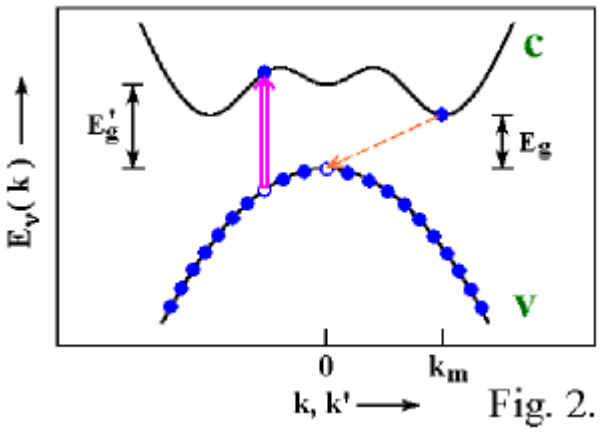

Fig. 2.11

Thus we are again dealing with three-particle collisions photon - electron - phonon, whose probability is small. Since in recombination there are always competition processes (especially radiative and nonradiative transitions at impurities) the processes of interest are hard to observe. The corresponding luminescence-yield generally is very low, so that interband

transitions of indirect materials cannot be used for light emission applications (Section 2.7).

2.4 Transitions between Valence and Conduction Bands at High Photon Energies

In the Sections 2.2 and 2.3 we have discussed the optical behaviour at photon energies in the vicinity of E_g on the basis of simplified band structures (e. g. Fig. 2.2). In the following we deal with (direct) upward transitions between arbitrary valence and conduction bands for real band structures. For this purpose we show again as an example, in Fig. 2.12, the $E_V(\mathbf{k})$ diagram of GaAs (see Fig. 1.4).

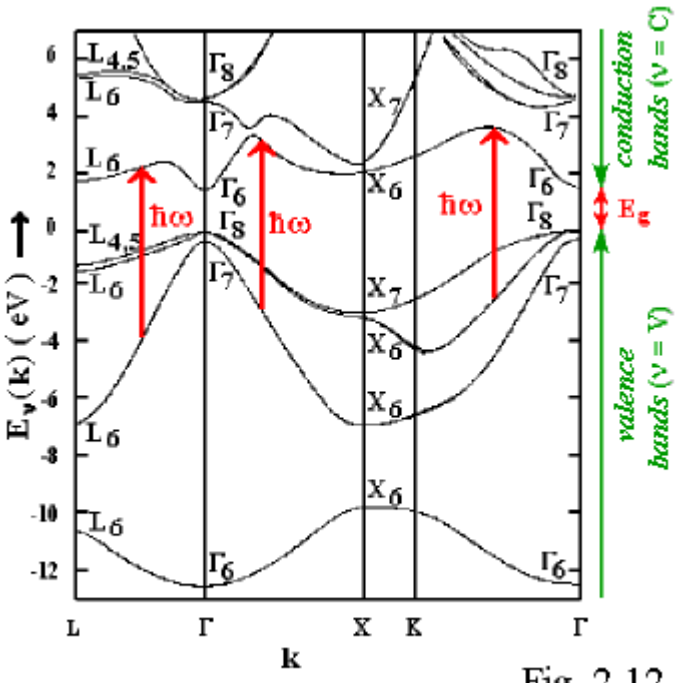

Fig. 2.12

Now we will discuss the absorption spectrum related to these transitions, using the imaginary part of the dielectric function (Appendix 2).

$$(2.15)\quad \varepsilon_2(\omega) \sim \sum_{C,V,\mathbf{k}} f_{CV}(\mathbf{k})\,\delta(E_C(\mathbf{k}) - E_V(\mathbf{k}) - \hbar\omega)$$

where the f-quantities are

$$(2.16)\quad f_{CV}(\mathbf{k}) \sim |\langle \mathbf{k}C|W_0|\mathbf{k}V\rangle|^2 / [E_C(\mathbf{k}) - E_V(\mathbf{k})]$$

The band indices C und V characterize the conduction and valence bands, respectively. (As before, the indices c and v (Sections 2.1, 2.2, and 2.3) refer to the *lowest* conduction band and the *highest* valence band, respectively.) The rest of the terms correspond to those used in Section 2.1.

The structure of Equ. (2.15) is rather transparent: Contributions to the absorption at the photon energy $\hbar\omega$ are made by all transitions, for which the vertical transition arrow (length $\hbar\omega$) fits into the separation of any combination of conduction and valence bands. In Fig. 2.12 we have included three such transitions(↑) for a given $\hbar\omega$. The δ function selects all transitions of that kind from the sum in Equ. (2.15). The contributions of the individual transitions are given by the quantities $f_{CV}(\mathbf{k})$, which are named ***oscillator strengths***. After Equ. (2.16) these are proportional to the squared magnitudes of the matrix elements of W_0 between the corresponding Bloch states (see Equ. (2.4)), i. e., as expected, proportional to the transition probabilities.

Taking into account the fact (being ensured both experimentally and theoretically) that the f's, for a given pair of bands, have only a weak **k** dependence, and replaces them by corresponding average values F_{CV} , we get

$$(2.17)\quad \varepsilon_2(\omega) \sim \sum_{C,V} F_{CV} \sum_{\mathbf{k}} \delta(E_C(\mathbf{k}) - E_V(\mathbf{k}) - \hbar\omega)$$
$$= \sum_{C,V} F_{CV}\, g_{CV}(\omega)$$

$$(2.18)\quad g_{CV}(\omega) = \sum_{\mathbf{k}} \delta(E_C(\mathbf{k}) - E_V(\mathbf{k}) - \hbar\omega)$$

The quantitiy $g_{CV}(\omega)$ introduced here, which is referred to as ***combined density of states*** , sometimes as ***interband density of states***, indicates how many "fitting" $\hbar\omega$ arrows exist for a given pair of bands C,V. This has to be discussed in the three-dimensional **k** space. One can derive the following expression for the combined density of states:

$$(2.19)\quad g_{CV}(\omega) = \frac{1}{4\pi^3} \int \frac{d\sigma}{|\mathrm{grad}_{\mathbf{k}}(E_C(\mathbf{k}) - E_V(\mathbf{k}))|}$$
$$[E_C(\mathbf{k}) - E_V(\mathbf{k}) = \hbar\omega]$$

This relation is analogous to the expression for the contribution $g_\nu(E)$ of one band ν to the ordinary density of states given in Equ. (1.13). In both cases we are concerned with integrals over surfaces of constant energy in **k** space. However, in the present case these are determined by $\hbar\omega$ and by the $E_\nu(\mathbf{k})$ functions of *two* bands.

The ω dependence of ε_2 obviously is given by the ω dependence of the combined density of states. In particular, the $g_{CV}(\omega)$ are responsible for the existence of structures in $\varepsilon_2(\omega)$ (by the way, also of structures in $\varepsilon_1(\omega)$, Appendix 2). It is found that structure appears at ω values at which there are,on the corresponding surface of constant energy, zeros of the integrand denominator, i. e. if the surface contains points at which

(2.20) $\mathrm{grad}_{\mathbf{k}} [E_C(\mathbf{k}) - E_V(\mathbf{k})] = 0$

Such points are named ***critical points***. One obtains the form of those structures by expanding $E_C(\mathbf{k}) - E_V(\mathbf{k})$ into a Taylor series around the critical point $\mathbf{k}_0$,

$$(2.21)\quad E_C(\mathbf{k}) - E_V(\mathbf{k}) = E_C(\mathbf{k}_0) - E_V(\mathbf{k}_0) +$$
$$+ \sum_{i=1}^{3} \frac{\hbar^2}{2\mu_i} (k_i - k_{0i})^2 + \ldots$$

and inserting this into Equ. (2.19). Because of Equ. (2.20) there are no terms linear in $\mathbf{k} - \mathbf{k}_0$. For the second derivatives of $E_C(\mathbf{k}) - E_V(\mathbf{k})$ we have written $\hbar^2/\mu_i$, i. e. we have introduced, similarly as in our earlier expansion in Equ. (1.10) to (1.12), parameters μ_i, having the dimension of masses. k_i and k_{0i} are the Cartesian components of the corresponding vectors in a coordinate system analogous to the one used in Equ. (1.10).

The contribution of a critical point to $g_{CV}(\omega)$ depends upon the signs of the μ_i. The structures expected for the four possible combinations of signs (denoted by M_0, M_1, M_2 and M_3) are shown in **Fig. 2.13**.

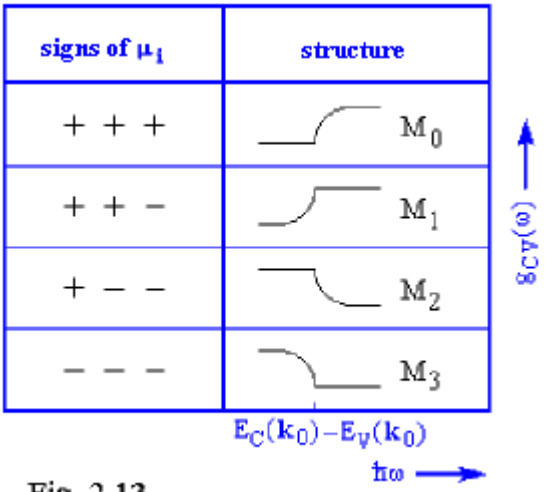

Fig. 2.13

Obviously M_0 (+++) und M_3 (---) describe minima and maxima of $E_C(\mathbf{k}) - E_V(\mathbf{k})$, respectively. This explains the shapes of the corresponding structures shown in Fig. 2.13. In the cases of M_1 and M_2 one is dealing with something like saddle points of this function.

In **Fig. 2.14** we present $\varepsilon_2(\omega)$ for GaAs (T = 300 K) [6], in an energy range beginning above E_g(about 1.4 eV) and comprising the visible and ultraviolet parts of the spectrum.

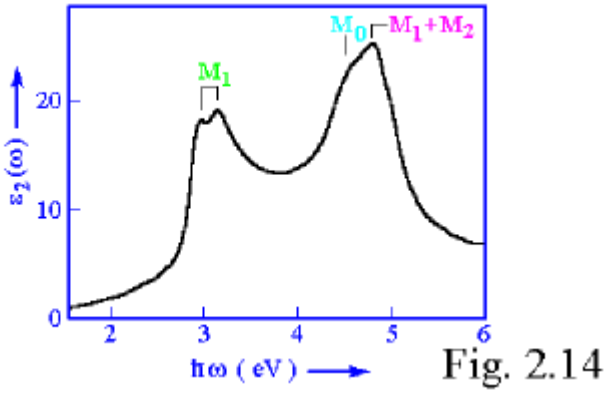

Fig. 2.14

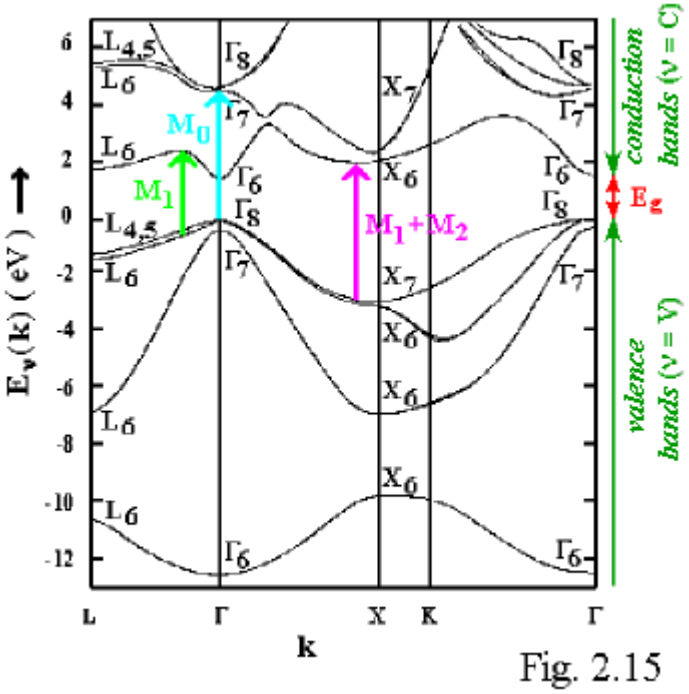

Fig. 2.15

The spectrum in Fig. 2.14 was obtained by ***ellipsometric measurements***. This method is based on the fact that linearly polarized light in general becomes elliptically polarized when reflected by an absorbing medium. The dielectric function can

be determined from the analysis of the ellipse parameters, requiring, contrary to the methods mentioned so far (Section 2.2, Appendix 1 and Appendix 3), no measurements of intensities [7].

The assignments of the structures to critical points are given in Fig. 2.14. In the $E_v(\mathbf{k})$-diagram, which we repeat as **Fig. 2.15**, the responsible transitions are characterized by corresponding colours.

When comparing Figs. 2.13 and 2.14 we have to note that, in the vicinity of structures, other **k** regions and band combinations generally contribute to ε_2, whereby the ω dependence may be considerably modified.

Remarkably, the optical absorption shows still a strong increase at high $\hbar\omega$ compared with the range around E_g.

2.5 Derivation of Information on Energy Band Structures

Studies of the optical spectra as dealt with in Section 2.4 contain information on the $E_v(\mathbf{k})$ dependences of valence and conduction bands. In this connection the structures due to critical points are of special importance. Unfortunately, the spectra cannot be evaluated *directly* with respect to $E_v(\mathbf{k})$, apart from elementary statements as the determination of E_g from the position of the interband absorption edge. The desired information can only be obtained by performing band structure calculations for the corresponding material and comparing the resultant spectra, in particular $\varepsilon_2(\omega)$, with the experimental data.

Obviously, this involves a solution of the Schrödinger Equ. (1.5) with the Hamilton operator Equ. (1.4), i. e. the determination of the corresponding eigenvalues $E_v(\mathbf{k})$and eigenfunctions $\psi_{\mathbf{k}v}(\mathbf{r})$ (Equ. (1.8)). It is shown by Equ. (2.19) and (2.16) that the $E_v(\mathbf{k})$ give the combined density of states $g_{CV}(\omega)$, whereas the $\psi_{\mathbf{k}v}(\mathbf{r})$, together with the energies, yield the oscillator strengths $f_{CV}(\mathbf{k})$ or F_{CV}. With Gl. (2.17) one then obtains theoretical $\varepsilon_2(\omega)$ curves.

The theoretical results critically depend upon the choice of the potential U(**r**). As already mentioned, both the atomic nuclei and the other electrons contribute to U(**r**). The nuclear contribution is determined by the Coulomb potential generated by the nuclear charges and is not problematic, since the kinds of nuclei and their positions are known (the latter being obtained from X-ray data). Problems come from the electronic part, since this is determined by the wavefunctions of the other electrons, being objects of the calculations themselves.

In a strongly simplified consideration one would expect that the contributions of the other electrons to the charge density, $e|\psi_{\mathbf{k}v}(\mathbf{r})|^2$, which determine their Coulomb field, are effective. In reality, the situation is much more complex, mainly due to the existence of many-electron effects.

In view of those difficulties, the problem can only be treated making use of considerable approximations [1]. From the degree of agreement between theory and experiment one can draw conclusions as to the quality of the approximations employed, i. e., in this manner, one obtains information concerning the correct U(**r**) and thereby information on the correct energy band structure and correct wavefunctions of the material investigated.

Apart from the optical spectra of valence band to conduction band transitions, one makes use, if available,of additional experimental data, especially X-ray absorption and emission spectra (see Chapter3), photoemission spectra [2], and experimental values of effective masses [2] (see also Section 2.6)

2.6 Transitions Between Sub-Valencebands

As already mentioned in Section 1.3, in many materials the $E_v(\mathbf{k})$ maxima of the three highest valence bands lie at $\mathbf{k} = 0$, and at this point these three bands approach each other rather closely (see Fig. 1.4). This is related to the fact that the corresponding Bloch states originate from p-states of the constituting atoms; as is well known, these states are degenerate (threefold without spin). As a consequence, simple kinds of band structure calculations lead to a contact of the three bands at $\mathbf{k} = 0$. More detailed theoretical studies show that the (partial) separation of bands observed is due to the existence of ***spin-orbit interaction*** and, in some cases, also to deviations from cubic crystal-symmetry.

Here we restrict ourselves to materials with diamond and zincblende structure, for which only spin-orbit coupling is effective. This coupling is based on the fact that electrons in Bloch states, due to their behaviour in the vicinity of atoms (Fig. 1.2) in general possess an orbital angular momentum interacting with the spin (analogous to the situation of electrons in isolated atoms).

Fig. 2.16 shows part of the sub-valence-band structure (roughly corresponding to the situation of Ge); with standard names and labels as used in the literature.

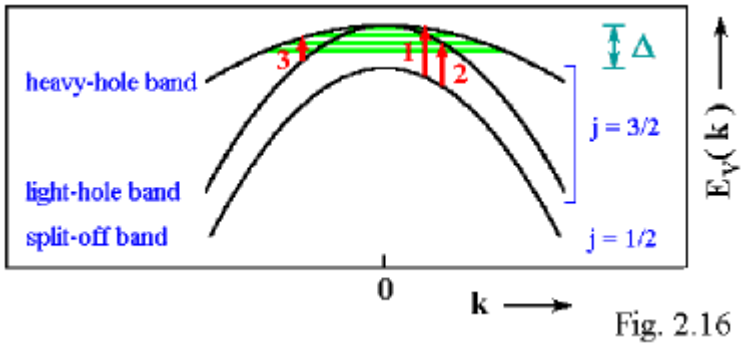

Fig. 2.16

The j-labels refer to the analogy with atomic p-states, in the presence of spin-orbit coupling. The names "heavy-hole band" and "light-hole band" point to the magnitudes of the effective masses, which are inversely proportional to the magnitudes of the second derivatives (curvatures) of $E_V(\mathbf{k})$(Equ. (1.11)).

The separation of the bands at $\mathbf{k} = 0$ (Δ) depends on the strength of the spin-orbit coupling for the material under consideration. In the Table the corresponding values are given for four substances.

	Δ(eV)
Si	0.044
Ge	0.30
GaAs	0.33 (see Fig. 1.4)
CdTe	0.96

The dependence on the material can be related qualitatively to the constituting types of atoms: Substances consisting of atoms (especially anions) with high nuclear charge numbers exhibit large Δ values and vice versa.

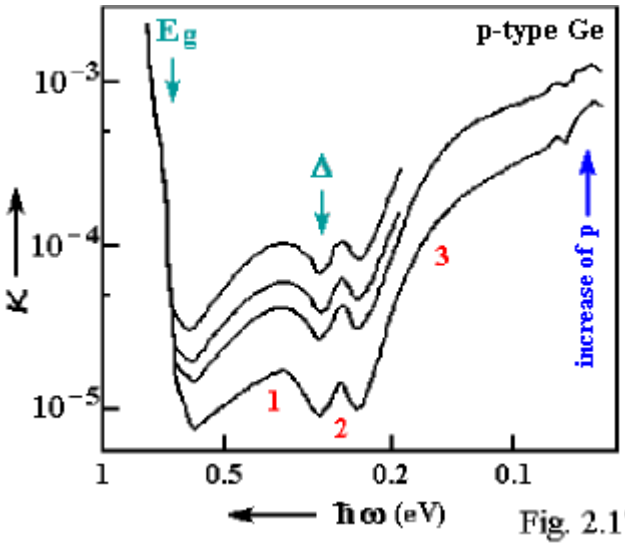

Fig. 2.17

In order that optical transitions between subbands can take place, one must have non-occupied final states, i. e. holes (defect electrons) have to exist. This requires (ignoring sophisticated experiments working with supplementary short-wavelength irradiation) doping the material with "shallow" acceptor impurities (p-type doping). As the temperature increases the acceptor levels receive (due to collisions with phonons) electrons from the valence bands. The holes generated in this way are distributed, in thermal equilibrium, over the valence bands according to Fermi-Dirac statistics. Preferentially they occupy the states having the highest energy; hence these are possible final states for upward transitions. In Fig. 2.16 we indicate this range by green hatching. As a consequence, three types of transitions can occur, designated in Fig. 2.16 by **1**, **2**and **3** (vertical transitions, Section 2.1). These give rise to three bands in the absorption

spectrum. Fig. 2.17 shows experimental results for p-type Ge [8]. In this Figure the absorption index κ (compare Appendix 2) is plotted versus the photon energy $\hbar\omega$, on a double logarithmic scale. The curve parameter is the hole concentration of the samples investigated. As to be expected, the three bands are located on the low-energy side of the interband absorption edge (marked by E_g (= 0.8 eV)). Due to the comparatively small number of free final states, their intensity is much lower than the intensity of the true interband absorption discussed earlier; it grows, as should be expected, with increasing p.

According to Fig. 2.17, the low- energy limit of band 1 and the high-energy limit of band 2, which are both given by Δ, coincide. The declining of bands 1 and 3 toward high energies and of band 2 toward low energies are mainly caused by the occupation of the final states with holes decreasing in these directions.

The quantitative description of these spectra is based on the same principles as in the case of interband spectra (Section 2.4), allowing for the doping- and temperature-dependent occupation of the electronic final states (and, partly, the **k** dependence of the oscillator strengths). We are not going to discuss these problems in detail.

From measurements of inter-subband spectra one can obviously obtain information on the $E_V(\mathbf{k})$ dependence of the valence bands. Especially the important parameter Δ can be extracted directly. In addition, one is able to determine - as from studies of *intraband transitions* to be discussed later- concentrations of current carriers (hole concentrations in the present case) in a pure optical manner (see Section 4.1 for more details).

2.7 Aspects of Applications

Here we shall briefly discuss some applications based on upward and downward transitions between valence and conduction bands of semiconductors.

Upward Transitions

In these applications one makes use of the fact that upward transitions generate electron-hole pairs influencing the electrical properties of the material.

When *spatially homgeneous material* is irradiated with photons in the interband range, an applied electric voltage leads to the motion of electrons and holes, which manifests itself (see Fig. 2.18, image part a) in the appearance of photocurrent (n- or p-photocurrent, depending upon the ratio of the lifetimes of the two kinds of particles, application as ***photoresistors***). In *p-n junctions* a change in the space charge distribution is brought about by optically generated electron-hole pairs. This leads to a photoinduced EMF (***photoelements***) or - under applied voltage - a significant effect on the current through the junction (***photodiodes***). This is illustrated in Fig. 2.18b; analogous phenomena can be realized in *Schottky barriers*.

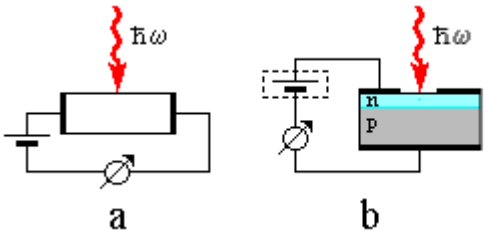

Fig. 2.18

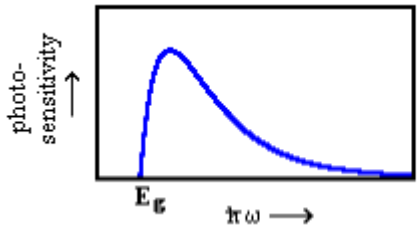

Fig. 2.19

As is well known, those structures are being used in many applications, including the detection of radiation (especially in the infrared spectral region) and the transformation of radiation energy into electrical energy (solar cells).

The minimum photon energy necessary fot these effects is obviously given by E_g. Hereby, in most cases, the sensitivity to radiation is limited, as indicated in Fig. 2.19, to a relatively narrow $\hbar\omega$ range above E_g. The decrease appearing at high energies is related, generally speaking, to the decrease of the penetration depth of the radiation, which occurs owing to the increase of the absorption coefficient . The penetration depth can diminish down to the order 10^{-5} cm. (For instance, in the case of photoresistors the decrease is frequently due to the growing effect of surface recombination).

Therefore the optimum choice of a material for a given spectral range depends rather critically on the corresponding E_g values. To achieve a good adjustment or to cover a larger range, one frequently uses systems of mixed composition: One starts, e. g. from two compounds AC and BC with different E_g values, from which one can produce systems of the type $A_xB_{1-x}C$ (metal sites partly occupied by A atoms, partly by B atoms). Then, by choosing the mixing ratio x (x between 0 and 1), the desired E_g and, consequently, the sensitivity range of interest can be realized, see Fig. 2.20. As an example, we refer to $Cd_xHg_{1-x}Te$, a material used for infrared detectors, for which E_g can be varied from about 1.4 eV (x = 1) to approximately 0 eV (small x).

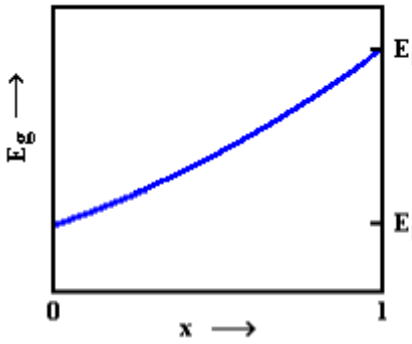

Fig. 2.20

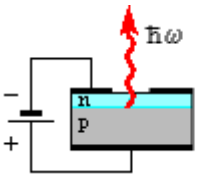

Fig. 2.21

For the theoretical treatment of the electronic states of such systems, one has to employ techniques which go beyond the methods used for normal bandstructure calculations (Section 2.5), since one no longer has translation symmetry, as occurs in the case of "pure" systems.

Downward Transitions

This group of applications is based on the radiative recombination of electrons in the lowest conduction band with holes in the highest valence bands (Section 2.2). Here the electron-hole pairs are generated in *p-n junctions* by applying voltage in the forward direction (injection electroluminescence), see Fig. 2.21. One makes use of this phenomenon in ***luminescence diodes*** (also often referred to as ***LED's*** (= light emitting diodes)).

Here the useful spectral region is also limited to photon energies in the vicinity of E_g, see Fig. 2.7. (This effect is even more pronounced than for the upward transitions.) In the present case this phenomenon mainly arises from relaxation processes (Section 2.2). The spectral range desired for the application is realized here, too, using systems of mixed composition, whose E_g values are chosen according to Fig. 2.20. $GaAs_xP_{1-x}$ is a material employed for luminescence diodes wich different emission wavelengths (varying the occupation of non-metal sites).

Strictly speaking, the injection electroluminescence is usually determined by transitions between impurity levels lying close to the band edges (e. g. "pair transitions betwen shallow donor and acceptor levels). As a consequence, the minimum photon energies are usually somewhat smaller than E_g. The emission spectra can be varied, as described earlier, by means of mixed compositions, because the impurity levels " are coupled to the corresponding bands".

p-n structures as shown in Fig. 2.21 can also be used to achieve laser action. However, it has been found that a much higher efficiency is obtained with the aid of more complex structures, including quantum wells (see Chapter 6, especially Section 6.4), as employed today in ***semiconductor lasers***.

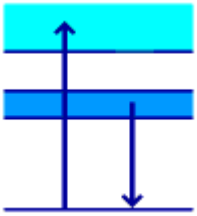

Chapter 3

Transitions Between Core Levels and Bands

In the preceding chapter we have dealt with transitions between valence and conduction bands. The corresponding photon energies typically are situated in the optical range (infrared, visible, or ultraviolet region).In the present short chapter we shall discuss transitions connecting the bands with deep lying, so-called core levels; the relevant spectra are generally found in the X-ray range.

Fig. 3.1 shows the energy spectrum (without **k** dependence, energy separations not to scale) of NaCl, comprising conduction and valence bands as well as core levels.

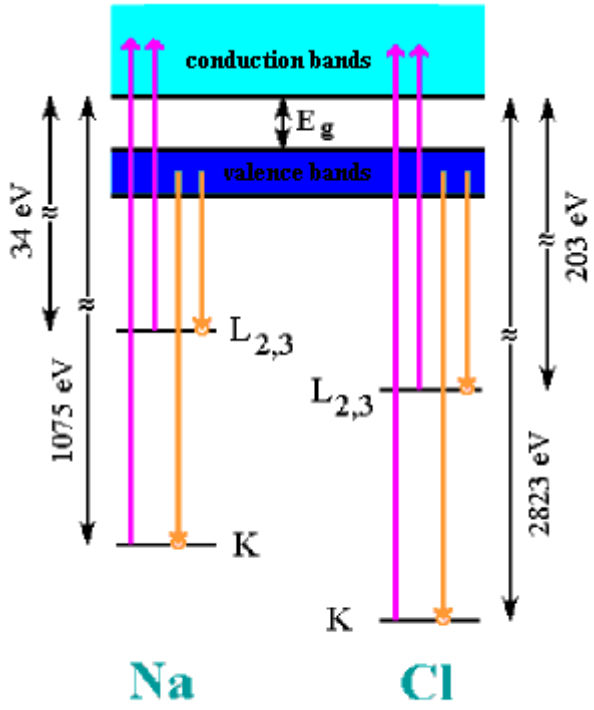

Fig. 3.1

As an example we present here data referring to the ionic compound sodium chloride, because in this case there are experimental results which very clearly demonstrate the usefulness of X-ray spectroscopy (see Fig. 3.2 below). The general aspects of the following discussion are also valid for semiconductor materials consisting of several kinds of atoms.

Electrons in core-level states are strongly bound to the atoms, hence they are similar to the states of free atoms.The wavefunctions are localized in the range of individual atoms, so that a description in terms of delocalized Bloch functions is no longer adequate. The energy levels do not form broad bands as found before, but are discrete as are the levels of isolated atoms. A general discussion of the different properties of valence band and conduction band states compared with the properties of core states is presented in **Supplement 4**.

In view of these facts the core states are characteristic of the individual sorts of atoms, which we illustrate in Fig. 3.1 by a side shift of the Na and Cl type levels. In this Figure we restrict ourselves to K-type levels (atomic 1s states) and L-type levels (atomic 2s and 2p states). Level splittings, which are present in reality, have been omitted.

In **Fig. 3.1** we represent radiative transitions that are of interest to us. These are

- upward transitions between core levels and conduction bands ↑, manifesting themselves in absorption spectra and
- downward transitions from valence bands to core levels ↓, detected in emission spectra (fluorescence spectra).

Of course downward transitions can only be observed if holes are created in the core levels, which are normally occupied by electrons; this requires supplying energy from outside (excitation by high-energy photons or high-energy electrons).

Absorption spectra are usually determined by transmission measurements in the X-ray range. The components of the experimental arrangements are usually the same as shown in Appendix 1, Fig. A1 for the optical case, although their technical structure is often basically different. However, one can omit the I_R measurements due to the low reflectivity. A similar situation is found for the arrangement for emission experiments, represented in Appendix 1, Fig. A2; of course, the excitation source involving a laser has to be replaced by a suitable high-energy excitation source.

Studies of those kinds of spectra yield information about the structure of valence and conduction bands. Let us demonstrate this for the example of upward transitions between a core level ρ and a conduction band C.

In this case the imaginary part of the dielectric function (Appendix 2) has the form (ignoring prefactors):

$$(3.1) \quad \varepsilon_2(\omega) \sim \sum_{\mathbf{k}} f_{C\rho}(\mathbf{k})\, \delta(E_C(\mathbf{k}) - E_\rho - \hbar\omega)$$

where E_ρ are energies of core levels and $f_{C\rho}(\mathbf{k})$ are oscillator strengths. One has the following relations between oscillator strengths and transition matrix elements:

$$(3.2) \quad f_{C\rho}(\mathbf{k}) \sim |\langle \mathbf{k}C|W_0|\rho\rangle|^2 / [E_C(\mathbf{k}) - E_\rho]$$

These expressions are completely analogous to Equ. (2.15) and (2.16), whereby instead of the initial states $|\mathbf{k}V\rangle$ and initial energies $E_V(\mathbf{k})$ entering there, the core states $|\rho\rangle$ and core energies E_ρ, respectively, appear. (In addition, the conduction band states are modified through the retroactive effect of the localized hole occurring in the core level, which we ignore in the following.) Because of the big separation between conduction bands and core levels (Fig.3.1) the denominator in Equ. (3.2) may be regarded as **k** independent, so that we have

$$(3.3) \quad f_{C\rho}(\mathbf{k}) \sim |\langle \mathbf{k}C|W_0|\rho\rangle|^2.$$

If, for the moment, we consider $f_{C\rho}$ as *totally* **k**-independent, we get from Equ. (3.1)

$$(3.4) \quad \varepsilon_2(\omega) \sim \sum_{\mathbf{k}} \delta(E_C(\mathbf{k}) - E_\rho - \hbar\omega) = g_C(E_\rho + \hbar\omega)$$

The sum over **k**, which includes, according to the δ-function all conduction band states with energy $E_\rho + \hbar\omega$, obviously is identical with the corresponding density of states g_C, at this energy (see Section 1.4). Consequently, we obtain here (due to the presence of discrete initial levels) information about the density of states itself, rather than the combined density of states as in our previous discussion.

However, the density of states function is considerably modified by the **k** dependence of $f_{C\rho}$, which has been ignored so far: This becomes evident by writing the matrix element in Equ. (3.3) as an integral over the wavefunctions

$$(3.5) \quad \langle \mathbf{k}C|W_0|\rho\rangle = \int \psi_{\mathbf{k}C}(\mathbf{r})^* W_0(\mathbf{r})\, \psi_\rho(\mathbf{r})\, d\mathbf{r}$$

The $\psi_\rho(\mathbf{r})$ are approximated by atomic wavefunctions:

$$(3.6) \quad \psi_\rho(\mathbf{r}) = R_{nl}(r)\, Y_{lm}(\theta,\phi)$$

r, θ and ϕ are spherical polar coordinates related to the position of the corresponding atomic nucleus; $R_{nl}(r)$ and $Y_{lm}(\theta,\phi)$ are radial functions and spherical harmonics. n, l, and m are atomic quantum numbers in the usual notation. Contributions to the integral in Equ. (3.5) are made only by the overlapping parts of the integrand factors, which are determined by the strongly localized ψ_ρ. Therefore it is useful to expand $\psi_{\mathbf{k}C}$ in wavefunctions of the atom for which ψ_ρ was chosen:

$$(3.7) \quad \psi_{\mathbf{k}C}(\mathbf{r}) \approx \sum_{n'l'm'} a_{n'l'm'}(\mathbf{k})\, R_{n'l'}(r)\, Y_{l'm'}(\theta,\phi)$$

For the matrix element we get

$$(3.8) \quad \langle \mathbf{k}C|W_0|\rho\rangle \approx \sum_{n'l'm'} a^*_{n'l'm'}(\mathbf{k}) \langle n'l'm'|W_0|n\,l\,m\rangle$$

.

Here $|n', l', m'\rangle$ are atomic states with wavefunctions $R_{n'l'}(r)\, Y_{l'm'}(\theta,\phi)$. The matrix elements on the right-hand side, corresponding to intraatomic radiative transitions, are subject to the familiar dipole selection-rule $l' = l \pm 1$.

If the initial level is of K(1s) type we have l = 0 and l'= 1. For L(2p) initial levels one gets l = 1, yielding l'= 0 or l'= 2. Hence, in the first case only the "p-parts" of the conduction band density of states make contributions to absorption,

while in the second case the "s-parts" and "d-parts" contribute. (These parts refer to the atomic sort, to which the core state ρ belongs.)

In Fig. 3.2 we show experimental absorption spectra of NaCl [9] for transitions starting from K (Na)-, K (Cl)-, L (Na)- and L (Cl)-levels. Here the absorption coefficient α is plotted on the vertical scale; see Appendix 2 for the relation between α and ε_2. The spectra have been shifted against each other, so that the absorption edges corresponding to the bottoms of the conduction bands (|) coincide (compare the energetic separations in Fig. 3.1). The lines appearing in the L-spectra below this limit originate from transitions into so-called ***exciton states***. In these states the excited electron remains localized, due to Coulomb attraction, in the vicinity of the hole generated in the L-shell.

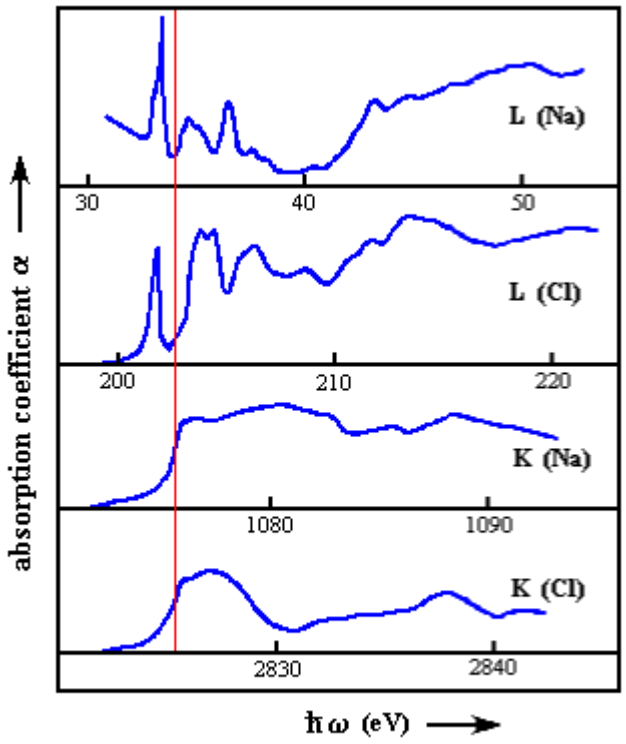

Fig. 3.2

Obviously the density of states of the conduction band is considerably modified by the selection effect described. In particular, there are big differences between K-and L-spectra, enabling conclusions to be drawn as to the character of the conduction-band wavefunctions, which is evident from the previous discussion. However, in a more detailed interpretation, one has to take into account that usually multi-electron excitations contribute to the spectra (see the following remarks).

An analogous situation is found for the emission spectra based on transitions from valence bands to core levels. These yield information on the various components of the valence-band density of states, depending on the type of final level.

Hence, in principle very detailed checks of band-structure calculations are obtained from X-ray spectra. However, it should be noted that the analysis of the spectra is often complicated (compared with the case of valence-band to conduction-band transitions) by a series of effects not mentioned so far. These include:

- Frequently, in addition to the one-electron transitions discussed here, many-electron processes contribute to the spectra, which is due to the strong localization of the core states.
- The attainable spectral resolution of the structures in the density of states is generally worse than in the optical region (absolute values at least several tenths of an eV compared to values in the meV range in the optical case).
- In the case of emission measurements, the spectral components of interest are often superimposed by contributions of different processes (e. g. contributions of "characteristic radiation" and "bremsstrahlung").

Consequently, to derive information about $E_v(\mathbf{k})$, one makes use, if possible, of data from the optical as well as from the X-ray range (see also Section 2.5).

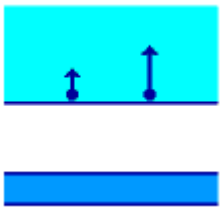

Chapter 4

Intraband Transitions

In the present Chapter we shall be concerned with spectra that are correlated with upward transitions *within an energy band*. Obviously such transitions can be observed only if the band is occupied *partially* by electrons. This situation occurs, e. g., in the case of semiconductors doped with shallow impurities becoming thermally ionized at not too low temperatures.

4.1 Absorption Spectra

Let us consider a material doped with shallow donors. Then, in the case of thermal ionization, we have electrons in the (lowest) conduction band, which accumulate near its bottom (assumed to be at $\mathbf{k} = 0$), see Fig. 4.1. Obviously, the occurrence of intraband transitions implies a change of the **k** vector (↗). Our previous discussion of indirect interband transitions (Section 2.3) indicates that interaction partners in addition to photons and electrons have to take part in the present processes.

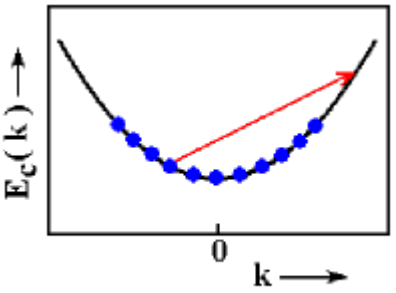

Fig. 4.1

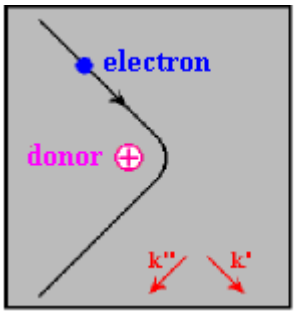

Fig. 4.2

It is found that two kinds of partners are important:

- *phonons.* In these processes, which resemble the indirect interband transitions, a phonon is emitted or absorbed during the absorption of the photon (momentum close to 0). Here the change of the momentum of the electron (change of **k**) is brought about by the phonon. These processes can be referred to as three-particle collisions photon - electron - phonon as before.
- *impurities.* These processes can be visualized as an electron-impurity collision taking part during the absorption of the photon (also something like a three-particle collision). The collision generally leads, as indicated in Fig. 4.2, to a deflection of the electron corresponding to a change of the **k** vector (**k'** → **k''**). Fig. 4.2 refers to a collision with one of the donors (being unevitably present as a consequence of doping), which is positively charged due to thermal ionization. Here the donor, which is essentially fixed in the crystal, only contributes to the change in **k** (elastic collision), while a contribution to the increase in energy merely comes from the photon.

As to be expected, intraband transitions give rise to a continuous optical absorption spectrum. We shall not deal here with the theoretical treatment.The quantitative form of the spectra significantly depends upon various features (e. g. temperature, details of the energy band structure). Let us consider a case that is frequently realized:

- nondegenerate semiconductor material (Fermi energy below the conduction-band minimum)
- photon energy $\hbar\omega$ large against the thermal energy $k_B T$
- transitions limited to the range of quadratic $E_c(\mathbf{k})$ dependence

In this case the spectral variation of the absorption coefficient α (Appendix 1 and Appendix 2) is approximately given by power laws:

(4.1) $\alpha(\omega) \sim n_{el}\, \omega^{-\beta} \sim n_{el}\, \lambda^{\beta}$

(n_{el} concentration of electrons in the conduction band, $\beta > 0$ parameter, λ light wavelength). For β one obtains the following values depending on the third collision partners:

	β
acoustic phonons	3/2
(longitudinal) optical phonons	5/2
charged impurities	7/2

(For the imaginary part of the dielectric function, $\varepsilon_2(\omega)$, we find, because of the relations given in Appendix 2 and the

weak ω dependence of the refraction index, approximately power laws, too. However, here the exponents are higher by the value 1 in each case.)

When comparing with experiment, one has to note that generally several types of collisions occur with similar frequency, the relative contributions being temperature dependent in a given system. (In particular, the frequency of the phonon collisions increases with growing temperature.) Hence, in real cases, one is often concerned with exponents deviating from the values given before.

The decrease of α with increasing photon energy $\hbar\omega$ (Equ. (4.1)) has the consequence that for semiconductors intraband transitions are mainly observed in the infrared region.

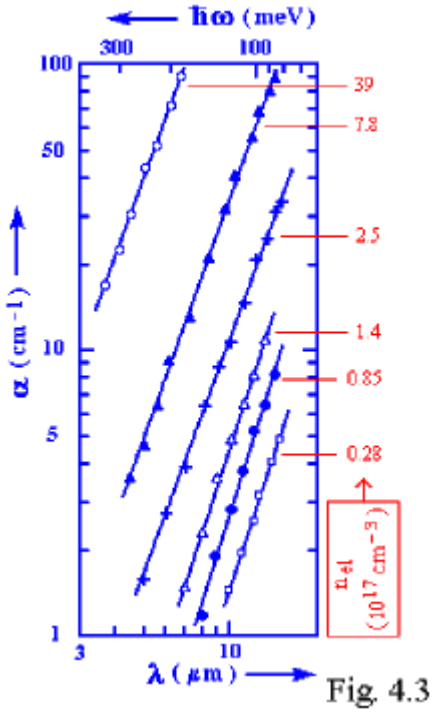

Fig. 4.3

Fig. 4.3 shows experimental absorption spectra of intra-conductionband transitions for n-type InAs (T = 300K) in a log α - logλ plot, with n_{el} (determined by electrical measurements) as a parameter [10]. In agreement with Equ. (4.1) we find a power-law form of the spectra and - within experimental accuracy - proportionality to n_{el}. The exponent β deduced from the straight-line slope is close to 3 in all cases, which suggests, according to the Table, that optical phonons and charged impurities are the dominant collision-partners.

Intra-valenceband transitions, which occur in p-type semiconductors, are usually masked by the transitions between sub-valencebands appearing in the same spectral region (see Section 2.6).

Making use of the intraband absorption as well as of the absorption due to transitions between sub-valencebands, it is - after corresponding calibration - possible to determine carrier concentrations in a pure optical (i. e. contactless) manner. (The detection limits are of the order 10^{15} and 10^{14}cm^{-3}, respectively.) The previous remarks show that one can also get insight into "scattering mechanisms" of the carriers from intraband absorption. This kind of information is conventionally obtained by means of electrical methods (measurements of conductivity and Hall effect), which require the production of electrodes. A remarkable application involves determining *spatially inhomogeneous distributions* of carrier concentrations in semiconductor material , in particular semiconductor devices, by scanning with a fine infrared beam having a wavelength in the range of the corresponding transitions.

In literature the spectra due to intraband transitions are usually referred to as ***free-carrier absorption spectra***, sometimes also as ***Drude-type absorption spectra***.

4.2 Reflection Spectra

Intraband transitions also manifest themselves in reflection spectra. To understand the shape of these spectra, we refer to the oscillator model discussed in Appendix 4. Due to the fact that electrons and holes occupying a band-edge range behave, in many respects, similarly to free particles(see Section 1.3), they can be characterized, in a simplified manner, as oscillators with the resonance frequency $\omega_0 = 0$ ("acceleration in an electric field without a restoring force"). As a consequence, we can use Fig. A5 to get a rough idea of the optical spectra. For $\omega_0 = 0$ we have to consider, in this Figure, only the ω ranges above the resonance frequency. To begin with, that means that the quantities ε_2 and κ, which

characterize the absorption, monotonously decrease with growing ω. This behaviour transfers to α(ω) and thus qualitatively corresponds to the theoretical and experimental results presented in Section 4.1 .

For the reflectivity R we expect on the basis of Fig. A5d a fairly weak variation at low ω, with values close to unity, then a steep drop to zero, followed by an increase to a nearly constant low level, see Fig. 4.4. The steep drop of R is referred to as the ***plasma reflection edge***. As in the general case (Appendix 4), the drop approximately coincides with the zero of $\varepsilon_1(\omega)$.

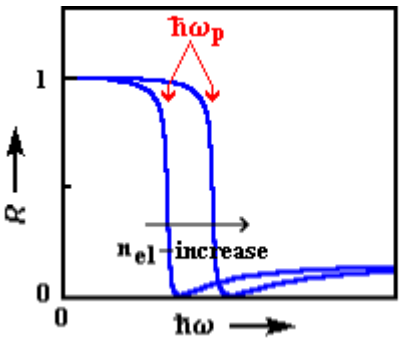

Fig. 4.4

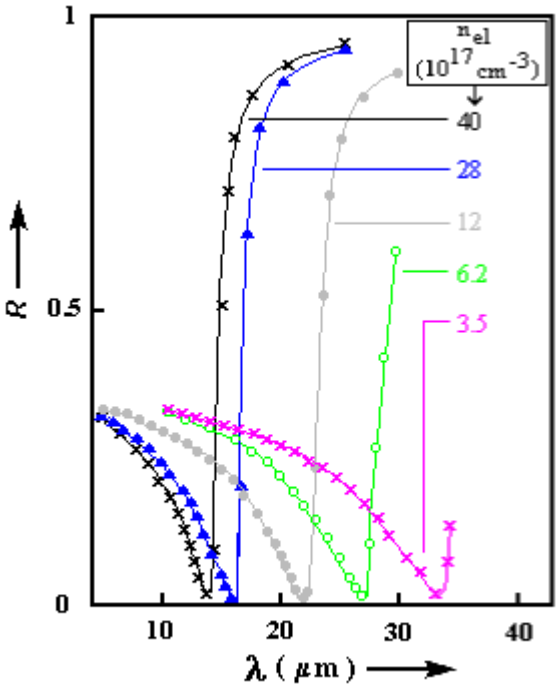

Fig. 4.5

To estimate the position of the edge for an n-type material, we use the oscillator formula Equ. (A4.6), specializing it to $\omega_0 = 0$, $\gamma = 0$, $A = 4\pi Q^2 N / M$ (Equ. (A4.4)), $Q = e$, $N = n_{el}$ and $M = m_c^*$ (effective mass of the conduction-band electrons). Then we obtain

(4.2) $\varepsilon_1(\omega) = \varepsilon_{oo} - 4\pi e^2 n_{el} / m_c^* \omega^2$

From this we get the zero (ω_p) of $\varepsilon_1(\omega)$:

(4.3) $\omega_p = (4\pi e^2 n_{el} / \varepsilon_{oo} m_c^*)^{1/2}$

ω_p is called ***plasma frequency***. In the case of semiconductors ω_p is typically located in the infrared range.

> The term plasma frequency originates from the fact that, strictly speaking, one is dealing with the the frequency of a characteristic vibration of the system of band electrons, which is similar to the characteristic vibration of a gas plasma. (This vibration cannot be excited directly by optical means.)

Fig. 4.5 shows experimental [11] reflection spectra $R(\lambda)$ (λ light wavelength) for n-type InSb, again with n_{el} as a parameter. The result is as expected: In particular, in the case of n_{el} values, for which the whole λ range could be investigated, we see practically complete reflection at large λ, and, at decreasing λ, the plasma reflection edge involving the drop of R to zero. With the parameter values for InSb (m_c^* near 0.03 m_0 (n_{el}-dependent), $\varepsilon_{oo} = 15.7$) and the n_{el} data given in the Figure, one obtains plasma frequencies corresponding to the edge wavelengths observed. The edge shift with n_{el} shows the trend expected after Equ. (4.3). (These results lead to an additional method for the optical determination of n_{el}.)

> Of course absorption spectra can only be observed, with sufficient accuracy, in the spectral range where the reflectivity is clearly below unity. (The spectra of InAs presented in Fig. 4.3 (m_c^* close to 0.03 m_0 (n_{el}-dependent), $\varepsilon_{oo} = 12.25$) are all situated on the high-energy side of the plasma edge.) By the way, high carrier concentrations giving rise to high reflectivity in a large part of the infrared region, sometimes complicate studies of phonon transitions, which are usually also located in this region (Section 8.2 and 8.3).

In the case of metals, where the n_{el} values are larger by many orders of magnitudes, one is concerned with much higher plasma frequencies; that is, among other things, the reason for the high reflectivity in the visible range.

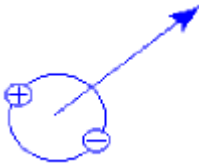

Chapter 5

Exciton Transitions

5.1 Exciton States

As already mentioned in the Overview Chapter, one can observe, at not too high temperatures, at photon energies slightly below the band gap E_g, lines in the absorption spectrum, which are due to the formation of "excitons". Analogous phenomena are found in the luminescence spectrum.

The appearance of exciton states cannot be understood on the basis of the one-electron approximation applied so far. For a given electron this approximation is related to the simple Hamilton operator

(1.4) $H = \mathbf{p}^2 / 2m_0 + U(\mathbf{r})$

It is important that here we are dealing with a definite potential $U(\mathbf{r})$, being independent of the states of the other electrons. Significant deviations from this condition occur in the case of an interband transition: Obviously, in the one-electron picture, such a transition leads to a change of the wavefunction (Bloch function) of one electron,

(5.1a) $\psi_{\mathbf{kv}}(\mathbf{r}) \rightarrow \psi_{\mathbf{kc}}(\mathbf{r})$

and thus changes the contribution of this electron to the charge density,

(5.1b) $e|\psi_{\mathbf{kv}}(\mathbf{r})|^2 \rightarrow e|\psi_{\mathbf{kc}}(\mathbf{r})|^2$

(see Section 2.1). The electrons remaining in the valence band "feel" that small change in the potential (change of the Coulomb energy and of more complex portions of interaction), resulting in a change of their wavefunctions. This, in turn, has an effect upon the wavefunction of the electron having performed the optical transition. This leads to the formation of electronic states unlike Bloch states, which has some influence on the optical spectra. Generally speaking, this influence is not strong, but there may be pronounced effects at photon energies near E_g (Section 2.1).

Fortunately, for semiconductors, these interaction processes, which are actually rather complex, can be treated theoretically in a rather simple way by using the hole concept: One only has to consider the *modification of the states of the electron in the conduction band and of the hole in the valence band - which carry a negative and positive charge, respectively - due to their mutual Coulomb interaction* . Hence, in such cases, we are dealing with a *two-body problem.*

To calculate these states the so-called ***effective mass approximation*** is used. To this end, masses - given by the effective masses of the corresponding band edges - are assigned to the two particles. (Later on we shall discuss the validity range of this approximation.)

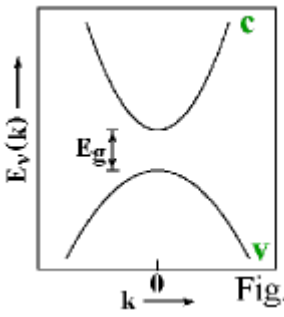

Fig. 5.1

In the following we refer to a material of cubic symmetry with band extrema at $\mathbf{k} = 0$, as represented in Fig. 5.1 (simplified compared with real band structures, see Fig. 1.4). In this case both effective masses are isotropic. The conduction band mass (definition in equation Equ.(1.11)), which we refer to as m_c^*, is positive. The valence band mass defined in an analogous way, m_v^*, is negative due to the sign of the second derivative (sign of the band curvature). Now we introduce effective masses of electron (m_e) and hole ((m_h):

(5.2) $m_e = m_c^* \qquad m_h = -m_v^*$

So both masses are positive. (The second relation in Equ. (5.2) corresponds to the general definition of the hole effective mass, which appears if the hole concept is introduced in a logical way [1].) Using the above assumptions on the band structure, the problem to be treated is reduced to the hydrogen problem of atomic physics: The proton is substituted by the hole, and the H-electron is replaced by our electron. The Schrödinger equation is

(5.3) $\{-(\hbar^2/2m_e)\Delta_e - (\hbar^2/2m_h)\Delta_h - e^2/[\,\varepsilon_{st}|\,(\mathbf{r}_e - \mathbf{r}_h)\,|\,]\}\Phi(\mathbf{r}_e,\mathbf{r}_h) = E\,\Phi(\mathbf{r}_e,\mathbf{r}_h)$

Here $\mathbf{r}_e$ and $\mathbf{r}_h$ are the position vectors of electron and hole, respectively. Δ_e and Δ_h are the Laplace operators acting on the respective coordinates, ε_{st} is the static dielectric constant, $\Phi(\mathbf{r}_e,\mathbf{r}_h)$ is a wavefunction for electron and hole. E is the energy of this two-particle system. Hence the terms in the curly brackets represent the kinetic energies and the Coulomb attraction of the particles, the latter being weakened by the electric polarization of the crystal (CGS system), which is approximated by the expression for a continuous medium.

The derivation of this so-called ***effective mass equation*** (5.3) is very time-consuming [12]. Roughly speaking, this derivation involves eliminating the potential $U(\mathbf{r})$, introducing effective masses instead of it, and transferring the real complex interactions into the simple Coulomb energy $-e^2/[\varepsilon_{st}|(\mathbf{r}_e - \mathbf{r}_h)|]$

> The functions $\Phi(\mathbf{r}_e, \mathbf{r}_h)$ as well as the functions ($\chi(\mathbf{R})$, $\phi(\mathbf{r})$) to be introduced later actually are not correct wavefunctions of the particles. They only rather roughly give the corresponding position dependences. This will be dealt with in more detail in Supplement 5. The effective mass approximation is frequently used in solid state physics, e. g. in the discussion of the electronic states of "shallow" impurities and the states of charge carriers in semiconductor quantum structures (Section 6.1).

Equ. (5.3) is solved in a manner analogous to treating the H-problem[13]. For better understanding the most important steps will be reproduced here. First we define coordinates (position vectors) for the center-of-mass and relative motion of the particles,

(5.4) $\mathbf{R} = [m_e\mathbf{r}_e + m_h\mathbf{r}_h] / [m_e + m_h] \qquad \mathbf{r} = \mathbf{r}_e - \mathbf{r}_h$

and introduce the total mass (M) and the reduced mass (μ) of the particles,

(5.5) $M = m_e + m_h, \qquad \mu^{-1} = m_e^{-1} + m_h^{-1}$

The transformation of Equ. (5.3) to the new coordinates **R** and **r** yields

(5.6) $\{-(\hbar^2/2M)\Delta_{\mathbf{R}} - (\hbar^2/2\mu)\Delta_{\mathbf{r}} - e^2/[\,\varepsilon_{st}|\mathbf{r}|\,]\}\,\Phi(\mathbf{R},\mathbf{r}) = E\,\Phi(\mathbf{R},\mathbf{r})$

The two first terms in the curly bracket describe the kinetic energy of the center-of-mass and relative motion, respectively. As to be expected, the potential energy (third term) only depends upon the relative coordinates.

Equ. (5.6) can be solved using the separation approach

(5.7) $\Phi(\mathbf{R},\mathbf{r}) = \chi(\mathbf{R})\,\phi(\mathbf{r})$.

For $\chi(\mathbf{R})$ we get

(5.8) $\chi(\mathbf{R}) = (V^{-1/2})\exp(i\mathbf{K}\mathbf{R})$

Here V is the volume of the crystal and **K** a propagation vector for the center-of-mass motion. The wavefunction component $\phi(\mathbf{r})$ of the relative motion is determined by the Schrödinger equation

(5.9) $\{-(\hbar^2/2\mu)\Delta_{\mathbf{r}} - e^2/[\,\varepsilon_{st}|\mathbf{r}|\,]\}\,\phi(\mathbf{r}) = \eta\,\phi(\mathbf{r})$.

The total energy E (Equ. (5.3) and (5.6)) consists of a contribution of the center-of-mass motion and a contribution (η) of the relative motion, the latter appearing in Equ. (5.9):

(5.10) $E = (\hbar^2/2M)\mathbf{K}^2 + \eta$.

The center-of-mass motion is a (quasi) free motion; this manifests itself in the form of the wavefunction component, Equ. (5.8), and the energy contribution $(\hbar^2/2M)\mathbf{K}^2$ in Equ. (5.10). Apart from the parameter values, Equ. (5.9) corresponds to the Schrödinger equation which is the usual starting point for the discussion of the H-atom; there one mainly restricts oneself to studying the relative motion of the particles. However, as we shall see shortly, the center-of-mass motion is highly important in the analysis of exciton transitions.

For discussing exciton spectra no further calculations are necessary. One has simply to make the following two

substitutions in the final expressions for the H-atom [13]:

(5.11) (reduced) mass of the electron in vacuum $\rightarrow \mu$, elementary charge $\rightarrow e / (\varepsilon_{st})^{1/2}$

In the case of positive η we are concerned with electron-hole-pair states, i. e. with non-bound states of electron and hole. Such states are also obtained on the basis of the one-electron-approximation; remember that the concept electron-hole-pair has been introduced earlier.

The bound states of electron and hole in semiconductors (exciton states in the original sense) are of special interest. These correspond to negative η values. In this case the wavefunctions for the relative motion $\phi(\mathbf{r})$ are characterized by quantum numbers n, l, and m as for an atom; thus one writes $\phi_{nlm}(\mathbf{r})$. (The spin quantum number is ignored here.) The lowest-energy state ("1s state") is the state with n = 1 and l = m = 0. In this case ϕ only depends on $|\mathbf{r}|$.We get

(5.12) $\phi_{100}(\mathbf{r}) \sim \exp(-|\mathbf{r}| / a_{exz})$

a_{exz} is the so-called ***exciton radius***, i. e. the average distance of electron and hole in the exciton. The substitution according to Equ. (5.11) yields

(5.13) $a_{exz} = (m_0 / \mu)\, \varepsilon_{st} a_H$

a_H is the Bohr radius. The energies η of the exciton states only depend on n. We have

(5.14) $\eta_n = -(1/n^2)E_D, \quad E_D = (\mu / m_0)\varepsilon_{st}^{-2} E_H.$

Here E_H is the ionization energy of the H-atom; Equ. (5.14) is obtained with the substitution (5.11). E_D is the ***dissociation energy*** of the exciton, i. e. the energy that has to be spent in order to split an exciton in the lowest bound state (n = 1) into an electron-hole pair of minimum energy (η = 0), if there is no center-of-mass motion in the two states (difference of the corresponding E values in Equ. (5.10) for the case $\mathbf{K}$ = 0).

As an example we put $m_e = 0.067\, m_0$, $m_h = 0.5 m_0$, $\varepsilon_{st} = 11$ (these values approximately correspond to GaAs) and, besides, $a_H = 5.29 * 10^{-9}$cm, $E_H = 13.55$ eV. We get

$a_{exz} = 9.8 * 10^{-7}$cm and $E_D = 6.6$ meV.

Obviously, E_D is a very small energy (in particular, much smaller than typical E_g values). This means that *the binding of electron and hole in the exciton is weak* . As a consequence, exciton effects can only be observed at lower temperatures; when heating the crystal the excitons are soon dissociated by collisions with phonons. For instance, for the above E_D value we do not expect exciton effects at room temperature. (Then E_D is much smaller than the thermal energy, $k_B T = 25$ meV.)

The weak binding of electron and hole also manifests itself in the fact that *a_{exz} is large against the size of the unit cells* ,which we outline in Fig.5.2. On the other hand, this result confirms that in the present case the description in terms of the effective-mass Equ. (5.3) is justified: For a given material such a treatment (possibly in some more complicated form) is correct, if a_{exz} (first calculated formally) has this property.

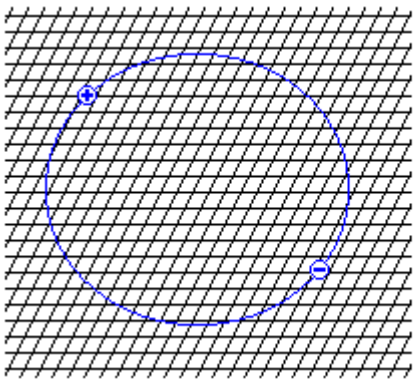

Fig. 5.2

In some sense, we are still dealing here with particles near the band edges, having the corresponding effective masses, their motion being only weakly disturbed by their mutual interaction. Because of the large separation of electron and hole, the

Coulomb field weakly varies between neighbouring unit cells. Consequently, on this scale the field is nearly homogeneous so that the potential in Equ. (5.3) may be approximated by a continuum expression.

In (nonmetallic) materials, for which the effective-mass equation is not applicable (e. g. ionic crystals, organic substances, and solid rare gases), there are, in general, also exciton states, their spatial extension being comparable with the size of the unit cells. In this case one is dealing with localized excited states, which are able to migrate through the crystal (analogously to the center-of-mass motion discussed earlier). These phenomena are referred to as ***charge-transfer excitons*** or ***Frenkel excitons***, depending on whether the wavefunctions are localized on small groups of atoms and on single atoms, respectively. In contrast, the extended excitons typically observed in semiconductors are called ***Wannier-Mott excitons.***

5.2 Optical Transitions

Let us first discuss which is the correct energy-momentum diagram for analysing optical transitions. Obviously the simple band-structure diagrams as Fig. 1.4 and Fig. 5.1, respectively, cannot be used, since the exciton states are related to more than one band (i. e. to conduction *and* valence bands).

We have to consider here the energy and momentum of the *electron system of the crystal*, specifically

- the ground state (all valence bands and deeper bands fully occupied with electrons, all conduction bands empty) and
- excited states with *one exciton* or *one electron-hole pair*.

We have collected the properties of those states ((quasi-)momentum $\hbar \underline{\boldsymbol{K}}$ and energy $\underline{E}$) in the following Table (valid for small $|\underline{\boldsymbol{K}}|$ and materials, whose band stucture can be approximated according to Fig. 5.1).

	ground state	excited states
momentum	$\hbar\underline{\boldsymbol{K}} = 0$	$\hbar\underline{\boldsymbol{K}} = \hbar\,\mathbf{K}$ nonzero
energy	$\underline{E} = 0$	$\underline{E} = E_g + (\hbar\mathbf{K})^2/(2M) + \eta$

In the ground state the momentum of the electron system vanishes, since the momenta of the individual electrons compensate each other (there are only fully occupied and empty bands). We have *put* the energy of the ground state equal to zero. The momentum of the system in the excited state must be given by the momentum of the exciton or electron-hole pair, i. e. by $\hbar\mathbf{K}$. To generate such an excited state, energy has to be added, namely (as in the simple picture considered earlier) E_g, if an electron-hole pair of minimum energy ($(\hbar^2/2M)\,\mathbf{K}^2 = \eta = 0$) is to be created. If the two particles get, in addition, a resultant center-of-mass energy and / or energy of relative motion, E_g has to be increased by the value $(\hbar^2/2M)\,\mathbf{K}^2+\eta$ (Equ. (5.10)).

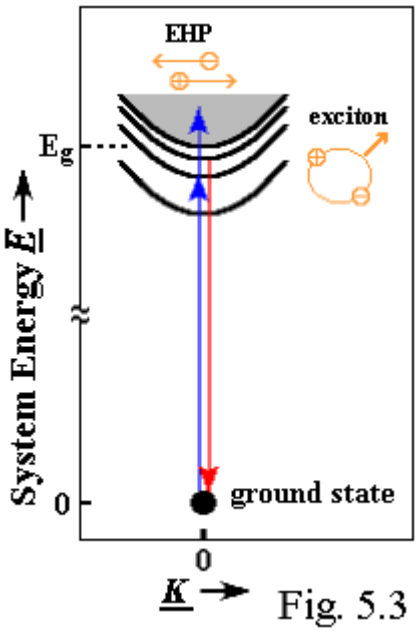

Fig. 5.3

For discussing optical transitions we shall use an $\underline{E}$ ($\underline{\boldsymbol{K}}$) diagram (see Fig. 5.3) (for a gradual construction of Fig.5.3 see the electronic version of the course). We plot these dependences along a straight line in $\underline{\boldsymbol{K}}$ space which passes through $\underline{\boldsymbol{K}} = 0$ and mark the energies 0 und E_g on the $\underline{E}$ axis.

The ground state is represented by a point at $\underline{\boldsymbol{K}} = 0$, $\underline{\boldsymbol{E}} = 0$, according to the Table.

We now consider the excited states.

Obviously, the discrete levels ($\eta < 0$, Equ. (5.14)) give rise to parabolas. The energies of the minima (situated at $\underline{\boldsymbol{K}} = 0$) are given by $\underline{\boldsymbol{E}} = E_g + \eta$ according to theTable. For non-negative η we get the (grey shaded) continuum, whose lower limit is the parabola $\underline{\boldsymbol{E}} = E_g + \hbar^2/2M)\ \mathbf{K}^2$ (corresponding to $\eta = 0$). The character of the states is indicated in the diagram (EHP = electron-hole pair). The $\underline{\boldsymbol{E}}$ axis is broken, because the picture is not to scale.

We are interested in optical transitions between the ground state and states with one exciton or one electron-hole pair. In upward transitions the exciton or electron-hole pair is created "out of nothing", in downward transitions the exciton or electron-hole pair is annihilated ("the electron jumps into the hole"). These processes are accompanied by the absorption and emission of a photon, respectively.

There is a fundamental selection rule for the $\underline{\boldsymbol{K}}$ vectors, which is based on the translation symmetry of the crystal, as the **k** selection rule in the simple way of consideration . According to this rule, only excitons and electron-hole pairs, whose momentum $\hbar\mathbf{K}$ agrees with the momenum of the photon $\hbar\mathbf{s}$, can be created or annihilated (law of momentum conservation) :

(5.15) $\underline{\boldsymbol{K}}\ (= \mathbf{K}) = \mathbf{s}$

In the present case, the momentum law can be simplified as earlier, taking into account that in the spectral ranges under discussion, $|\mathbf{s}|$ is small compared with the size of the Brillouin zone. Thus instead of Equ. (5.15) we can usually write

(5.16) $\underline{\boldsymbol{K}}\ (= \mathbf{K}) = 0$

It is easily realized that, in the cases of the creation and annihilation of electron-hole pairs, Equ. (5.16) is equivalent to the old **k** selection rule (see Supplement 6). Of course, in addition to the law of momentum conservation, we have the energy balance:

(5.17) $E_g + \eta = \hbar\omega,$

i. e. the energy of the excited states (Table, specialized to the case $\underline{\boldsymbol{K}} = 0$) must be equal to the energy of the photons involved. Hence, in the $\underline{\boldsymbol{E}}(\underline{\boldsymbol{K}})$ diagram, the optical transitions are to be represented by vertical arrows of length $\hbar\omega$, which begin or end at the ground state point (Fig.5.3).

η assumes discrete values in the negative range (see Equ. (5.14)), and this transfers to the corresponding $\hbar\omega$ values. Hence, as is also visible in Fig. 5. 3, line spectra are found here. The line structure occurs, although the overall energy spectrum is continuous; it is a consequence of the $\underline{\boldsymbol{K}}$ selection rule (Equ. (5.15) and (5.16)).

5.3 Absorption Spectra

Now we discuss what should be the form of the absorption spectra due to upward transitions; later on we shall compare the results with experiment.

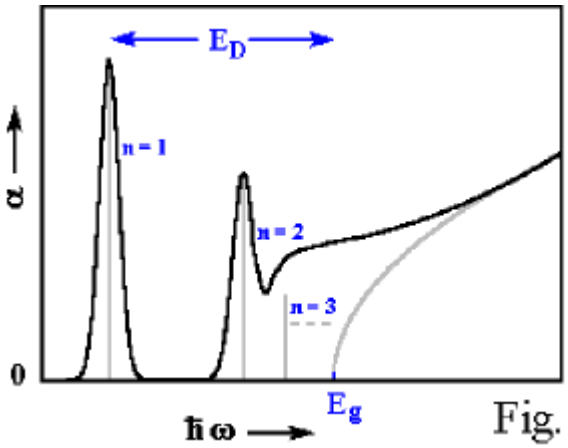

Fig. 5.4

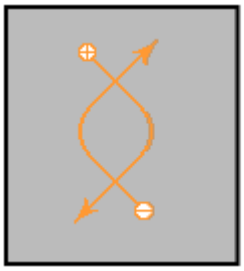

Fig. 5.5

The expected behaviour is shown in Fig. 5.4. Here we plot the absorption coefficient α against the photon energy $\hbar\omega$ (for a gradual construction of Fig.5.4 see the electronic version of the course). From the previous consideration (Section 5.2)

we expect that the transitions to exciton states give rise to infinitely sharp lines at positions corresponding to the various n - values. This is indicated in Fig. 5.4 by grey lines (—) taking into account the theoretical result that the line intensities decrease with increasing n. In experiment we are dealing with finite linewidths (black spectrum), due to the fact that an exciton generated in a state with $\boldsymbol{K} = 0$ after some time goes into other states (in particular states with nonzero $\boldsymbol{K}$, Fig. 5.3). This originates from the interaction with phonons or impurities (lifetime broadening).

Since on approaching E_g, the separation of the lines decreases, only the lines with the smallest n can be resolved, while those with higher n melt into a quasi-continuum. At $\hbar\omega = E_g$ this quasi-continuum passes *continuously* to the "real" continuum based on the formation of elctron-hole pairs. At somewhat higher $\hbar\omega$ values, the spectrum deviates from the (—) curve expected from the primitive considerations. In Fig. 5.4 we have assumed that only two exciton lines are resolvable.

At $\hbar\omega$ values a little above E_g the absorption curve lies higher than expected in the simple consideration. This is due to the Coulomb attraction between electron and hole (Equ. (5.3)) being now taken into account. It has the consequence that - also in the absence of binding - there is a mutual influence between the motions of the two particles. Fig.5.5 visualizes the effect of this interaction.

However, these effects only appear at small particle-energies, as are present a little above E_g. At high energies the particles practically " ignore each other", moving "along straight lines". In the quantum-mechanical picture, this means that a description on the basis of the one-electron approximation, i. e. in terms of Bloch states, is again adequate. As a consequence, at larger distances from E_g the spectra join the naive curve (—), and the previous discussion (Chapter2) is, in general, justified. By the way, there are analogous effects in the absorption spectrum of the H - atom close to the ionization energy, due to the Coulomb interaction between electron and proton [13].

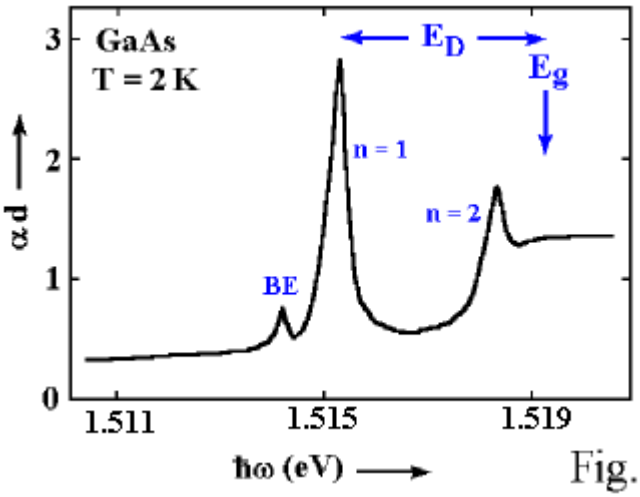

Fig. 5.6

Let us now compare these results with experiment. Fig.5.6 shows an absorption spectrum of GaAs measured [14] at a very low temperature (2 K) . Here the quantity αd (d sample thickness, about 2 μm) is plotted against the photon energy (near-infrared region). As indicated by the labels, the two most intense lines originate from the creation of excitons with n = 1 and n = 2. At high $\hbar\omega$, these lines are followed by the continuum. The additional line characterized by "BE" is due to the formation of a so-called ***bound exciton***, i. e. an exciton bound to an impurity. We shall not give here a discussion of this phenomenon. Apart from the BE line, the spectrum corresponds to our construction in Fig. 5.4 (which we have deliberately performed for a situation similar to the GaAs case). The position of E_g (= 1.5192 eV at the temperature of the measurements) and the E_D value are indicated.

> The experimental E_D value of about 4.2 meV somewhat deviates from the value obtained earlier using GaAs parameters (Section 5.1), because the simplified valence band structure taken as a basis in Equ. (5.3) and Fig. 5.1 does not correspond to the real situation in GaAs (Fig. 1.4) .

In Fig.5.7 we represent the temperature dependence of the absorption spectrum of GaAs at higher temperatures [15}. Let us first look at the 21 K spectrum. Here (and also in the 90 K and 186 K spectra) we only see the n = 1 line and a subsequent continuum. The n = 2 line is no longer visible, due to strong broadening. This effect in part originates from the temperature increase compared with Fig. 5.6 (shorter lifetime due to more frequent collisions with phonons), in part probably from a higher defect-concentration in the corresponding sample (lower crystal-perfection, measurements of earlier origin). When going to still higher temperatures, two main effects are observed:

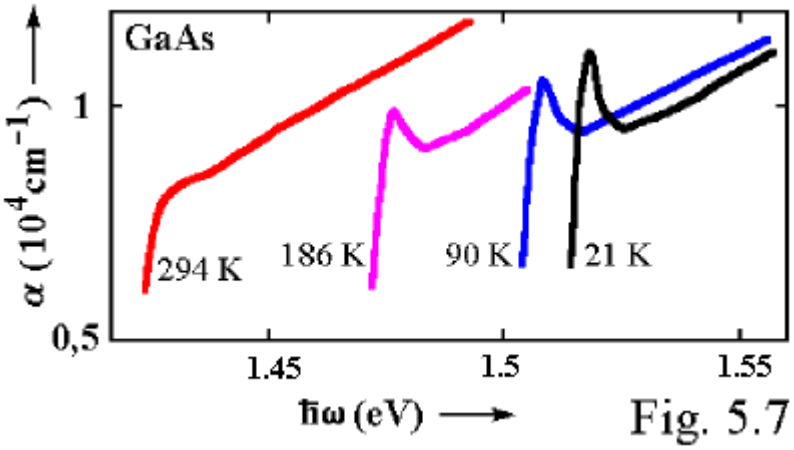

Fig. 5.7

- A shift of the spectrum to lower photon energies . This is related to the decrease of E_g occurring with growing temperature. We shall not discuss this effect, which also originates from the interaction of the electron system with phonons, in detail.
- The n =1 line undergoes additional broadening, due to more frequent collisions with phonons, and, finally, at 294 K, is no longer observable. In the last case, the spectrum is qualitatively similar to the spectrum expected in the absence of exciton effects (Fig. 2.4). This situation can be roughly characterized by saying that the states of electron and hole are less affected by their mutual interaction than by the collisions with phonons.

Hence the disappearance of exciton effects on heating is generally to be expected, and is indeed observed for all materials. In the GaAs case this already occurs at relatively low temperatures. This originates fom the fact that here the dissociation energy E_D is rather small (weak coupling between electron and hole). In Section 5.5 we shall compare the E_D values for various substances.

5.4 Other Optical Spectra

For materials with direct band structure, upward transitions in the exciton region (transitions in which excitons are created) can also be detected in **reflection spectra** . Fig. 5.8 shows, as an example, a reflection spectrum of CdTe [16] in the range of the n = 1 and n = 2 transitions. The n = 1 structure qualitatively agrees with the dependence expected on the basis of the oscillator model (Appendix 4). This is also true, within experimental accuracy, for the very weak n = 2 structure. The n = 1 structure can be described by special parameter combinations (relatively large ε_{oo} values and relatively small A values). The maximum value of R for n = 1 approximately corresponds to the value expected at the resonant photon energy (Appendix 4) at which that sort of excitons is generated.

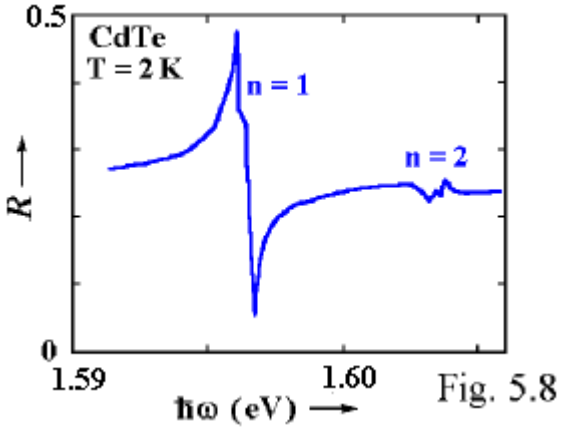

Fig. 5.8

Downward transitions in the exciton region can be studied by measurements of **photoluminescence spectra**. We now represent the relevant processes in the $\underline{E}$ ($\underline{K}$) diagram introduced earlier (see Fig. 5.9). Of course, the excitation of photoluminescence by laser radiation of sufficiently high photon energy ($\hbar\omega_L > E_g$) is subject to the $\underline{K}$ selection rule Equ. (5.16). We indicate this process in Fig. 5.9 (left-hand part) by ⇧. From the electron-hole pair state now occupied ***relaxation*** with phonon emission (⇩) into lower- energy states takes place rapidly. Then radiative transitions can start from the $\underline{K} = 0$ states (Fig. 5.9, right-hand part).

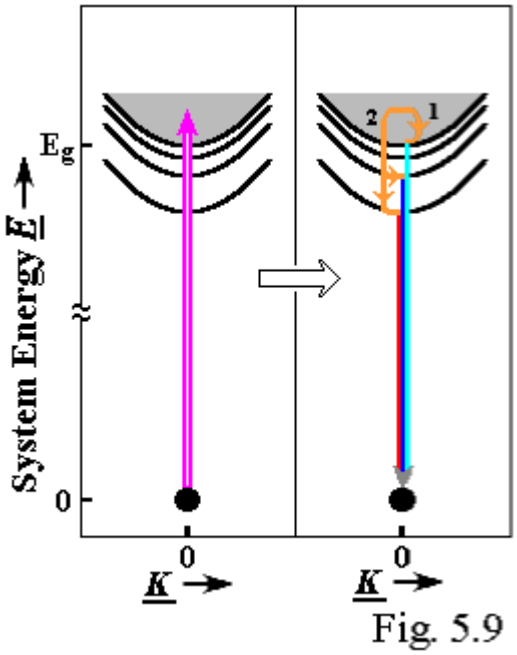

Fig. 5.9

There are two possibilities:

1. Relaxation to the lower edge of the electron-hole pair continuum, which is the starting point for the radiative recombination of electrons and holes (↓). This type of relaxation and recombination processes has been already described on the basis of the simple $E_v(\mathbf{k})$ diagram in Section 2.2.
2. Relaxation to one of the exciton parabolas with subsequent radiative transition from the minimum of this parabola ($\underline{\boldsymbol{K}} = 0$) (↓↓).

The radiative transitions of type 2 are called ***annihilation transitions***, since we are concerned with the destruction (annihilation) of an exciton in each case.

> From a linguistic point of view, it is incorrect to refer to the "recombination" of excitons, because one is dealing here with the destrucion of *one* particle.

On the basis of Fig. 5.9 we expect that all types of transitions manifest themselves as *lines* in the luminescence spectrum. The lines due to exciton annihilation (type 2) should nearly coincide with the absorption lines originating from the corresponding reverse transitions (Fig. 5.3). The line due to the recombination of electrons and holes (type 1) should lie directly above E_g.

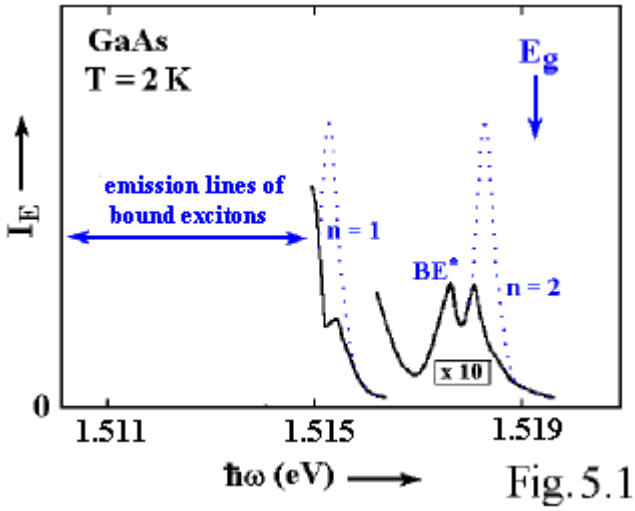

Fig. 5.10

It is important to note that the line intensities are determined both by transition probabilities and and the occupation of the initial states (Fig. 5.9). Because the relaxation processes are very fast, mainly the lowest-energy states become occupied before radiative transitions can occur. Hence, transitions at small photon energies - in particular in the case of low temperatures - are favoured even more clearly than in the absorption spectrum (Fig. 5.4) .

In Fig.5.10 we show a corresponding part of the photoluminescence spectrum of GaAs [17]. For comparison we also reproduce here the absorption spectrum presented in the preceding Section (Fig. 5.6). In Fig. 5.10 the emitted light intensity I_E is plotted as a function of photon energy $\hbar\omega$ (see Appendix 1). The assignment to the n = 1 and n = 2 states

is indicated.

An essential complication lies in the fact that the luminescence light is partly absorbed before leaving the crystal. This "reabsorption" is especially strong in spectral regions in which the absorption coefficient α is large. Consequently, dips appear in the spectrum at energies where originally emission peaks are expected. The variation of the intensity to be expected without this reabsorption effect is represented as a dotted curve (⋆ ⋆ ⋆ ⋆ ⋆) in Fig. 5.10.

The preference of the low-energy initial states is clearly visible (compare n = 1 with n = 2, taking into account the different ordinate-scales). The electron-hole recombination is completely absent at the temperature of the measurements. The line labelled BE* is attributed to the annihilation of a bound exciton in a higher excited state. As already mentioned, many (intense) lines which are also due to bound excitons, are found at energies below the spectrum shown in Fig. 5. 10 .

By the way, it should be noted that, compared with other materials, relatively few transitions of "free" excitons can be observed in the emission spectrum of GaAs; this is related to the low E_D value (see Section 5.5).

5.5 Comparison of Exciton Effects for Various Semiconductor Materials

As stated at the end of Section 5.3 , the strength of exciton effects in a given substance is determined by the magnitude of their exciton dissociation energy. In the following Table we have compiled the (experimental) E_D values for important semiconductor materials.

	Ge	Si	InSb	GaAs	GaP	CdS	CdSe	CdTe	ZnO	ZnS	ZnSe	ZnTe	Cu_2O
E_D (meV)	2.7	14.3	0.5	4.2	19.5	30.5	15.5	10.5	59	39.5	19.9	13.2	98
	indirect	indirect			indirect								

Clearly in most cases the values are much larger than for GaAs. An extremely small value is found for InSb, where exciton effects usually can be completely neglected. For materials with direct band-structure, large E_D values generally lead to the appearance of several (more than two) exciton lines (also observable at higher temperatures). Spectra with many lines are particularly found for some Cu compounds (here represented by Cu_2O). For indirect materials there is no line stucture in the absorption spectrum, because in this case excitons can only be created with the assistance of phonons (having a continuous energy spectrum).

> As already mentioned, there are considerable deviations from the values obtained (Equ. (5.14)) for the case of an idealized band structure (Fig. 5.1). However, the trends expected from that equation (dependence on ε_{st} and on the effective masses) are represented fairly well. This is also true for materials crystallizing in the non-cubic wurtzite structure (CdS, CdSe, ZnO, partly ZnS). In the cases where, due the more complicated band structure, several exciton series are observed, the values presented here are to be regarded as corresponding averages.

Chapter 6

Electronic Transitions in Semiconductor Quantum Structures

So far we have been dealing with the optical behaviour of homogeneous solids having macroscopic dimensions. If the dimensions are reduced to the µm or nm range, one may get systems with quite different properties, which have become important for applications, particularly in optoelectronics [18, 19]. We shall discuss this kind of phenomena in the present Chapter.

To illustrate the physically important effects, we first consider the simplest type of such structures, the so-called ***single quantum well***. These are layer structures of the kind represented in Fig. 6.1. As a specific example, we discuss the combination A = GaAs, B = $Al_xGa_{1-x}As$ (x mixing ratio, compare Section 2.7), which, so far, plays a most important role in applications. The small thickness d of the A layer is essential. We concentrate on the case that d is some 10 nm (some 10^{-6} cm), and the dimensions parallel to the interfaces are in the macroscopic range.

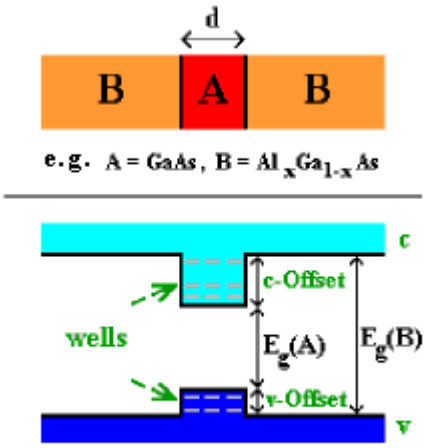

Fig. 6.1

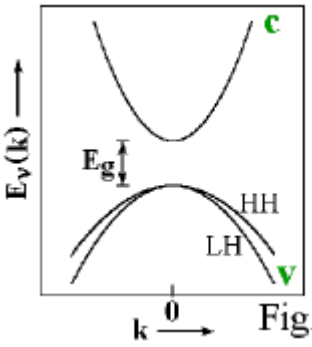

Fig. 6.2

The standard method used for producing such structures is ***molecular beam epitaxy*** (MBE), see Supplement 7.

6.1 Electronic States and Energy Spectrum

6.1.1 General

First we again refer to the specific case of the GaAs-AlGaAs system (Fig. 6.1). The essential effects result from the different positions of the lower conduction-band edges and the upper valence-band edges in the three regions. AlGaAs has the largest band gap (E_g), the conduction-band edge being shifted upward, the valence-band edge downward with respect to GaAs. Thus wells parallel to the interfaces are formed, both for electrons and for holes. In Fig. 6.1 we represent the behaviour of the bands along a straight line perpendicular to the interfaces. The magnitudes of the jumps in the band edges are referred to as ***band offsets***. Of course, these depend upon the combination of materials employed (on the x-value in the present case). If we combine different kinds of materials, we may also find cases where, in the central region, there is a well only for one type of particles, while there is a barrier for the other type.

The electronic energy spectrum is determined by the fact that perpendicular to the interfaces - at not too high energies - the particle states are forced to localize in the A region as in a potential box, while parallel to the interfaces a quasi free motion occurs. Since potential boxes have discrete energy - levels, we expect that this effect manifests itself in a corresponding structure of the energy spectrum, as indicated by – – – in Fig. 6.1.

In the following we shall discuss this question in more detail, starting from a band structure of the kind shown in Fig. 6.2. This band structure corresponds to the lowest edge of the conduction band and the upmost edge of the two highest valence bands of GaAs (Fig. 1.4). Qualitatively this picture also describes the situation for $Al_xGa_{1-x}As$ at not too high x. The labels HH and LH stand for the names "heavy-hole band" and "light-hole band" , respectively, already used earlier .

> Strictly speaking, an energy band structure characterized by a **k** dependence cannot be defined in the case of a mixed compound as $Al_xGa_{1-x}As$, because we are concerned here with a random distribution of Al and Ga atoms over the metal sites, so that there is no translation symmetry. However, it has been shown that for small portions of one sort of atoms (e. g. for small x values), the energy spectrum can be approximated by interpolated band structure functions $E_V(\mathbf{k})$ (" interpolation" between the the contributions of the two sorts of atoms).

As in the case of a homogeneous macroscopic crystal, the quantitative discussion is based on a Hamilton operator in the one-electron approximation:

(1.4) $H = \mathbf{p}^2 / 2m_0 + U(\mathbf{r})$

Of course, the potential $U(\mathbf{r})$ is different in the type A and type B regions (and, as a whole, does not have translation symmetry). In many cases, it can be assumed that within these regions U agrees with the potential in the corresponding homogeneous materials (apart from the effect of mechanical deformations which are due to the different sizes of the unit cells of A and B) and that abrupt transitions occur at the interfaces. Under these conditions the problem can frequently be treated - for not too small d (d much larger than the size of the unit cells) - using procedures similar to the effective mass approximation .

Now we shall discuss in more detail the conduction band states, because in this case we have a comparatively clear situation due to the simple band structure (Fig. 6.2).

6.1.2 Conduction Band States

In this case we start from the following effective mass equation for the envelope function $\Phi(\mathbf{r})$:

(6.1) $\{- (\hbar^2/2m_c^*(z)) \Delta + U_c(z)\}\Phi(\mathbf{r}) = E\, \Phi(\mathbf{r})$

$U_c(z)$ is a box-type potential which represents the difference between the lowest conduction band edges of the materials A and B, with the box walls corresponding to the offset U_0 (Fig. 6.3). Here the coordinate system has been chosen in such a way that the z axis is perpendicular to the interfaces. U_c is normalized to zero in region A. $m_c^*(z)$ is the effective mass at the band edge, which is, in general, different for A and B, i. e. z-dependent (Fig. 6.3). In the following we ignore the z-dependence (which is normally weak), using, instead, an average value. Δ and E are the Laplace operator and the energy, respectively, as usual.

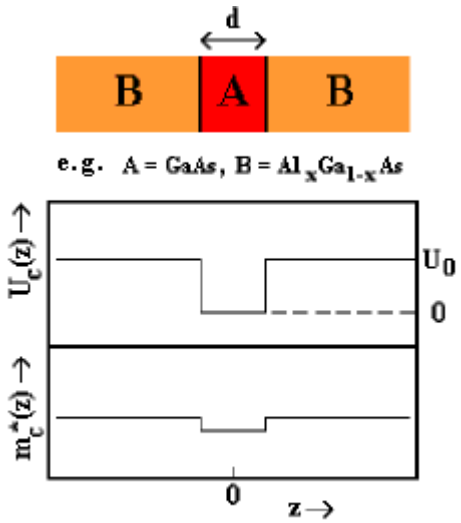

Fig. 6.3

We start with the expression

(6.2) $\Phi(\mathbf{r}) = \exp(i\mathbf{k}_t\mathbf{r})\, \chi(z)$

where we have introduced a propagation vector $\mathbf{k}_t = \{k_x, k_y, 0\}$, which is perpendicular to the z axis. For the definition of $\chi(z)$ we obtain

(6.3) $- (\hbar^2/2m_c^*)\chi\,''(z) + U_c(z)\chi(z) = \varepsilon\, \chi(z).$

where

(6.4) $E = (\hbar^2/2m_c^*)\, \mathbf{k}_t^2 + \varepsilon$

The factor $\exp(i\mathbf{k}_t\mathbf{r})$ in Equ. (6.2) and the term $(\hbar^2/2m_c^*)\, \mathbf{k}_t^2$ in Equ. (6.4) express the quasi-free motion perpendicular to the z axis. Equ. (6.3) describes the effect of the box-type potential acting in the z direction, and determines the factor $\chi(z)$

in the wavefunction in (6.2) as well as the contribution ε to the total energy in (6.4).

For $\varepsilon < U_0$ the box Equ. (6.3) yields discrete levels which we shall refer to as ε_N, enumerating them with the index N. The corresponding wavefunctions $\chi_N(z)$ are localized (Fig. 6.4). For $\varepsilon \geq U_0$ we obtain a continuous ε spectrum and delocalized χ functions.

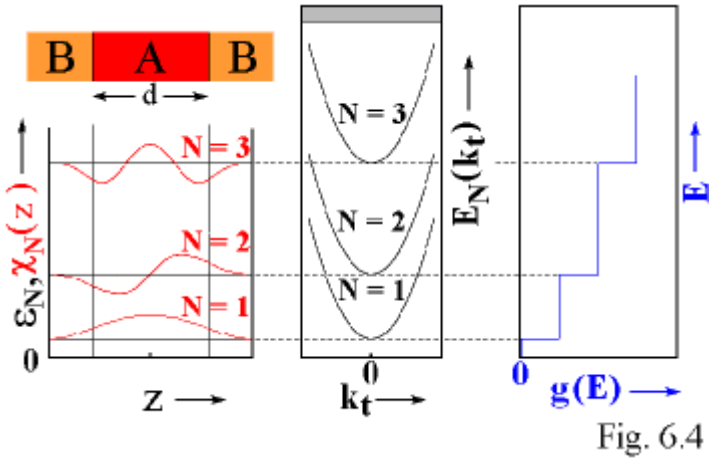

Fig. 6.4

In the discrete ε range the total energy E depends on $\mathbf{k}_t$ as well as on N. We write

(6.5) $E_N(\mathbf{k}_t) = (\hbar^2/2m_c^*)\,\mathbf{k}_t^2 + \varepsilon_N \qquad N = 1,2,....$

Hence, in that range the spectrum consists of overlapping bands which are numbered by N. The states within the bands are characterized by the propagation vector $\mathbf{k}_t$. We illustrate this in Fig. 6.4. According to Equ. (6.4) the energy spectrum is determined, as a whole, by ε, which depends on the parameters U_0 and d.

In Fig. 6.4 we also give the density of states with respect to energy, g (E), (compare Section 1.4). In the subband region g(E) shows a step-like behaviour. Approximately, each subband makes a constant contribution to g (E) ("two-dimensional density of states").

The results of ε calculations [20] are compiled in Fig. 6.5. In this Figure the quantity ε / E_0 is plotted against the quantity U_0 / E_0 (the latter on a logarithmic scale). Here one uses the nomalization energy

(6.6) $E_0 = (\hbar^2/2m_c^*)\,(\pi / d)^2$

The lower subband edges ε_N are indicated by —; the boundary to the continuous region $\varepsilon = U_0$ is marked by —. To get the spectrum for a given U_0 (and a given E_0), one has to move, at the corresponding abscissa value, upward starting from the ordinate value 0 (e. g. ↑). Hereby one obtains a series of subbands, before passing the boundary to the continuous region ε. The number of subbands (number of discrete box-levels ε_N) decreases with decreasing U_0 (starting point shifted to the left).

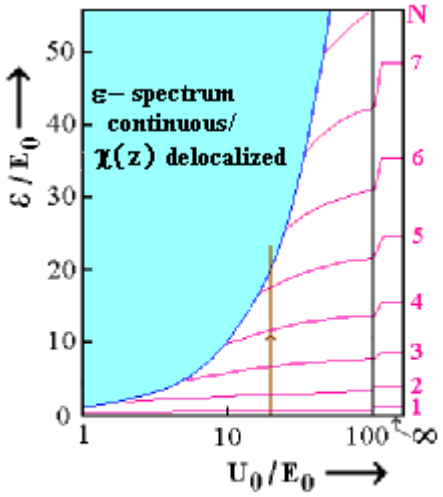

Fig. 6.5

(6.6) $E_0 = (\hbar^2/2\,m_c)(\pi/d)^2$

Let us now consider the dependence on the well diameter d at a given U_0. This dependence is contained in in the expression for E_0 (Equ. (6.6)). With decreasing d, one moves to the left on the abscissa axis, so that the number of ε_N decreases. Simultaneously, the growth of E_0 leads to an increase of the ε_N (due to ε = (ordinate ε/E_0) * E_0).

All these results correspond to expectation , remembering the behaviour of the quantum-mechanical states in a potental box [13].

A particularly simple situation - in mathematical respect - is found in the case of infinite offset (box with infinitely high walls), which is shown on the right-hand side of the Figure. The corresponding formulae (Supplement 8) are often used for making estimates.

For U_0 tending to zero, we return to the case of a homogeneous material. A corresponding extrapolation in Fig. 6.5 yields a single conduction band without substructure, its minimum energy being ε = 0, as expected. Then, the total energy E (Equ. (6.5)) also has a minimum value of 0. On the other hand, for U_0 values different from zero, the minimum of the spectrum (minimum of the N = 1 subband) lies at positive energy values. This phenomenon is referred to as ***confinement effect***. Obviously this effect grows with increasing U_0 and decreasing d, as also expected from the properties of the potential box.

> This effect may be attributed to the uncertainty relation of quantum mechanics $\Delta p\,\Delta z \geq \hbar$. The localization to a range of about d occurring compared with the homogeneous case (infinite Δz) , leads to an uncertainty of the quasi-momentum in z direction, Δp. That means, in particular, that the quasi-momentum no longer can assume a zero value, i. e. that the minimum energy possible increases.

For instance, for A = GaAs, B = $Al_{0.3}Ga_{0.7}As$, $m^*_c = m^*_c(GaAs) = 0.067\ m_0$, U_0 = 245 meV, d = 10 nm one obtains a confinement of about 25 meV.

Among other things, the confinement effect results in an increase of the minimum photon energy for interband transitions in the well region, compared with the homogeneous case. This has important consequences for optoelectronic applications (Section 6.4).

6.1.3 Valence Band States

For these states the situation is much more complicated, because we have to deal with two bands which are in contact in the homogeneous case (Fig. 6.2). In the case of the layer systems the contact is removed and the corresponding wavefunctions become "mixed". This is mainly due to the lowering of symmetry compared with the homogeneous case. Among other reasons, contributions to this effect are generally made by the mentioned mechanical deformations which have low-symmetry (uniaxial) components. The effects on the valence band spectrum depend, in a detailed manner, upon the properties of the combined materials, and cannot be described, as before, by two parameters (offset and effective mass).

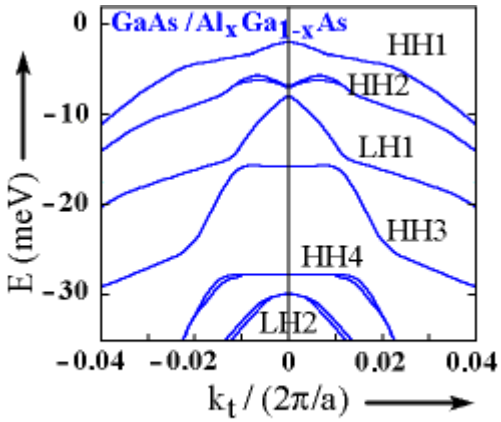

Fig. 6.6

In Fig. 6.6 we show a calculation [21] of the valence band spectrum for the case A = GaAs, B = $Al_{0.25}Ga_{0.75}As$, with d = 20 nm. The energies are represented, as before, as a function of a propagation vector $\mathbf{k}_t$ parallel to the interfaces in the vicinity of $\mathbf{k}_t = 0$ (normalized to 2π / a, a = average lattice constant of the homogeneous materials, $\mathbf{k}_t \| [110]$).

The subbands exhibit a rather complicated $\mathbf{k}_t$ dependence. In spite of the mixing effects mentioned, they can be still assigned to the original band components HH and LH (Fig. 6.2) and are correspondingly labelled. The energy of the upper valence-band edge for homogeneous A type material is nomalized to 0. The confinement effects for holes (downward shift) is larger in the LH case than in the HH case. This trend can be attributed to the different effective masses, being consistent with the mass dependence of the energy levels of the potential box [13].

Strictly speaking, the results given in Fig. 6.6 do not refer to simple quantum wells, but to so-called superlattices, i. e. a combination of many (about 70 in the present case) A nnd B type layers which are arranged periodically in the z direction (Section 6.1.4).

6.1.4 Superlattice States

Using epitaxy techniques, one is able to produce layer systems which consist of stacks along the z axis including a large number of alternating A type and B type layers. If all A layers - among themselves - and all B layers - among themselves - have the same thickness, d_A and d_B, respectively (Fig. 6.7), a periodic structure is obtained which constitutes a three-dimensional *lattice*, in the sense of our earlier definition . Such a structure (typically including 50 to 100 A and B type layers) is referred to as a ***superlattice***. If d_A and d_B are chosen to be some 10^{-6} cm (10 nm), the diameter of the unit cells of the superlattice in z direction is of the same order (length of the corresponding primitive lattice-vector $a_{SG} = d_A + d_B$), the dimensions in the perpendicular directions being of the order 10^{-8} cm, as before .

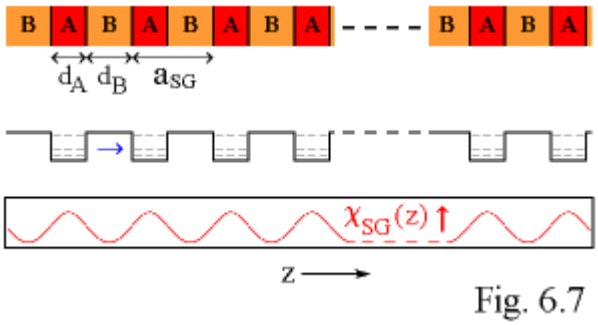

Fig. 6.7

This periodic structure gives rise to a periodic potential which can be represented by a combination of potential boxes as shown in Fig. 6.7. Now the electrons are able to tunnel from well to well (⟶). If the barrier thicknesses d_B are small enough, states delocalized in the z direction (χ_{SG}) also arise in the case $\varepsilon < U_0$ instead of the localized states (χ_N shown in Fig. 6.4). Thereby the discrete box-levels ε_N change into bands which, however, have very small widths, of typically ≤ some meV for the lowest bands. The main effect on the energy spectrum as a whole (E, see Equ. (6.4)) involves some broadening of the lower subband edges. We show this effect in Fig. 6.8, making use of the density of states g (**E**). The broadening has maximum magnitude for the highest subbands, since the probability of tunnelling increases as the upper edge of the barriers is approached.

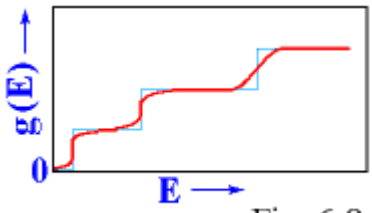

Fig. 6.8

These phenomena are similar to the effects which occur when composing a simple crystal out of atoms (see the discussion in Supplement 4) .

The main reasons for producing and investigating superlattices include planned -or already realized- applications, beyond the possibilities that can be achieved with simple quantum wells or a small number of combined quantum wells (e. g. applications based on electrooptical effects). Moreover, experiments are often performed with superlattices having relatively large barrier thicknesses, because the effects of the individual wells add up and, consequently, can be measured with greater accuracy.

6.2 Interband and Exciton Transitions

We shall now discuss transitions between valence and conduction bands and the corresponding spectra - including their modification by exciton effects - referring again to the simple quantum-well. First we shall consider **upward transitions** for the case (Fig. 6.9) that the well is irradiated with photons of energy $\hbar\omega$ in the direction perpendicular to the interfaces. Interband transitions can take place, if $\hbar\omega$ is at least equal to the separation beween the lowest conduction subband and the highest valence subband.

Fig. 6.9

It is found that there is a selection rule for the propagation vector $\mathbf{k}_t$ (consequence of the translation symmetry in the directions parallel to the interfaces),

(6.7) $\Delta\mathbf{k}_t = 0$,

i. e. transitions can only occur between valence band and conduction band states having the same $\mathbf{k}_t$. We illustrate this in a E($\mathbf{k}_t$) diagram which we obtain by combining a valence band diagram as Fig. 6.6 with a conduction band diagram as Fig. 6.4 (see Fig. 6.10). The transitions are represented according to Equ. (6.7) by vertical arrows ↑. We have only drawn transitions between subbands with the same N-value, because these usually possess the highest probability.

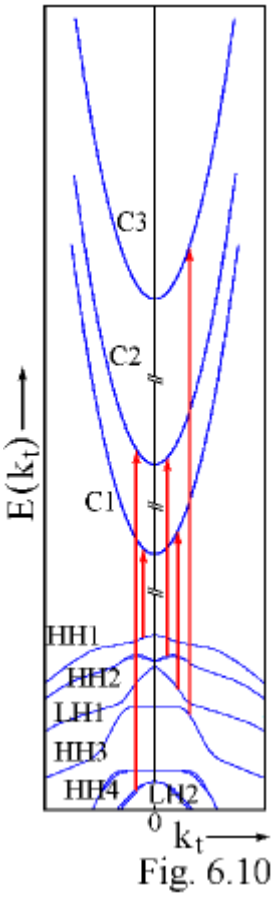

Fig. 6.10

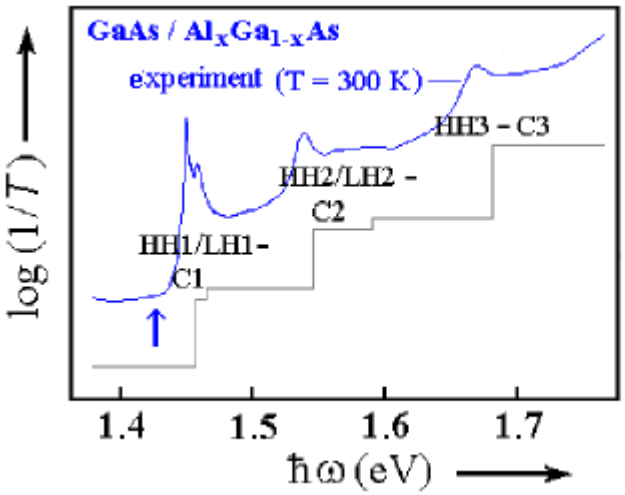

Fig. 6.11

We now show what kind of absorption spectrum we should get for a typical structure of the type considered (A = GaAs, B = $Al_{0.3}Ga_{0.7}As$, d = 10 nm). We may expect that the spectrum consists of contributions of the *combined densities of states* of the valence bands and conduction bands involved in the the transitions (Equ. (2.17)), as in the homogenous case.

We shall assume - starting from the properties of the simple density of states g (E) (Fig. 6.4) - that in the present case each subband combination gives rise to a step with a subsequent near constant behaviour . Thus we obtain a spectrum as represented in **Fig. 6.11** (—). The assignment to the transitions (Fig. 6.10) is given. It should be noted that the energetic separations in Fig. 6.10 are not drawn to scale, and that the system parameters in the two Figures are somewhat different.

> Since we are concerned with an optically inhomogeneous system we cannot describe the spectrum by an absorption coefficient α. Therefore we return to the transmittivity T (Appendix 1), which is the directly measured quantity, plotting log $(1/T)$ versus ħω (in the homogeneous case log $(1/T)$ is often approximately proportional to α).

In addition to the expected spectrum **Fig. 6.11** shows an experimental spectrum [22] (—, shifted, for clarity, in vertical direction), which has been measured on a corresponding superlattice (50 periods, $d_A = d_B = 10$ nm). It differs qualitatively from the expected picture, in showing lines instead of steps, which broaden with increasing N. The lines are due to transitions into *exciton states*, that are based on one-particle states corresponding to the edges of conduction-valence-band combinations (analogously to the case of homogeneous materials, Section 5.1). The electrons and holes constituting the excitons are localized in the A regions (in the same A region in the case of superlattices). Since the well dimensions are typically comparable with the exciton radius of the corresponding homogeneous material the exciton is compressed in z-direction, as already suggested in **Fig. 6.12**. This has two consequences:

- When the charge densties of electron and hole approach, the Coulomb attraction and, hence, the dissocation energy E_D are increased. This leads to a larger stability of the exciton states with respect to temperature growth and the action of electric fields. Due to the first property, exciton absorption lines are still distinctly visible at 300 K, in contrast to macroscopic GaAs (Fig. 5.7) . The second property is the basis of (future or already realized) applications of quantum wells for light modulation. The confinement effect is quite evident in Fig. 6. 11; the low-energy limit of the spectrum in the homogeneous case has been marked by ↑ in this Figure.
- The transition probability for the generation of excitons increases due to the growth of the corresponding transition matrix elements. ("It is easier to create an excited state of the system, if the electron and hole states overlap more strongly".)

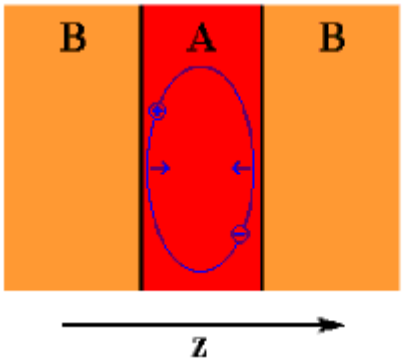

Fig. 6.12

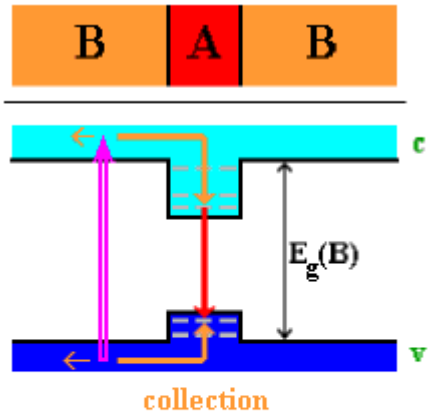

Fig. 6.13

The broadening of the exciton lines which occurs with growing energy (Fig.6.11) probably originates from the broadening trend in the subband edges of the superlattices (Fig. 6.8).

We conclude with some remarks concerning **downward transitions** which are observed in photoluminescence spectra. If a quantum-well structure is irradiated with photons whose energy is larger than the bandgap of the B-material(see Fig. 6.13), excitation transitions ⇑ leading to the creation of high-energy electron-hole pairs take place. In the present case the relaxation (—) mainly results in a ***collection*** of the two kinds of particles in the wells, whereby electrons and holes end up in the corresponding subbands and finally, sometimes, in exciton states. This is followed by radiative recombination (↓) or radiative annihilation. Due to the collection effect the luminescence yield is usually increased compared with that of homogeneous material:

- The "meeting probability" of electron and hole as well as the probabilities of radiative recombination/annihilation greatly increase due to the approach of the two particles (see also the previous remarks on the behaviour of upward transitions).
- The structures produced by epitaxy usually have excellent crystallographic quality - epecially in the well regions - which decreases the rates of undesired types of downward transitions near lattice defects.

Of course the confinement effect is also reflected in the photoluminescence spectra. Here exciton annihilation processes are dominant over electron-hole pair recombination, more distinctly than for homogeneous systems; this is mainly related to the high E_D-values.

6.3 Intersubband Transitions

Transitions between conduction subbands or valence subbands can occur, if varations in the degree of occupation are produced within the well regions by doping with donor and acceptor impurities, respectively. In the following we consider upward transitions between conduction subbands for the case in which the N = 1 subband is partly occupied with electrons due to thermal ionization of shallow donors (Fig. 6.14). The $\mathbf{k}_t$ selection rule Equ. (6.7) is valid also in this case. So, e. g. transitions to the the N = 2 subband are possible (↑) .

Owing to the energy relation Equ. (6.5) we get a vertical subband separation independent of $\mathbf{k}_t$, i. e. we expect *one absorption line* at

(6.8) $\hbar\omega = E_2 - E_1 = \varepsilon_2 - \varepsilon_1$.

Fig. 6.15 shows experimental absorption spectra [23] referring to two GaAs-$Al_{0.3}Ga_{0.7}As$-superlattices with different d_A values (6.5 and 8.2 nm) (50 periods, d_B = 10 nm in both cases, wells doped with Si donors). For clarity the spectra are vertically shifted relative to each other. The dominant absorption line is attributed to subband transitions of the type of Equ. (6.8) in each case. In addition, there are weaker lines about 88 and 96 meV in both cases, which are due to phonon transitions (multiphonon processes, Section 8.3) . As to be expected, the intersubband peak is located at higher $\hbar\omega$ in the case of the 6.5 nm sample.

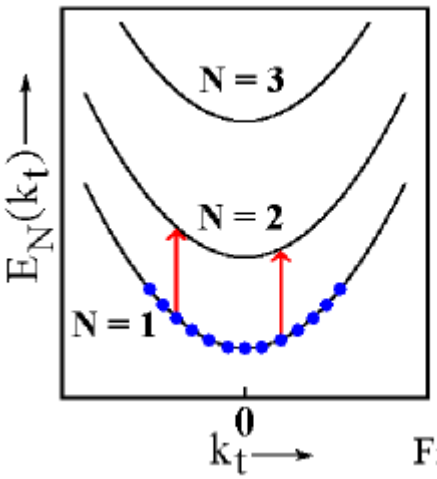

Fig. 6.14

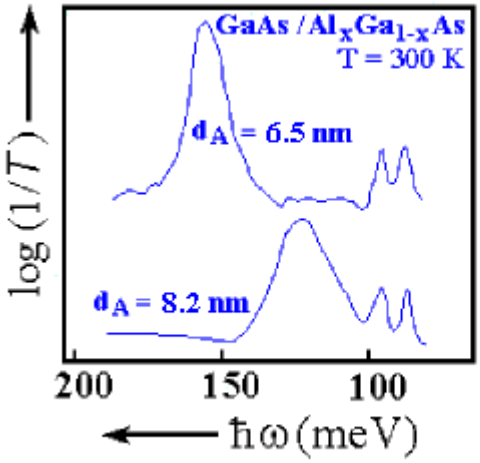

Fig. 6.15

The observed positions of these peaks are obtained, to some approximation, using Fig. 6.5, Equ. (6.6) and Equ. (6.8) together with the offset value U_0 = 245 meV for the present material combination (E_0 = 132 bzw. 83 meV and referring to the m_c* value (0.067 m_0) of GaAs).

> An experimental problem is due to the fact that intersubband transitions can be observed as electrical dipole transitions only if the incident light has a polarization component perpendicular to the interfaces (parallel to the z-axis). That means that in the usual configuration as represented in Fig. 6.9 absorption of this kind is not visible because of the transversal character of the radiation. To avoid this problem obliquely instead of normally incident light is used in the experiments. Then - especially if incidence under the Brewster angle is employed - the electric field of the radiation has a significant z- component.

Unlike the case of homogeneous material we are dealing here with transitions between states which are induced merely by the interaction with photons, and do not require the participation of additional interaction partners (compare Chapter 4). Consequently, the transition probabilities (in the suitable geometric configuration) are relatively high. In particular, this refers to the N = 1 → 2, transitions discussed earlier, which can be illustrated by the fact that the change of the wavefunctions $\chi_N(z)$ (Fig. 6.4) is accompanied by a large change of the electric dipole moment.

Of course, the transition probabilities of the corresponding radiative downward transitions are high, too, in particular for the backward processes N = 2 → 1, where the relaxation times are of the order 10^{-13} s. The observed linewidths (Fig. 6.15) mainly originate from lifetime broadening.

It should be noted that at high photon energies upward transitions from the subbands to the continuum levels above U_0 ("ionization transitions") are possible. These transitions, which involve the generation of mobile carriers, may become the basis for the development of infrared photodetectors [23a].

6.4 Semiconductor Lasers

As already mentioned in Section 2.7, the semiconductor lasers currently employed are mainly based on quantum well structures.

Let us explain the principle of operation using Fig. 6.16, which is a modification of Figures 6.1 and 6.13. Here the B -

regions are assumed to be doped with "shallow" donors or acceptors. At environmental temperature these regions show n-type and p-type conduction, respectively, due to thermal ionization. Because of the gradients of the carrier concentrations existing between the B-regions on the one hand, and the A-regions on the other hand, electrons and holes partly undergo diffusion into the A-regions. Thereby the diffusion is slowed down through the action of the opposite

space charge originating from the impurities (positive charge of the donors acting on electrons, negative charge of the acceptors acting on holes).

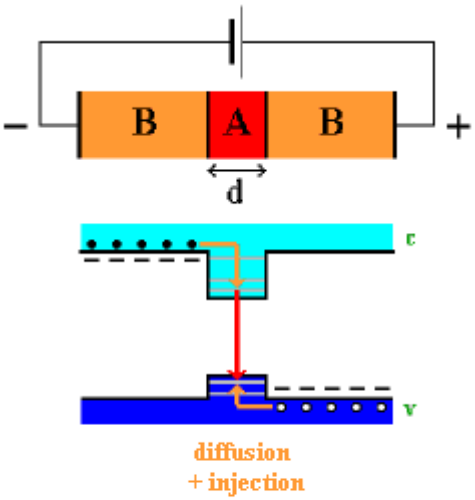

Fig. 6.16

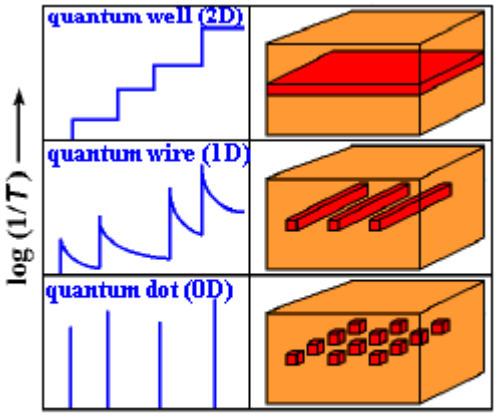

Fig. 6.17

If electrodes are deposited upon the B-regions and an electric voltage of the polarity shown in Fig. 6.16 (forward direction) is applied, we are concerned with an additional collection of carriers (injection); these can recombine radiatively. (Generally, there are also exciton annihilation transitions.) As a consequence, we are dealing here with ***electroluminescence***. In the presence of sufficiently strong injection, population inversion may occur, and - if by suitable surface treatment the structure is made to obtain resonator properties - laser action is possible.

The efficiency of such systems is considerably higher than for lasers based on simple p-n junctions (see Section 2.7). The most important advantages are:

1. Low threshold current and high emission yield: Due to the small well diameters, the rates of the radiative recombination / radiative annihilation are large, while the rates of undesired competitive processes occurring at defects are small (owing to the perfection of the epitaxial material), see our remarks in Section 6.2 concerning the luminescence yield. The collection effect leads to to a population inversion starting already at low injection current. Furthermore, there are favourable conditions because, due to the different E_g values, the refractive index in the A-regions is usually higher than in the B-regions, thus concentrating the radiation field in the A-regions.
2. The laser wavelength can be varied within wide limits by changing the well diameter d (changing the confinement energy). In particular, a decrease of d results in a decrease of the laser wavelength. For instance, one can reach the visible spectral range in the case of a GaAs well (about 0.7 µm, to be compared with about 0. 9 µm for homogeneous GaAs).

A further phenomenon which is favourable for the achievement of population inversion and laser effect, is the energetic concentration of "laser active" states. This phenomenon is due to the decrease of the active region, i. e. to the fact that we are concerned here with a near-two-dimensional system. This result suggested experiments attempting to obtain further improvements by going to systems with one or zero dimension [18,19], which typically have diameters of some nm in two and three dimensions, respectively. Such systems are referred to as ***quantum wires*** and ***quantum dots***, respectively.

As shown in Fig.6.17 a decrease of the number of dimensions (2D - 1D - 0D) leads to an increase in the spectral concentration of the optical transitions. We illustrate this with the help of schematic pictures of absorption spectra, as expected from the corresponding combined densities of states (Section 6.2, ignoring exciton effects). As far as quantum dots are concerned we approach the case of big molecules, which manifests itself in the line type character of the spectrum. To exploit these possibilities, one needs procedures for the production of systems containing a large number of quantum wires or quantum dots with -if possible- *the same dimensions* (note that the desired effects are strongly disturbed by deviations of size, due to the size dependence of the confinement energies). At present intense efforts for solving these problems by means of epitaxy techniques (Supplement 7) are under way.

Chapter 7

Lattice Vibrations and Phonons: Basic Concepts

After this excursion to the field of quantum structures, we shall now deal again, in the two final chapters, with processes in homogeneous crystalline materials, more specifically with phonon processes.

> To understand the corresponding optical transitions, it is necessary to be familiar with the vibrational properties of crystals. However, as experience shows, most students do not have a good knowledge in this respect. This is partly because the general mathematical treatment (involving equation systems with many indices) is deterrent at first sight . Therefore, in lectures, oversimplified kinds of presentation (e. g. restriction to linear chain models) are often employed. On the other hand. the consequent treatment of vibrational states is conceptually no more difficult than the treatment of electronic states. In view of this situation, we shall give an analysis of that matter in the present Chapter, restricting ourselves to the basic ideas (a detailed discussion may be found e. g. in [3]).

The vibrational states will be treated using a model which does not have a direct connection with our earlier discussion of electronic states (Section 1.2) . In this model it is assumed that the crystal *consists of particles ("atoms") having certain masses, which are - to some extent - mobile and that certain forces are active between them* .

The existence of these forces has the following consequences:

- There is a certain equilibrium configuration of the atoms corresponding to the minimum of the potential energy of the system (starting point of the discussion in the previous Chapters).
- The forces have restoring character, i. e. the atoms are able to perform vibrations around the equilibrium positions.

For the moment we admit forces of any range (Fig. 7.1, ♦♦♦♦♦) . These vibrations are referred to as ***lattice vibrations***, although, what is meant is not a motion of the lattice, but of the individual atoms.

> Strictly speaking, there is no precise definition of the term "atoms" in solid state physics, since the electrons cannot be assigned to a definite atomic nucleus (nonlocalized electronic wavefunctions ψ_{kv} (**r**), see Section 1.2). The vibrations actually involve motions of the nuclei, in which the electrons are partly "dragged away". This effect, which involves changes of the wavefunctions, can be taken into account in more detailed theoretical treatments [24]. The results include a determination of the "force constants" to be introduced later.

7.1 Classical Description

Understanding the subject is made relatively easy by the fact that many vibrational properties can be discussed in classical terms.

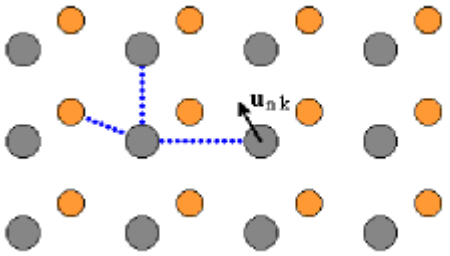

Fig. 7.1

Let us first introduce ***displacements*** of the atoms from their equilibrium positions, $\mathbf{u}_{n\,k}$, as illustrated in Fig. 7.1. The indices n and k are used to number the unit cells in the crystal and the atoms in the unit cell, respectively. Then the ***potential interaction energy of the atoms*** is a function of the cartesian components $u_{n\,k\,\alpha}$ of the atomic displacements (α = x,y,z). We denote this function by $\Phi(u)$ (u totality of the $u_{n\,k\,\alpha}$) and expand it into a Taylor series around the equilibrium positions $u_{n\,k\,\alpha} = 0$. Taking into account that in this case the first derivatives are zero, there are no first-order terms , and we get

$$(7.1)\quad \Phi(u) = \Phi(0) + (1/2)\sum_{\substack{n'\,k'\,\alpha' \\ n''\,k''\,\alpha''}} \left(\frac{\partial^2\Phi(u)}{\partial u_{n'k'\alpha'}\,\partial u_{n''k''\alpha''}}\right)_0 u_{n'k'\alpha'}\,u_{n''k''\alpha''}$$

As usual, we have omitted all terms of higher than second order, i. e. we are working in the so-called ***harmonic approximation***. This name originates from the fact that the characteristic vibrations obtained on this basis are harmonic vibrations (pure sine and cosine type vibrations, as explained later).

The second derivatives are considered as parameters ("force constants"); we shall denote them by

$$(7.2)\quad \phi_{n'k'\alpha'n''k''\alpha''} = \left(\frac{\partial^2 \Phi(u)}{\partial u_{n'k'\alpha'}\,\partial u_{n''k''\alpha''}}\right)_0$$

By calculating the first derivative with respect to the u's, of Equ. (7.1), and changing signs we obtain the forces active in a certain configuration of displacements. This leads to the equation of motion for the atom nk in α direction:

$$(7.3)\quad M_k \frac{d^2 u_{nk\alpha}}{dt^2} = -\sum_{n'k'\alpha'} \phi_{nk\alpha n'k'\alpha'}\; u_{n'k'\alpha'}$$

M_k is the mass of the atoms of type k. The right-hand side of this equation gives the sum of the forces originating from the atomic displacements.

> The double summation over the three types of indices in Equ. (7.1) can be replaced by a single summation taking into account that in the sum all pairs of atoms are counted twice, then the factor 1/2 disappears.

We are interested in *normal vibrations* (also referred to as *normal modes*), i. e. vibrations having a definite frequency ω:

$$(7.4)\quad u_{nk\alpha}(t) = v_{nk\alpha} \exp(i\,\omega\, t)$$

Entering into Equ. (7.3) , we obtain an equation system for the $v_{nk\alpha}$:

$$(7.5)\quad M_k\,\omega^2\, v_{nk\alpha} = \sum_{n'k'\alpha'} \phi_{nk\alpha n'k'\alpha'}\; v_{n'k'\alpha'}$$

This system consists of a big number of equations (three times the number of atoms in the crystal). However, this system can be transformed to a system of very few equations making use of the presence of translation symmetry. To get this result we choose the relation

$$(7.6)\quad v_{nk\alpha} = (M_k)^{-1/2}\, w_{k\alpha} \exp(i\,\mathbf{q}\,\mathbf{R}_n)$$

as the starting point. The w's are amplitude factors that are independent of n. The $\mathbf{R}_n$ are lattice vectors; the quantities **q** are propagation vectors characterizing the desired wave-like solutions. More precisely, we are looking for solutions which have the same structure as Bloch waves (solutions of the electronic problem): A prefactor that is independent of the cell index n, i. e. having the periodicity of the lattice (corresponding to the Bloch factor) and a wave-type factor.

This choice leads to a system of equations for $w_{k\alpha}$:

$$(7.7)\quad \omega^2\, w_{k\alpha} = \sum_{k'\alpha'} D_{k\alpha k'\alpha'}(\mathbf{q})\, w_{k'\alpha'}$$

$$(7.8)\quad D_{k\alpha k'\alpha'}(\mathbf{q}) = \sum_{n'} \phi_{nk\alpha n'k'\alpha'} (M_k M_{k'})^{-1/2} \exp(i\,\mathbf{q}\,(\mathbf{R}_{n'} - \mathbf{R}_n))$$

Although the index n appears explicitly on the right-hand side of Equ. (7.8) , the quantities $D_{k\alpha k'\alpha'}$ are n - independent in the case of a sufficiently large crystal. This is a consequence of translation symmetry (see **Supplement 9**). This result implies that the Bloch - type relation (7.6) with n - independent w's is justified. Hence, in (7.7) we are dealing with a system of only a few linear homogeneous equations, which can be treated using the familiar algebraic procedure. Denoting by r the number of atoms in the unit cell, we are concerned with 3r equations. These equations can be written in matrix form:

$$(7.9)\quad \omega^2\, \mathbf{w} = D(\mathbf{q})\, \mathbf{w}$$

Here **w** is a three-dimensional vector with the components $w_{k\alpha}$ and D(**q**) is a 3r × 3r matrix with the elements $D_{k\alpha k'\alpha'}(\mathbf{q})$, which is referred to as ***dynamical matrix***. Equ. (7.9) is an eigenvalue equation, i. e. an equation for determining the eigenvalues ω^2 and the eigenvectors **w**. The first quantity gives the frequencies, the latter the amplitudes and the directions of the vibrations.

> Hence the vibrational behaviour of a given crystal is determined by its dynamical matrix. According to Equ. (7.8) this matrix depends, for definite **q**, on the masses of the atoms (which are well known) involved and the lattice vectors $\mathbf{R}_n$ (which can be

obtained from X - ray structure data). The force constants are unknown quantities that can be determined, if necessary, by fitting to experimental data. However, many general results can be deduced without a knowledge of the specific values of the ϕ's.

The eigenvalues are obtained by solving the secular equation

(7.10) $\det[D(\mathbf{q}) - \omega^2 \mathbf{E}] = 0$

($\mathbf{E}$ is the 3r × 3r unit matrix). It can be shown that this equation always has 3r real and positive solutions. Denoting these by $\omega_j(\mathbf{q})^2$ (j = 1,...3r) we get the same number of eigenfrequencis $\omega_j(\mathbf{q})$. If $\mathbf{q}$ is varied, each of these functions covers a certain range for each j, i. e. the frequency spectrum consists of 3r ***vibrational branches (bands)***. As in the case of the electronic propagation vector$\mathbf{k}$, $\mathbf{q}$ can be limited to the Brillouin zone (Section 1.2). According to the procedure described in that Section, we are concerned, of course, with the same Brillouin zone as in the electronic case.

Two additional general properties are important:

- In each case, there are three branches for which $\omega_j(\mathbf{q} = 0) = 0$; these are called ***acoustic branches***.
- The $\omega_j(\mathbf{q})$ are even functions of $\mathbf{q}$, i. e. one has $\omega_j(-\mathbf{q}) = \omega_j(\mathbf{q})$.

If there is more than one atom per unit cell, we are concerned, in addition to the acoustic branches, with 3r - 3 further branches (***optical branches***).

Let us now discuss the *vibrational configurations* . In view of Equ. (7.4) and (7.6) these are given by the expressions

(7.11) $(M_k)^{-1/2} w_{k\alpha}(\mathbf{q}, j) \exp(i\mathbf{q}\,\mathbf{R}_n) \exp(i\omega_j(\mathbf{q})t)$.

Here one has to use eigenvectors and eigenfrequencies, i. e. one is dealing with running waves (Bloch - type waves) with a propagation vector $\mathbf{q}$, which determines the wavelength (= $2\pi / |\mathbf{q}|$) and the direction of propagation. Thereby each atom is vibrating with the same frequency $\omega_j(\mathbf{q})$, while the phases and amplitudes are, in general, different. The vectors ($w_{k\,x}$,$w_{k\,y}$, $w_{k\,z}$) are directed perpendicular and parallel to $\mathbf{q}$, in the cases of "transverse" and "longitudinal" vibrations, respectively.

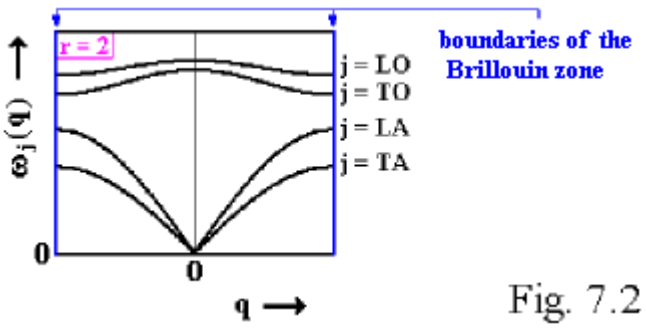

Fig. 7.2

Thus the spectrum of eigenvalues and the structure of the vibrational states are similar to the energy spectrum and the structure of wavefunctions, respectively, in the electronic case. An important difference lies in the fact that there is only a finite number of bands in the case of the vibrations.

Now we consider materials with two atoms per unit cell, in particular materials with diamond, zincblende, or rocksalt structure . In Fig. 7.2 we qualitatively represent the functions $\omega_j(\mathbf{q})$ along a straight line in the Brillouin zone passing through $\mathbf{q} = 0$ (compare Fig. 1.3)

The acoustical branches (one longitudinal (LA) and two transverse (TA)) and the optical branches (also one longitudinal (LO) and two transverse (TO)) are indicated. The picture refers to a high-symmetry direction in $\mathbf{q}$ space (e. g. Γ - L), where the transverse branches coincide.

In Fig. 7.2 the TO and LO branches are separated at $\mathbf{q} = 0$. This is found for all materials having a polar component of binding (different types of atoms). In the absence of polar binding (only one type of atoms as for the diamond structure) the optical branches are in contact at this point.

The maximum values of $\omega_j(\mathbf{q})$ typically are of the order 10^{13} to 10^{14} s^{-1}.

In a crystal of finite size the realizable $\mathbf{q}$ vectors form a fine-mesh network in the Brillouin zone , analogously as the $\mathbf{k}$

vectors in the electronic case (Supplement 1). Ignoring this fine structure, it can be stated that each point in a diagram as

Fig. 7.2 corresponds to a normal vibration.

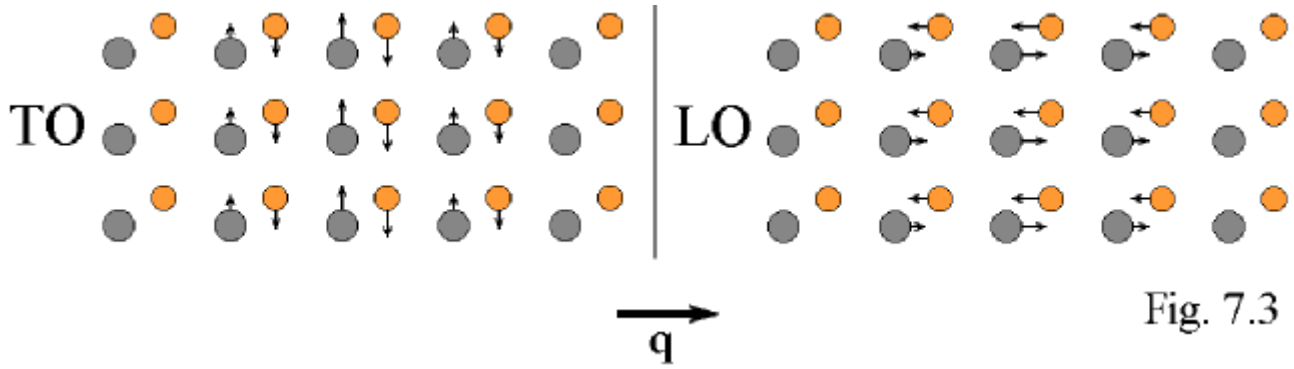

Fig. 7.3

In Fig. 7.3 we illustrate the TO and LO vibrational configurations for a crystal with two atoms per unit cell (schematic picture). These are "snapshots" of the patterns of atomic displacements within the range of half a wavelength. The different vibrational phases are evident. As time goes on, the pattern moves in **q** direction, whereby the displacements of the individual atoms vary periodically (Equ. (7.11)) . It is a characteristic feature of the optical vibrations, that in every unit cell the displacements of the two types of atoms are opposite. Because of the opposite charges of the atoms ("ions") an *electrical dipole moment* results in each unit cell. As a consequence, a direct interaction with electromagnetic radiation can occur (see Section 8.2 for details) . This is the reason for referring to these vibrations as "optical vibrations". In contrast, the displacements within the unit cell have the same direction in the case of acoustic vibrations. The latter name originates from the fact that at large wavelengths (small |**q**|) these vibrations turn into sound waves (audible frequencies).

7.2 Quantum Mechanical Description: Oscillator Picture

We start with the *Hamilton operator of the system of atoms*, accepting Equ. (7.1) and (7.2) for the potential energy and putting Φ(0) = 0 (normalization of energy),

$$(7.12)\quad H = (1/2)\sum_{n k \alpha} \frac{p^2_{n k \alpha}}{M_k} + (1/2)\sum_{\substack{n' k' \alpha' \\ n'' k'' \alpha''}} \phi_{n' k' \alpha' n'' k'' \alpha''}\, u_{n' k' \alpha'}\, u_{n'' k'' \alpha''}$$

Note that the u's are now operators; the p's are the momentum operators canonically conjugate to the u's . Because the potential energy contains terms of second order in the coordinates, Equ. (7.12) reminds us of the Hamiltonian of a system of harmonic oscillators. By means of a coordinate transformation we can arrive at an expression including only *pure quadratic terms*:

$$(7.13)\quad u_{n k \alpha} = (V_0/V)^{1/2} \sum_{\mathbf{q} j} [(M_k)^{-1/2} w_{k \alpha}(\mathbf{q}, j) \exp(i \mathbf{q} \mathbf{R}_n)] Q_{\mathbf{q} j}$$

V_0 and V are the volume of the unit cell and of the crystal, respectively; the $Q_{\mathbf{q} j}$ are the new coordinates (***normal coordinates***). The quantities in square brackets correspond to the classical normal vibrations (compare Equ. (7.11)).

> In Equ. (7.13) we consider eigenvectors **w** normalized to unity (dimensionless quantities). As a consequence, the dimension of the Q's is (mass$^{1/2}$ × length), and the u's have the dimension of lengths, as should be the case.

Each normal coordinate is assigned to a normal vibration. The transformation yields

$$(7.14)\quad H = (1/2)\sum_{\mathbf{q} j} \{ |P_{\mathbf{q} j}|^2 + \omega_j(\mathbf{q})^2 |Q_{\mathbf{q} j}|^2 \}$$

The $P_{\mathbf{q} j}$ are the momenta canonically conjugate to the $Q_{\mathbf{q} j}$. In deriving Equ. (7.14) we have made use of Equ. (7.7) and (7.8).

Obviously Equ. (7.14) is the Hamilton operator of a system of harmonic oscillators (of unit mass), each oscillator being assigned to a normal vibration (i. e. to a point in a diagram of type Fig. 7.2). The frequencies of the oscillators agree with

the frequencies $\omega_j(\mathbf{q})$ of the normal vibrations. Thus, by introducing normal coordinates, we have transformed the real physical system of coupled atoms into *a system of uncoupled harmonic oscillators*. The ***oscillator picture*** enables one to discuss, in a transparent manner, the processes connected with lattice vibrations.

We write the Schrödinger equation corresponding to the new Hamilton operator in the form

(7.15) $H\,|.....,\, l_{\mathbf{q}\,j},.....\rangle = W_l\,|.....,\, l_{\mathbf{q}\,j},.....\rangle \qquad l_{\mathbf{q}\,j} = 0,\, 1,\, 2,.....$

We characterize the *state of the system* by numbers which indicate the *state of the individual oscillators* (ground state $l_{\mathbf{q}\,j} = 0$, excited states $l_{\mathbf{q}\,j} > 0$). W_l are the corresponding energy eigenvalues (l = totality of the $l_{\mathbf{q}\,j}$):

(7.16) $$W_l = \sum_{\mathbf{q}\,j} \hbar\omega_j(\mathbf{q})\,(l_{\mathbf{q}\,j} + \tfrac{1}{2})$$

Since we are concerned with uncoupled oscillators, W_l is given simply by the sum of the contributions of the individual oscillators (see e. g. [13]):

7.3 Quantum Mechanical Description: Phonon Picture

There is a further possibility of describing lattice vibrations, viz. - as costomary now - by a system of particles. In order to introduce this picture, we start from Equ. (7.16), in a somwhat rewritten form:

(7.17) $$W_l = \sum_{\mathbf{q}\,j} \hbar\omega_j(\mathbf{q})\, l_{\mathbf{q}\,j} + \tfrac{1}{2}\sum_{\mathbf{q}\,j} \hbar\omega_j(\mathbf{q})$$

The dependence on the vibrational state is determined by the first term. The second term ("zero-point energy") , which is a constant for a given material, will be ignored in the following. We can reinterpret Equ. (7.17): We can assume that we are dealing with *a system of particles without mutual interaction* (***phonons***) which are able to occupy particle states ($\mathbf{q}$ j). The energies of the states (***phonon states***) are given by $\hbar\omega_j(\mathbf{q})$, their quasi-momenta by $\hbar\mathbf{q}$,; the $l_{\mathbf{q}\,j}$ are corresponding occupation numbers. We can illustrate this situation by assuming that the curves in diagrams of the type Fig. 7.2 (ordinate multiplied by $\hbar$, Fig. 7.4) are occupied with such particles.

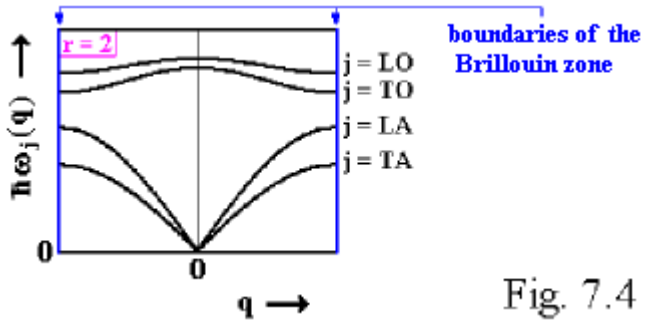

Fig. 7.4

The total energy of the system is obtained with the help of Equ. (7.17), by multiplying the energies of the phonon states ($\mathbf{q}$ j) with the numbers of the phonons residing there and summing over the energies thus achieved. According to this new interpretation, the state of the system $|.....,\, l_{\mathbf{q}\,j},.....\rangle$ (Equ. (7.15)) is specified by the occupation numbers for all phonon states ($\mathbf{q}$, j).

> We can give a " portrait" of a phonon, using, as an example, Fig. 7.3: If there is only one phonon in the corresponding state, the atoms are vibrating in the way shown in the picture, with minimum total energy (ignoring the zero-point energy).

We now refer to the $\hbar\omega_j(\mathbf{q})$- curves (compare Fig. 7.4) as ***phonon dispersion curves***. (We have used a similar Figure in Supplement 3 when discussing indirect interband transitions.) The maximum $\hbar\omega_j(\mathbf{q})$ values typically are of the order of several ten meV.

> The phonon dispersion curves are an analogy of the electronic band structure functions $E_\nu(\mathbf{k})$. Sometimes it is useful to introduce a ***phonon density of states*** similarly to the electronic density of states. This is obtained in a manner analogous to Equ. (1.13), replacing $\mathbf{k}$ by $\mathbf{q}$, ν by j, and $E_\nu(\mathbf{k})$ by $\hbar\omega_j(\mathbf{q})$. The factor before the integral is now $1 / 8\pi^3$.

In experimental studies there is usually no information about the individual occupation numbers $l_{\mathbf{q}j}$, but only about *average* occupation numbers present in thermal equilibrium. These are given by a Bose-type distribution function:

(7.18) $\langle l_{\mathbf{q}j}\rangle(T) = (\exp[\hbar\omega_j(\mathbf{q})/k_BT] - 1)^{-1}$

where T is the measurable crystal temperature defined by this distribution. Since, according to their introduction (Section 7.2) the values of $l_{\mathbf{q}j}$ are not restricted to a finite range, the phonons may be regarded as Bose particles.

The mathematical formulation adequate to the phonon picture is obtained by means of an additional coordinate transformtion. We introduce new dimensionless coordinates $b_{\mathbf{q}j}$ by:

(7.19) $Q_{\mathbf{q}j} = [\hbar/2\omega_j(\mathbf{q})]^{1/2}\,(b_{\mathbf{q}j} + b_{-\mathbf{q}j}^{+})$

(7.20) $P_{\mathbf{q}j} = i[\hbar\omega_j(\mathbf{q})/2]^{1/2}\,(b_{\mathbf{q}j}^{+} - b_{-\mathbf{q}j})$

As usual, the symbol $^+$ refers to adjoint operators. There are no momenta canonically conjugate to the new coordinates. The corresponding transformation of the Hamilton operator Equ. (7.14) gives

(7.21) $$H = \sum_{\mathbf{q}j} \hbar\omega_j(\mathbf{q})\left(b_{\mathbf{q}j}^{+} b_{\mathbf{q}j} + \tfrac{1}{2}\right)$$

The quantities $b_{\mathbf{q}j}^{+}$ and $b_{\mathbf{q}j}$ have the properties of creation and destruction operators, respectively, such as introduced for the treatment of many-particle systems in the second-quantization formalism [13]. Denoting the state of our system, as before, by $|\ldots, l_{\mathbf{q}j}, \ldots\rangle$, we have

(7.22) $b_{\mathbf{q}j}^{+}\,|\ldots, l_{\mathbf{q}j}, \ldots\rangle = [l_{\mathbf{q}j} + 1]^{1/2}\,|\ldots, l_{\mathbf{q}j} + 1, \ldots\rangle$

(7.23) $b_{\mathbf{q}j}\,|\ldots, l_{\mathbf{q}j}, \ldots\rangle = [l_{\mathbf{q}j}]^{1/2}\,|\ldots, l_{\mathbf{q}j} - 1, \ldots\rangle$

i. e. , apart from prefactors, the result is a *state of the system* with one phonon more and less, respectively, in the phonon state ($\mathbf{q}$ j) (indices of b^+ and b), while the phonon numbers in the other states remain unchanged. The combinations $b_{\mathbf{q}j}^{+}\,b_{\mathbf{q}j}$ appearing in Equ. (7.21) are so-called particle-number operators, whose eigenvalues are $l_{\mathbf{q}j}$. The energy eigenvalues of the system are therefore, as to be expected, given by Equ. (7.17). Apart from the zero-point contribution, Equ. (7.21) corresponds to the general form of the Hamilton operator for a system of non-interacting particles obtained in second quantization [13].

7.4 Summary

In the following Table we make a comparison of the three kinds of describing lattice vibrations presented in the preceding Sections.

coordinates	**picture**	**(q, j) characterizing**	**meaning of the $\omega_j(q)$**
$u_{n\,k\,\alpha}$	coupled atoms	classical eigenvibrations	frequencies
$Q_{\mathbf{q}j}$	non-coupled oscillators	oscillators	frequencies or $(1/\hbar)\times$energy steps
$b_{\mathbf{q}j}^{+}$, $b_{\mathbf{q}j}$	non-coupled particles = phonons	phonon states	$(1/\hbar)\times$phonon energies

Chapter 8

Phonon Transitions

8.1 Interaction of Phonons with Radiation

We now discuss the change of the vibrational state of the crystal (change of the number of phonons) induced by monochromatic electromagnetic radiation (Fig. 8.1). As in our earlier treatment of electronic transitions, we start with a classical radiation field (frequency ω), considering transitions between states of the system, in the present case states of the phonon system. More exactly, we regard transitions between an initial state |i> and a final state |f> of the system, specified by phonon occupation numbers :

(8.1a) $|i\rangle = |\ldots\ldots, l_{\mathbf{q}\,j}, \ldots\ldots i\rangle$

(8.1b) $|f\rangle = |\ldots\ldots, l'_{\mathbf{q}\,j}, \ldots\ldots i\rangle$

Fig. 8.1

Then, in general, the transition probability is given, analogously to the electronic case (Equ.(2.4)), by

(8.2) $P = (2\pi / \hbar) |\langle f |H_{pr}| i \rangle|^2 \, \delta (W_f - W_i \pm \hbar\omega)$

H_{pr} is the interaction operator between the phonon system (p) and the radiation field (r) . W_f and W_i are the energies of the states |f> and |i>, respectively (compare Equ.(7.17)). The ± sign in the argument of the δ functio takes into account that, in addition to transitions with the absorption of radiation ($W_f > W_i$, $\hbar\omega = W_f - W_i$), processes with the induced emission of radiation ($W_f < W_i$, $\hbar\omega = W_i - W_f$) can occur. We shall return to this point later on.

We shall use the dipole approximation for the interaction with the radiation field

(8.3) $H_{pr} = - \mathbf{M}\,\mathbf{E}_0$

Here **M** is the electric dipole moment of the crystal *produced by the displacements of the atoms* and $\mathbf{E}_0$ the amplitude of the electric field of the elctromagnetic wave.

Thus, **M** depends on the atomic displacements $\mathbf{u}_{nk}$. In the case of vanishing displacements we have **M** = 0; for small displacements we expect small magnitudes of **M**. Therefore, it is reasonable to make a Taylor expansion with respect to the $\mathbf{u}_{nk}$; we write symbolically

(8.4) $\mathbf{M} = \{ u \} + \{ u\,u' \} + \{ u\,u'\,u'' \} + \ldots\ldots = \mathbf{M}_1 + \mathbf{M}_2 + \mathbf{M}_3 + \ldots\ldots$

The symbols { } stand for sums containing terms of first, second, and third order in the $\mathbf{u}_{nk}$, respectively (sums over nkα). We refer to the contributions $\mathbf{M}_1$, $\mathbf{M}_2$ and $\mathbf{M}_3$ as ***first, second and third order dipole moments*** , respectively.

Obviously, first-order dipole moments result from the displacement of atoms having an excess charge ("ions"). Thus an atom with the excess charge Q displaced by $\mathbf{u}_{nk}$ makes the contribution $Q\mathbf{u}_{nk}$. Such contributions can only occur in substances consisting of different kinds of atoms, i. e. in so-called ***polar materials***. Higher-order dipole moments are found for *all* substances including substances which consist of only one type of atoms (***non-polar materials***). As illustrated in Fig. 8.2 these are due to the fact that the electron charge distribution is not rigidly coupled to the motion of the nuclei (o), but is deformed during the displacement (deformation of the electron shell and exchange of charge with neighbouring atoms (⇆)). These effects are also dependent on the displacements of the neighbouring atoms, so one is dealing with contributions of displacements of several atoms.

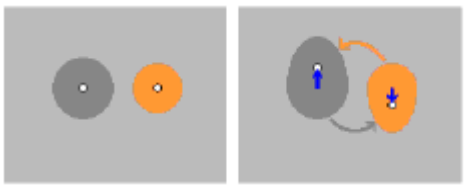

Fig. 8.2

It is appropriate to use, instead of the atomic displacements, the coordinates $b_{\mathbf{q}\,j}^{+}$ and $b_{\mathbf{q}\,j}$ corresponding to the phonon picture . Since there are linear relationships between the u's and the b's (compare Equ.(7.13), (7.19) and (7.20)), the new series expansion has a struture analogous to Equ. (8.4):

(8.5) $\mathbf{M} = \mathbf{M}_1 + \mathbf{M}_2 + \mathbf{M}_3 + ...$

$\mathbf{M}_1 = \{ b_{\mathbf{q}\,j}^{+} \} + \{ b_{\mathbf{q}\,j} \}$

$\mathbf{M}_2 = \{ b_{\mathbf{q}\,j}^{+} b_{\mathbf{q}'\,j'}^{+} \} + \{ b_{\mathbf{q}\,j}^{+} b_{\mathbf{q}'\,j'} \} + \{ b_{\mathbf{q}\,j} b_{\mathbf{q}'\,j'}^{+} \} + \{ b_{\mathbf{q}\,j} b_{\mathbf{q}'\,j'} \}$

$\mathbf{M}_3 = \{$ combination of three-b terms $\}$

We have now used symbols { }, similarly as in Equ. (8.4). In the present case, these stand for sums over **q** j and **q**' j', respectively. Here the expansion coefficients are three-dimensional vectors.

8.2 First-Order Dipole Moment / One-Phonon Transitions

A dipole moment proportional to the displacements is found for optical vibrations (Fig. 7.3). Here the coupling to electromagnetic radiation is restricted to the case in which $\mathbf{M}_1$, i. e. also the displacements have components in the $\mathbf{E}_0$ direction (scalar product in Equ. (8.3)) and in which the propagation vector of the vibration (**q**) agrees with that of the radiation (**s**). Since the radiation has transverse character, i.e. $\mathbf{E}_0$ is perpendicular to **s**, the relevant vibrations are also transverse.

The agreement of **s** and **q** can be interpreted, similarly to the cases of interaction treated earlier (e. g Section 5.2) , as being due to the momentum balance for collisions in which phonons take part (transformation processes photon - phonon in the present case).

As already discussed in connection with electronic transitions, the magnitude of **s** is always small against the size of the Brillouin zone in the spectral range considered. (This is the condition for the validity of the dipole approximation Equ. (8.3).) Consequently, **q** is also small and may be assumed to be approximately zero.

The restrictions described imply that the sums in $\mathbf{M}_1$ in Equ. (8.5) are always reduced to a single term, viz. to the term with

(8.6) $\mathbf{q} = 0, \quad j = TO$

in each case. Hence, due to this *selection rule*, we can write

(8.7) $\mathbf{M}_1 = \text{const} \times b_{0,TO}^{+} + \text{const} \times b_{0,TO}$

We replace **M** in Equ. (8.3) by $\mathbf{M}_1$, insert this in the matrix elements in Equ. (8.2) and take into account Equ. (8.7). We obtain matrix elements of the type

(8.8) $\langle ....., l'_{\mathbf{q}\,j}, ...| b_{0,TO}^{+} | ....., l_{\mathbf{q}\,j}, ... \rangle$ and $\langle ....., l'_{\mathbf{q}\,j}, ...| b_{0,TO} | ....., l_{\mathbf{q}\,j}, ... \rangle$

According to Equ. (7.22) and (7.23) we get

(8.9) $b_{0,TO}^{+} | ....., l_{\mathbf{q}\,j}, ... \rangle = [l_{0,TO} + 1]^{1/2} | ....., l_{0,TO} + 1, ... \rangle$

(8.10) $b_{0,TO} | ....., l_{\mathbf{q}\,j}, ... \rangle = [l_{0,TO}]^{1/2} | ....., l_{0,TO} - 1, ... \rangle$

i. e. apart from the prefactors we are dealing, on the right-hand side, with eigenstates of the phonon system, in which the particle states (**q** = 0, j = TO) contain one phonon more or less, while the occupation of the other particle states corresponds to the kets on the left-hand side, i. e. corresponds to the initial state |i> of the system. Thus in the case of the matrix elements (8.8) we are concerned with scalar products between system-eigenstates, which, because of the orthonormality of these states, are non-zero only if the states combined in the scalar products are identical.

That means that under the action of $\mathbf{M}_1$ transitions occur only if *exactly one phonon* with **q** = 0 and j = TO is generated or annihilated. Because of the energy balance (argument of the δ function in Equ. (8.2)) we are dealing, in the first case, with transitions involving the absorption of a photon ($-\hbar\omega$), in the second case with transitions involving the induced emission of a photon ($+\hbar\omega$). In both cases we have

(8.11) $\hbar\omega = \hbar\omega_{TO}(0)$

We refer to these two types of processes as ***one-phonon transitions***. These transitions are indicated in the $\hbar\omega_j(\mathbf{q})$ diagram (Fig. 7.4) (see Fig. 8.3a). There is only a single point in this diagram taking part in these processes. Considering that the maximum phonon energies are typically some 10 meV, we see that usually, at not too low temperatures *in thermal equilibrium*, the state ($\mathbf{q} = 0$, j = TO) is occupied with some probability (compare Equ. (7.18); $k_B \times 300$ K is about 25 meV). That is why it is really important to allow for induced emission processes (↓) when discussing optical properties. (Obviously this is less important in the range of interband and exciton transitions, because the excitation energies are much higher in these cases.)

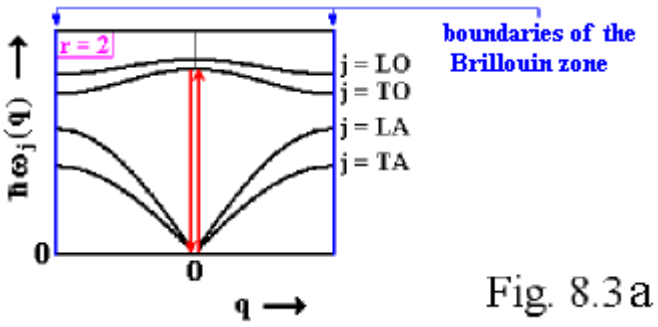

Fig. 8.3a

Of course, there are, besides the induced emission, also spontaneous emission transitions, in which phonons are annihilated (via one- or multiphonon transitions) and photons are generated. These appear, e. g., in the heat radiation of solids, making contributions, in particular, in the middle infrared region.

In order to keep the presentation transparent, we now introduce a Table, in which we give the previous results of this Section:

mechanism	processes	band	momentum balance	energy balance	type of material
first-order dipole moment ($\mathbf{M}_1$)	one-phonon processes	j = TO	$\mathbf{q} = 0$	$\hbar\omega = \hbar\omega_{TO}(0)$	polar

On the basis of Fig. 8.3 we expect that the absorption spectrum due to one-phonon transitions, of a polar material with two atoms per unit cell, consists of a single line at $\hbar\omega = \hbar\omega_{TO}(0)$. We show this in Fig. 8.4a, plotting the absorption index κ against $\hbar\omega$. There are contributions to the line intensity from absorption processes (↑) as well as induced emission processes (↓).

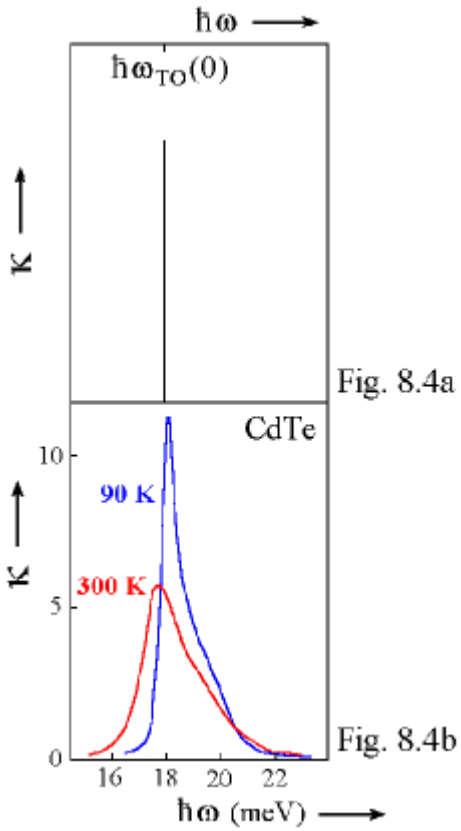

We compare this result in **Fig. 8.4b** with experimental spectra of CdTe [25], which have been determined by reflection measurements at two temperatures using a Kramers-Kronig analysis. The maximum values of κ are of the order 10. This corresponds to ε_2 values of some tens and α values above 10^4 cm^{-1}. These large intensities are comparable to the values found for interband and exciton transitions (e. g. Fig. 2.14 and Fig. 5.7).

In contrast to expectation (Fig. 8.4a), the absorpton lines in Fig. 8.4b have finite widths, growing with increasing temperature. We are dealing here with *lifetime broadening*: After some time, the phonons created in the optical transitions transform into other types of phonons. Such processes ("phonon-phonon scattering") are not to be expected on the basis of the previous treatment (Section 7.3). As will be remembered, we have been concerned with eigenstates of the system having definite phonon occupation numbers $l_{\mathbf{q}j}$. We shall discuss such processes - which are due to deviations from the harmonic approximation - in detail in **Supplement10**.

The shift of the line maximum toward lower energies, which occurs as the temperature increases, originates from the fact that the phonon energies are, to some extent, temperature dependent. This phenomenon is also due to anharmonic effects.

The quantitative pieces of information which can be obtained, by studying the one-phonon absorption line, include:

- $\hbar\omega_{TO}(0)$ (from the line position)
- the phonon lifetime τ_{TO} (from the line width) and
- the so-called ***effective charge*** (magnitude of the excess charge) of the atoms Q_{eff} (from the line intensity)

For a material consisting of two different kinds of atoms ("ions") the effective charges have, of course, opposite sign. As Q_{eff} increases , the interaction with the radiation field becomes stronger, and, consequently, the line intensity grows. To be more precise, the area under the absorption line (nearly independent of temperature, Fig. 8.4b) is proportional to Q_{eff}^2.

As an example, we give some values for CdTe: $\hbar\omega_{TO}(0)$ = 17.5 meV (corresponding to the peak position of $\varepsilon_2(\omega)$ at low temperatures), τ_{TO} (90 K) = 3.8×10^{-12} s, Q_{eff} = 0.83e.

> The τ_{TO} value is equal to about 16 times the period of a classical ($\mathbf{q} = 0$, j = TO) vibration. The classical analogon of the phonon lifetime is the *attenuation time* of the vibration. The attenuation is relatively weak in the present case, which is a final justification of using the harmonic approximation and, consequently, of introducing the phonon concept.
>
> The Q_{eff} value obtained is very far from the value one would naively expect for bivalent Cd and Te

in a corresponding ionic compound. Of course, the reason lies in the modified distribution of electronic charge which strongly deviates from the ionic case. (It is well known that this deviation is correlated with the presence of an appreciable covalent component of binding.)

For discussing experimental results, only the corresponding reflection bands are given in many cases. As we are concerned here with a single spectrally isolated resonance, we expect that the reflection band is similar to the corresponding band deduced from the oscillator model in Appendix 4. There we have to identify the oscillator frequency ω_0 with $\omega_{TO}(0)$ and to consider - in view of the finite phonon-lifetime - a nonzero attenuation coefficient (γ).

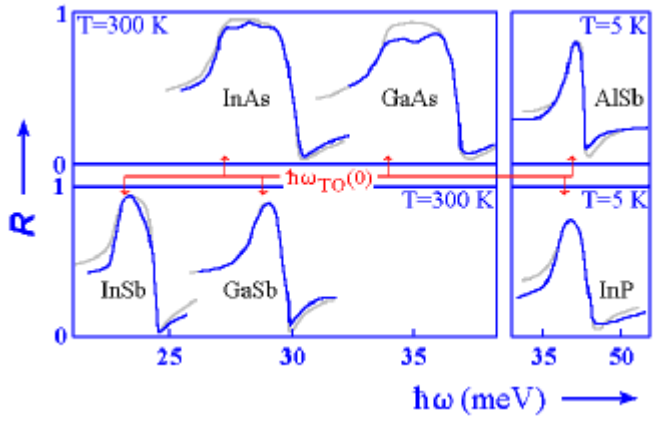

Fig. 8.5

Fig. 8.5 shows corresponding reflection bands of some III-V semiconductors (—, reflectivity R against $\hbar\omega$ after [26]). The $\hbar\omega_{TO}(0)$ values are marked in the Figure. The spectra largely agree with the expected behaviour, in particular, the maximum values are close to unity (almost perfect reflection). The grey curves have been calculated from the oscillator model [26] (fitting parameters ε_{oo}, ω_0, A, and γ, compare Appendix 4).

The reflection band is often referred to as ***Reststrahlbande***. This German term which means "residual ray band" is related to the historically first method for spectral decomposition of infrared radiation: After multiply reflecting the radiation emitted by an infrared source, at a set of crystals consisting of the same material (NaCl in the historical experiments), the part lying in the range of maximum reflectivity will be dominant, i. e. originate from a relatively narrow region of the spectrum. (Later on, the strong ω dependence of the refraction index in the range close to the $\omega_{TO}(0)$ resonance (Fig. A5c) was used for spectral decomposition by means of prisms.)

8.3 Higher-Order Dipole Moments / Multiphonon Transitions

As an example of a higher-order dipole moment we discuss here the influence of a second-order dipole moment ($\mathbf{M}_2$). The procedure is analogous to the treatment of $\mathbf{M}_1$ in Section 8.2.

We replace $\mathbf{M}$ in Equ. (8.3) by $\mathbf{M}_2$ (Equ. (8.5)) and insert this into the matrix elements in Equ. (8.2). This results in several types of matrix elements including

(8.12) $\langle f|b_{\mathbf{q}j}^{+}\, b_{\mathbf{q}'j'}^{+}|i\rangle$, $\langle f|b_{\mathbf{q}j}^{+}\, b_{\mathbf{q}'j'}|i\rangle$, $\langle f|b_{\mathbf{q}j}\, b_{\mathbf{q}'j'}^{+}|i\rangle$ and $\langle f|b_{\mathbf{q}j}\, b_{\mathbf{q}'j'}|i\rangle$

Arguments analogous to the considerations following Equ. (8.9) and (8.10) lead to the conclusion that ***two-phonon transitions*** occur under the action of $\mathbf{M}_2$. More precisely - bearing in mind the matrix elements in Equ. (8.12) as well as the energy balance - the following kinds of transitions are obtained

(8.13a) Generation of two phonons: $\hbar\omega = \hbar\omega_j(\mathbf{q}) + \hbar\omega_{j'}(\mathbf{q}')$ → [a] (Sum process)

(8.13b) Generation and annihilation of one phonon: $\hbar\omega = \hbar\omega_j(\mathbf{q}) - \hbar\omega_{j'}(\mathbf{q}')$ → [b1] → [b2] (Difference processes)

(8.13c) Annihilation of two phonons: $\hbar\omega = \hbar\omega_j(\mathbf{q}) + \hbar\omega_{j'}(\mathbf{q}')$ → [c] (Sum process)

We illustrate these processes in the Figures [a], [b1], [b2] and [c], representing photons and phonons by → and →, respectively. Obviously, in the cases [a] and [b1 we are concerned with the absorption of photons, in the cases [b2] and [c] with the induced emission of photons. Transitions of type [a] und [c] are referred to as ***sum processes***, transitions of type [b1] und [b2] ***difference processes***.

There are selection rules with respect to the propagation vectors also for two-phonon processes; viz.

(8.14) $\mathbf{q} \pm \mathbf{q}' = 0$

where the + and - signs denote sum and difference processes, respectively. These selection rules can be interpreted as momentum balances for the "collisions" of types [a] to [d] (generalization of the collision concept, compare Section 2.1), taking into account that the photon momentum (originally on the right-hand side of Equ. (8.14) is negligible. There is no selection rule with respect to the bands involved (j, j'). We now show examples of type [a] and [b1] transitions in Fig. 8.3b (↑↑).

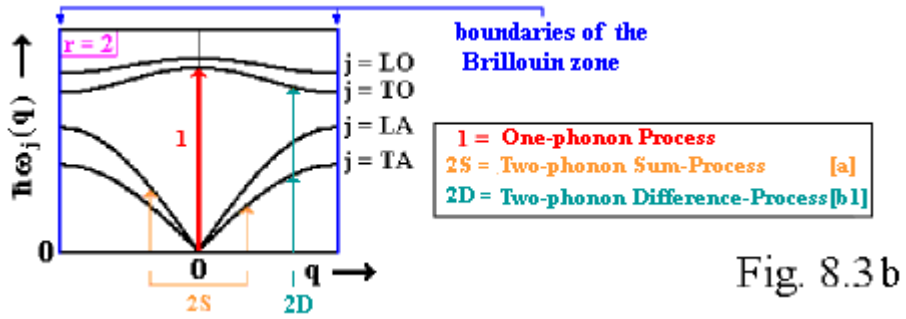

Fig. 8.3b

The dipole moments of higher than second order give rise to corresponding transitions of higher order; the probability of such transitions generally decreases wifh growing order.

Now we supplement our Table which has been set up earler for listing the relevant processes:

mechanism	processes	band	momentum balance	energy balance	type of material
first-order dipole moment ($\mathbf{M}_1$)	one-phonon processes	j = TO	$\mathbf{q} = 0$	$\hbar\omega = \hbar\omega_{TO}(0)$	polar
second-order dipole moment ($\mathbf{M}_2$)	two-phonon processes	no restriction	$\mathbf{q} \pm \mathbf{q}' = 0$	$\hbar\omega = \hbar\omega_j(\mathbf{q}) \pm \hbar\omega_{j'}(\mathbf{q}')$	polar and non-polar
:	:	:	:	:	:

In the following we try to find out what kind of absorption spectrum is to be expected for two-phonon transitions. We first consider the case of sum processes, using Equ. (8.13a) and (8.13c), as well as Equ. (8.14) with the + sign. We get

(8.15) $\hbar\omega = \hbar\omega_j(\mathbf{q}) + \hbar\omega_{j'}(\mathbf{q})$

Here we have taken into account the relation $\omega_{j'}(-\mathbf{q}) = \omega_{j'}(\mathbf{q})$ (see Section 7.1). We represent in **Fig.8.6** the right-hand side of this equation in a schematic picture, along a straight line in $\mathbf{q}$ space. Starting fron Fig. 7.4 we have considered various combinations of j and j'. According to Equ. (8.15) experiment yields all "two-phonon states" ($\mathbf{q}$, j, j') for which the ordinate in Fig. 8.6 is equal to the chosen photon energy $\hbar\omega$ ("determined by tuning the monochromator"). We have included $\hbar\omega$ with the suitable slitwidth (═) in **Fig.8.6**.

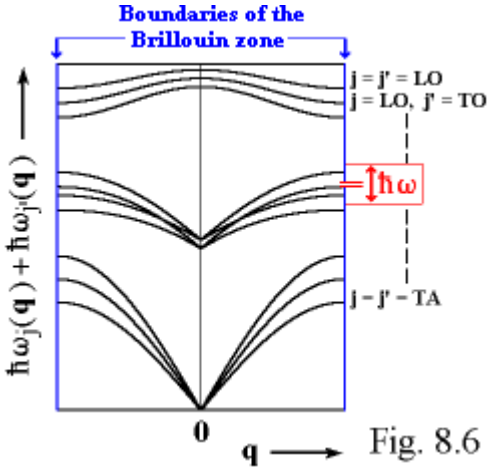

Fig. 8.6

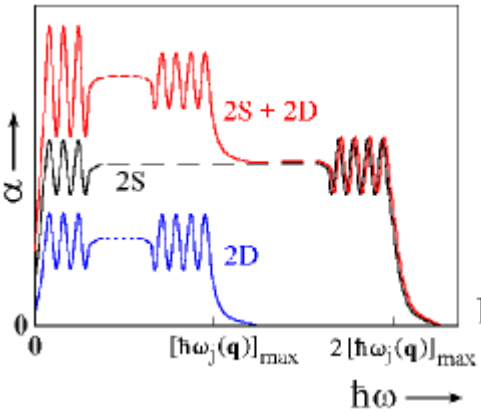

Fig. 8.7

The absorption spectrum then results essentially from the number of two-phonon states falling into the slitwidth interval,

for the various $\hbar\omega$ values. In qualitative respect, the following features can be inferred from Fig. 8.6:

- We are concerned with a continuous spectrum.
- There is a high-energy limit of the spectrum, viz. at $\hbar\omega = 2 \times [\hbar\omega_j(\mathbf{q})]_{max}$.
- The spectrum has structure, because the number of two-phonon states is strongly $\hbar\omega$ dependent. The number of two-phonon transitions that can occur in the slitwidth interval increases with the slope of the functions $\hbar\omega_j(\mathbf{q}) + \hbar\omega_{j'}(\mathbf{q})$.

The discussion of difference processes is performed in an analogous way. Equ. (8.13b) and (8.14) (- sign) yield

(8.16) $\hbar\omega = \hbar\omega_j(\mathbf{q}) - \hbar\omega_{j'}(\mathbf{q})$

On the basis of a diagram similar to Fig. 8.6 we find that the spectrum has properties analogous to that of sum processes. The main difference is that now the high-energy limit is at $[\hbar\omega_j(\mathbf{q})]_{max}$ (in Equ. . (8.16) realized by the fact that the first term on the right-hand side has a maximum, and the second term has a minimum (equal to zero)).

We illustrate in Fig. 8.7 the spectral regions of sum processes (2S) and of difference processes(2D), which, of course, are superposed in experiment (2S + 2D).

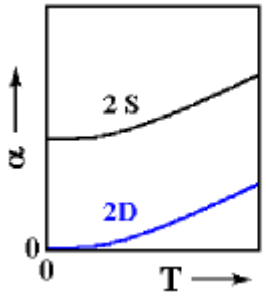

Fig. 8.8

In order to decide whether a certain peak in an experimental spectrum is due to a sum process or a difference process one can make use of the different temperature dependences of the two kinds of transitions: In case of type [b1] and [b2] transitions (Equ. (8.13b)) we are dealing with a collision of a photon with a phonon which is already present in the crystal. The frequency of such collisions is, of course, dependent upon the number of suitable "offered" phonons. This number tends to zero when approaching absolute zero temperature (Bose distribution, Equ. (7.18)), the same occurs with the intensity of the peaks due to difference processes. In contrast, type [a] (Equ. (8.13a)) sum processes can also take place at the lowest temperatures. Strictly speaking, the frequency of these processes also decreases on cooling; however, a considerable amount is left (Fig. 8.8). This temperature dependence of the sum processes can be explained by the fact that the "induced emission of phonons" occurs less frequently due to the decreased number of phonons, while the "spontaneous emission of phonons" is not affected by this trend.

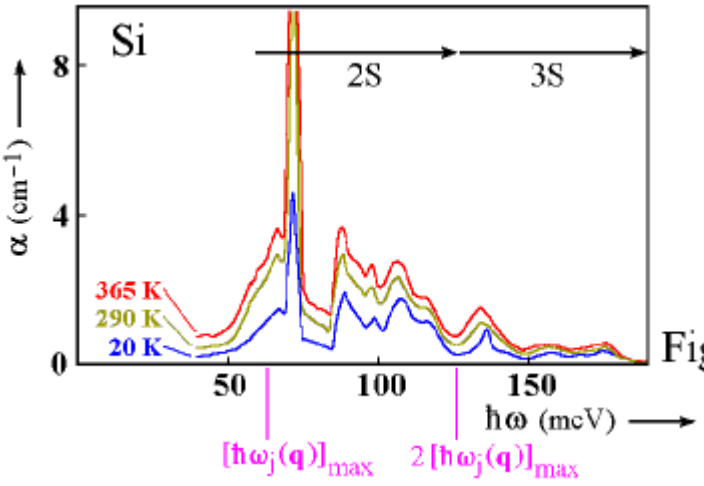

Fig. 8.9

Multiphonon transitions can be studied in a most convenient way for nonpolar materials, because there is no interference by one-phonon processes. (In the case of polar materials, $\hbar\omega_{TO}(0)$ is usually located just within the two-phonon spectrum Fig. 8.7.) In Fig. 8.9 we show the absorption spectrum of Si due to multiphonon transitions, measured [27] at three temperatures. Here the absorption coefficient α is plotted against $\hbar\omega$. In the case of Si $[\hbar\omega_j(\mathbf{q})]_{max}$ is about 63 meV; the

corresponding limits of the two-phonon sum and difference region are included in the diagram. In addition, *three-phonon*

sum processes (3S) are observed here, which make a relatively great contribution for this material. As expected, a

spectrum with appreciable structure is found, which, in the range considered, solely originates from sum processes. As the temperature is lowered, the light intensity decreases in the way expected.

The structures were used to get information about phonon dispersion curves $\hbar\omega_j(\mathbf{q})$. Thereby a certain model for the force constants was employed (dependence on $nk\alpha$, range of action). Considering these quantities as fitting parameters, ($\hbar\omega_j(\mathbf{q}) + \hbar\omega_{j'}(\mathbf{q})$) diagrams as Fig. 8.6 were obtained. By choosing the values of the force constants, line positions and line intensities could be described quantitatively. Hence, in this way it was possible to get reliable results on the phonon dispersion curves of Si, consistent with data from other methods of investigation (e. g. inelastic scattering of neutrons).

It is apparent from the ordinate values in Fig. 8.9 that the absorption due to multphonon transitions is very weak (compared with the intensity of one-phonon peaks). Such spectra can be measured with adequate accuracy only if relatively thick samples of sufficient purity are available. A low impurity content is especially important, since impurities give rise to interfering contributions of comparable intensity in the relevant spectral region (e. g. transitions at impurity centers and intraband transitions). In this respect, Si is a positive example because of the highly developed crystal-growth technology for this material.

8.4 Final Remarks

In the present Chapter we have dealt with the basic aspects of spectra due to phonon transitions. It should be mentioned that phonon spectroscopy has also become an important tool for the characterization of materials. This concerns, in particular, analysing the composition and structure of mixed systems, and studies of "defect centers" giving rise to ***local modes*** and ***resonance modes*** .

A most informative methodic variant which has not been discussed here is ***Raman spectroscopy***. This method involves measuring a component of light scattering, in which the light frequency is changed due to the interaction between the electron system and the phonon system. In a future extension of this course the basic ideas of Raman spectroscopy will be included.

Appendices

Appendix 1. Elementary Experimental Procedures

In this Appendix we briefly consider simple arrangements for measuring spectra of upward and downward transitions. (For didactic reasons we have included part of this discussion in Section 2.2, where the connection between optical transitions and experimental quantities plays a role for the first time.) Upward transitions manifest themselves mainly in absorption and reflection spectra, while downward transitions make their appearance in luminescence spectra.

For studying **upward transitions** (excitation transitions) one freqently uses a combination of transmission and reflection measurements; see Fig. A1.

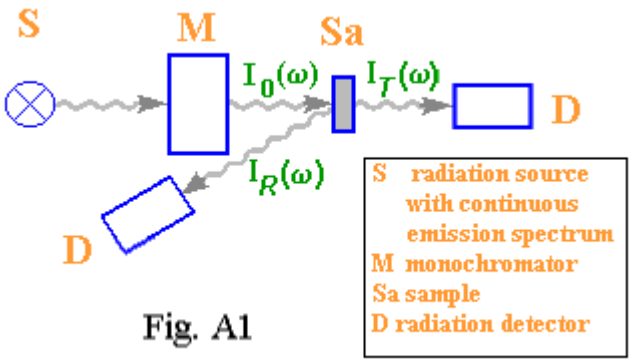

Fig. A1

At each frequency **ω**, to which the monochromator is tuned, the intensities transmitted and reflected by the sample, $I_T(\omega)$ and $I_R(\omega)$, respectively, are measured, and, in addition, in a "blank test", the incident intensity $I_0(\omega)$. Then one has, in simple cases (e. g. cubic symmetry, no interference effect)

(A1.1) $\quad T(\omega) = (1 - R(\omega))^2 \, e^{-\alpha(\omega)d}$

$T(\omega) = I_T(\omega) / I_0(\omega)$ and $R(\omega) = I_R(\omega) / I_0(\omega)$ are referred to ***transmittivity*** and ***reflectivity***, respectively; d is the sample thickness; α is the ***absorption coefficient*** (dimension cm^{-1}), a quantity describing the attenuation of light per unit length.

The absorption spectrum α(ω) can be determined, after correspondingly resolving Equ. (A1.1) , from the measured functions $I_T(\omega)$, $I_R(\omega)$ and $I_0(\omega)$. Equ. (A1.1) shows that the accuracy with which α is determined critically depends on the sample thickness d. Optimum conditions are obtained if the product α d has a value about 1.

> (Because of the exponential d-dependence, the spectral variation of αhas hardly influence on $T(\omega)$ in the case of small d, while at large d-values $T(\omega)$, i. e. $I_T(\omega)$, is too small to give reliable experimental results.)

For many types of transitions (e. g. valence-band to conduction-band transitions, exciton transitions) one is dealing with α values of the order 10^4 to 10^6 cm^{-1}. Hence, in these cases ideal conditions are met for sample thicknesses of the order 10^{-5} cm = 100 nm. For many materials this can be realized by employing epitaxial layers. (Thereby the evaluation has to be done using expressions that are more complex than Equ. (A1.1) .)

If such layers are not available, it is also possible to get information on upward transitions from reflection spectra $R(\omega)$ (see Appendix 3 and Appendix 4), which can also be obtained by means of the arrangement shown in Fig. A1. In these experiments one can also use thicker samples.

The observation of luminescence spectra aiming at the investigation of downward transitions (deexcitation transitions) requires a supply of energy "from outside" ("excitation"). Depending on the type of energy supply, these measurements are referred to as studies of photo-, cathodo-, electrotroluminescence e. t. c. Here we only deal with photoluminescence, involving excitation by optical irradiation. The principle of the experimental arrangement is shown in Fig. A2 .

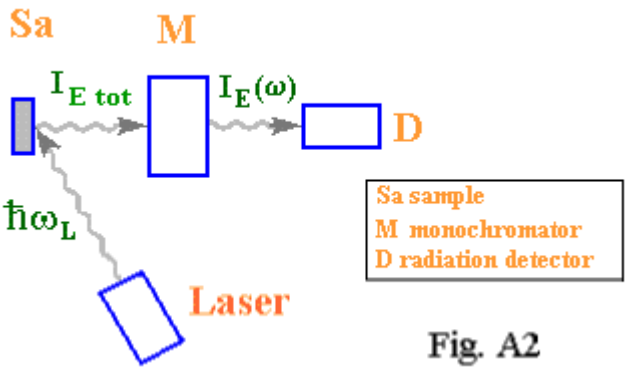

Fig. A2

Generally the excitation leads to the emission of a whole spectrum of photon energies (totat intensity I_{Etot}). Then the spectral decomposition is performed by the monochromator (emerging intensities $I_E(\omega)$). The photon energy $\hbar\omega_L$ of the laser employed for the excitation is chosen corresponding to the downward transition to be studied (usually $\hbar\omega_L > \hbar\omega$).

Appendix 2. Material Parameters Describing the Effect of the Radiation Field

As we know, radiation acting on a solid leads, under certain conditions, to upward transitions which manifest themselves in the absorption spectrum. However, there are further effects of such transitions noticable in other optical properties, such as refraction and reflection (see Appendix 4 for a physical discussion). Starting from Maxwell's equations, the overall reaction of the solid is described in terms of (ω dependent) material parameters [1].

In solid state spectroscopy it is customary to work with two combinations of parameters (dimensionless quantities):
- using a ***complex refractive index***:

(A2.1) $\eta(\omega) = n(\omega) + i\,\kappa(\omega)$

(n normal ***refraction index***, κ ***absorption index***) or
- using a ***complex dielectric function***

(A2.2) $\varepsilon(\omega) = \varepsilon_1(\omega) + i\,\varepsilon_2(\omega)$.

The two variants are connected through the relations

(A2.3) $\eta^2 = \varepsilon, \quad \varepsilon_1 = n^2 - \kappa^2, \quad \varepsilon_2 = 2n\kappa$

(limiting ourselves to the case of nonmagnetic materials and cubic symmetry).

Of the optical phenomena determined by these parameters, the properties of upward transitions are reflected in the most direct way by the phenomenon of *absorption*. Hence, if possible, the latter effect is used for getting information on those transitions. In Appendix 1 we describe a procedure involving transmission measurements. The absorption coefficient $\alpha(\omega)$ determined in these measurements can be used to evaluate the absorption index by means of

(A2.4) $\alpha(\omega) = 2\,\kappa(\omega)\,\omega / c$

The physical relation between the parameters will be discussed in Appendix 4, on the basis of an oscillator model.

Appendix 3. Evaluation of Reflection Spectra by Means of Kramers-Kronig Analysis

In Appendix 1 we have illustrated how absorption spectra can be determined by means of transmission measurements. As we have mentioned, this procedure is applicable only if sufficiently thin samples are available. In the absence of such samples, the desired information can be obtained *from pure reflection data* using the method described in the following. That method can be applied in all cases in which the transitions of interest have a sufficiently strong effect on the reflection spectrum (e. g. valence-band to conduction-band transitions, exciton transitions).

In order to explain the procedure, we consider the reflection from a thick sample for normal incidence of radiation. In this case, the reflectivity is given by

(A3.1) $R(\omega) = [(n(\omega) - 1)^2 + \kappa(\omega)^2] / [(n(\omega) + 1)^2 + \kappa(\omega)^2]$.

Here n is the refractive index, κ the absorption index (Appendix 2). Hence, for each ω, the measurement of R yields only *one* combination of the two quantities n and κ. In principle, a second combination of n and κ can be obtained by measuring, in addition, the phase shift ψ appearing for reflection:

(A3.2) $\psi(\omega) = - 2\kappa(\omega) / [n(\omega)^2 + \kappa(\omega)^2 - 1]$

Since measurements of phase shifts are relatively difficult and time-consuming, these are avoided by using a so-called ***Kramers-Kronig relation*** between R and ψ:

$$(A3.3)\quad \psi(\omega) = -\frac{\omega}{\pi}\, P\int_0^{\infty} \frac{\ln R(\omega')}{\omega'^2 - \omega^2}\, d\omega'$$

Here P is the principal value of the integral. Equ. (A3.3) means that one has only to measure the quantity R, which is needed in any case (Equ. (A3.1)) . However, a sufficiently large spectral range has to be covered. From this Equation, ψ (ω) is obtained by numerical integration. Inserting the result into Equ. (A3.2), one has, together with Equ. (A3.1) , two equations for the two unknown quantities n and κ. If desired, one can get from these, with the aid of Equ. (A2.3) (Appendix 2), the real and imaginary part of the dielectric function ε(ω).

Appendix 4. Optical Spectra in the Oscillator Model

In this Appendix we shall discuss the response to the radiation field of a system having discrete energy levels, and the corresponding optical spectra. Examples are spectra in the exciton and phonon regions (Sections 5.2 and 8.2).

> Strictly speaking, in all these cases one is dealing with *continuous energy spectra*, in which, due to *selection rules*, only transitions into single levels are possible, see e. g. Fig. 5.3 in Chapter 5 (exciton transitions). Thus, in discussions of the optical behaviour, one can pretend to be concerned with discrete levels.

The following point is of particular importance: Optical upward transitions, i. e. transitions with the absorption of radiation, can, of course, occur only if the photon energy ħω coincides with the separation of the corresponding levels, ΔE . However, there is also an effect of the radiation field in cases when ħω somewhat deviates from ΔE (Fig. A3). In such cases the system remains in the ground state, but a field-induced "admixture" of states of the upper level (time-dependent with the field frequency ω) occurs. One result is a time-dependent (electric and / or magnetic) polarization of the material [1].

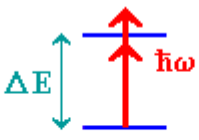

Fig. A3

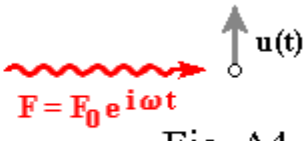

Fig. A4

A system for which the situation can be discussed - and generalized later on - in a most simple manner, is the one-dimensional harmonic oscillator. This system has only discrete energy levels. It is found that the optical behaviour comes out in an essentially correct way, if we consider the *classical* instead of the quantum mechanical oscillator. For easier illustration we begin with the classical case.

Classical Oscillator

Let us consider a classical oscillator with mass M, spring constant K, eigenfrequency (in the absence of attenuation) $\omega_0 = (K/M)^{1/2}$ and charge Q, which performs forced vibrations under the influence of the electric field $F = F_0 e^{i\omega t}$ of an electromagnetic wave (F_0 amplitude, ω frequency), see Fig. A4. Referring to the displacement at time t as u(t), we have the equation of motion

(A4.1) $M\, u''(t) = -K\, u(t) + Q\, F_0\, e^{i\omega t} - M\gamma\, u'(t)$

On the right-hand side, the first term is the restoring force, and the second term is the force due to the electric field. The third term describes the ***attenuation***, which we assume, as usual, to be proportional to the first derivative with respect to the time, of the dicplacement. γ (> 0) is the so-called attenuation coefficient. For formal reasons, the quantity M is incorporated in the proportionality factor.

It is well known that Equ. (A4.1) can be solved by putting $u(t) = u_0 \, e^{i(\omega t + \phi)}$: The oscillations occur with the field frequency ω, and are phase-shifted relative to the field by the angle ϕ. u_0 is the real amplitude. Calculation [28] yields

(A4.2) $u_0 = (Q \, F_0 / M) / [(\omega_0^2 - \omega^2)^2 + \gamma^2 \, \omega^2]^{1/2}$

(A4.3) $tg \, \phi = - \gamma \, \omega / (\omega_0^2 - \omega^2)$

Let us now regard a system of oscillators of the same kind (N oscillators per unit volume). The reaction of this system to the field can be described by the complex dielectric function

(A4.4) $\varepsilon \, (\omega) = 1 + (4\pi \, Q^2 \, N / M) \, [(\omega_0^2 - \omega^2) + i \, \gamma \, \omega] / [(\omega_0^2 - \omega^2)^2 + \gamma^2 \, \omega^2]$

Application to Solids

Surprisingly, the results can be applied, with minor modifications, to solid-state excitations of the kind mentioned earlier, although these have quantum-mechanical character, and their energy spectra substantially deviate from that of the harmonic oscillator: One has simply to identify ω_0 with $\Delta E / \hbar$ (Fig. A3) and to modify Equ. (A4.4) in the following way:

- The prefactor of the second term in Equ. (A4.4), $4\pi \, Q^2 \, N / M$, is replaced by a new (calculable) quantity, which we shall call A.
- We take into account that in the ω range around the excitation frequency ω_0 there are generally other (higher-frequency) excitations contributing to the real part of $\varepsilon(\omega)$ (a physical explanation will be given later). This effect is described by substituting the quantity "1" in Eq. (A4.4) by a real constant ε_{oo} (> 1)

In this way we get:

(A4.5) $\varepsilon \, (\omega) = \varepsilon_{oo} + A \, [(\omega_0^2 - \omega^2) + i \, \gamma \, \omega] / [(\omega_0^2 - \omega^2)^2 + \gamma^2 \, \omega^2]$

and, separately, for the real and the imaginary part:

(A4.6) $\varepsilon_1(\omega) = \varepsilon_{oo} + A \, [(\omega_0^2 - \omega^2)] / [(\omega_0^2 - \omega^2)^2 + \gamma^2 \, \omega^2]$

(A4.7) $\varepsilon_2(\omega) = A \, \gamma \, \omega / [(\omega_0^2 - \omega^2)^2 + \gamma^2 \, \omega^2]$

ε_2 characterizes the absorption of radiation (transitions from the ground state to an excited state), ε_1 describes the radiation-induced polarization of the solid-state system (admixture effect, discussed previously)

The attenuation coefficient γ entering Equ. (A4.5) to (A4.7) characterizes the transfer of excitation energy to "oscillators" which do not interact directly with the radiation field (e. g. in the exciton case the energy transfer to states with nonzero $\mathbf{K}$, see Section 5.2). In principle, such complicated processes lead to an ω dependence of γ, which, however, can be usually neglected.

Optical Spectra in the Oscillator Interpretation

In the following Fig. A5 we present the ω dependences of the relevant quantities for the set of parameters

$\varepsilon_{oo} = 5, \; A / \omega_0^2 = 1, \; \gamma / \omega_0 = 0.01$

We shall discuss these dependences in the classical oscillator picture.

As to be expected, the amplitude of the oscillations u_0 (Equ.(A4.2)) shows resonance behaviour (sharp peak at $\omega = \omega_0$, see Fig.A5a). At frequencies well below ω_0, the phase shift ϕ (Equ. (A4.3)) is practically zero. As the frequency increases, a delay gradually develops (ϕ smaller than zero). After passing the resonance, the oscillation rather abruptly

goes out of phase ($\phi = -\pi$).

The ω dependence of the optical quantities can be explained by taking into account the variation of u_0 and ϕ:

$\varepsilon_2(\omega)$ (Gl. (A4.7)) describes , as visible in **Fig.A5b**, an absorption line at ω_0, corresponding, as to be expected, to the $u_0(\omega)$ curve. The magnitude of the quantity ε_1(Equ.. (A4.6)), which is determined by the dielectric polarization, is found to increase when approaching the resonance frequency. The phase behaviour $\phi(\omega)$ (Fig. A5a) is the reason why ε_1 has positive values in the ω region below ω_0, and , on passing ω_0, jumps to negative values. (As ω grows, ε_1 generally becomes positive again, due to the ε_{oo} term.)

Fig.A5c shows the ω dependences of the refraction index n and of the absorption index κ (see Appendix 2), which are obtained by reversing Equ. (A2.3)

(A4.8) $\quad n = [(1/2)(\varepsilon_1 + (\varepsilon_1^2 + \varepsilon_2^2)^{1/2}]^{1/2}$

(A4.9) $\quad \kappa = [(1/2)(-\varepsilon_1 + (\varepsilon_1^2 + \varepsilon_2^2)^{1/2}]^{1/2}$

from $\varepsilon_1(\omega)$ and $\varepsilon_2(\omega)$. $n(\omega)$ is mainly determined by $\varepsilon_1(\omega)$. At a greater distance from the ε_2- absorption line one has approximately $n(\omega) = \varepsilon_1(\omega)^{1/2}$. Near ω_0 the transition of ε_1 to the negative region manifests itself by a jump of n to very small values. $\kappa(\omega)$ corresponds, as expected, to an absorption line at approximately ω_0.

Finally, making use of Gl. (A3.1), we get the ω dependence of the reflectivity R shown in **Fig.A5d**

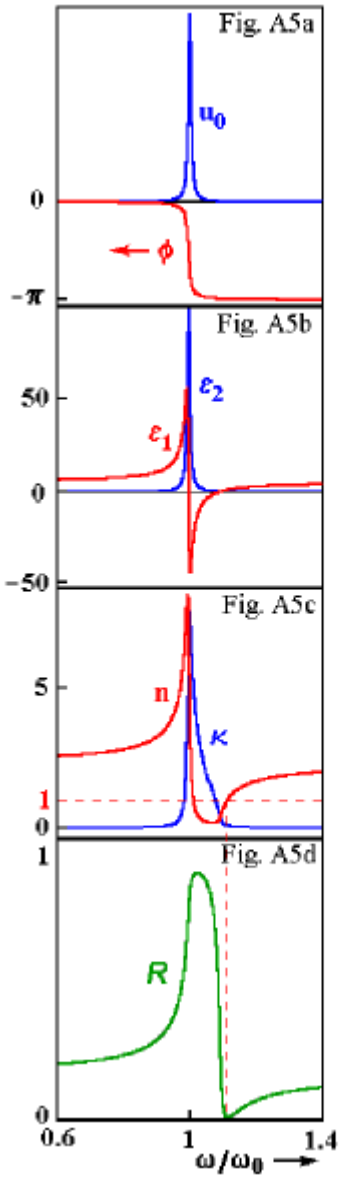

Fig. A5

(A4.10) $R = [(n - 1)^2 + \kappa^2] / [(n + 1)^2 + \kappa^2]$

Outside the κ absorption line R is mainly determined by n. As ω_0 is approached from small ω, R increases due to the growth of n.

Beyond ω_0 R nearly reaches unity (perfect reflection) . This originates from the small value that n assumes in this region. Later we have a steep drop to zero, afterwards R slowly increases again. The position of the steep edge approximately corresponds to the higher-energy zero of $\varepsilon_1(\omega)$. The R value of zero is located near the point where n, during its rise, passes unity. The vanishing of the reflection is due to the fact that at this frequency the radiation practically does not feel the border between vacuum and the medium, because in both regions the refraction index (and also ε_1) has the value unity.

In cases where transmission studies are impossible, the pronounced structure in $R(\omega)$ enables one to obtain information on excitations of the type of interest from reflection measurements.

The width of the structures under consideration (Fig. A5) strongly depends upon the parameter ratio γ / ω_0, the structure becoming sharper as this ratio decreases.

In conclusion, we shall deal with the reason for introducing the parameter ε_{oo} in Equ. (A4.5), referring to Fig. A5b: Passing through ω_0 from high to low ω values we see that (according to Equ. (A4.6)) ε_1 increases by A / ω_0^2 in the horizontal regions. Physically, this is due to the fact that the oscillators can follow a field frequency well below ω_0, but not a field frequency considerably above ω_0. Hence, all other types of oscillators having eigenfrequencies *higher* than ω_0 contribute to the ε_1 values of the considered oscillator, and this is taken into account by introducing the quantity ε_{oo}.

Supplements

Supplement 1. Occupation of the Energy Bands with Electrons

First we should note that only a finite number of electrons can be accommodated in each band (ν) of a crystal of finite size. This is because only a finite number of **k** vectors really correspond to Bloch states $\psi_{k\,\nu}(\mathbf{r})$. These **k** vectors form a fine-mesh network with equidistant net points in the Brillouin zone. We illustrate this behaviour in our $E_\nu(\mathbf{k})$ diagram (introduced in Fig. 1.4) (Fig. E1, see the magnifying-glass symbol on the **k** axis). The total number of allowed **k** vectors is equal to the number of unit cells (N_c) in the crystal, i. e. of the order 10^{22} to 10^{23} in a macroscopic crystal.

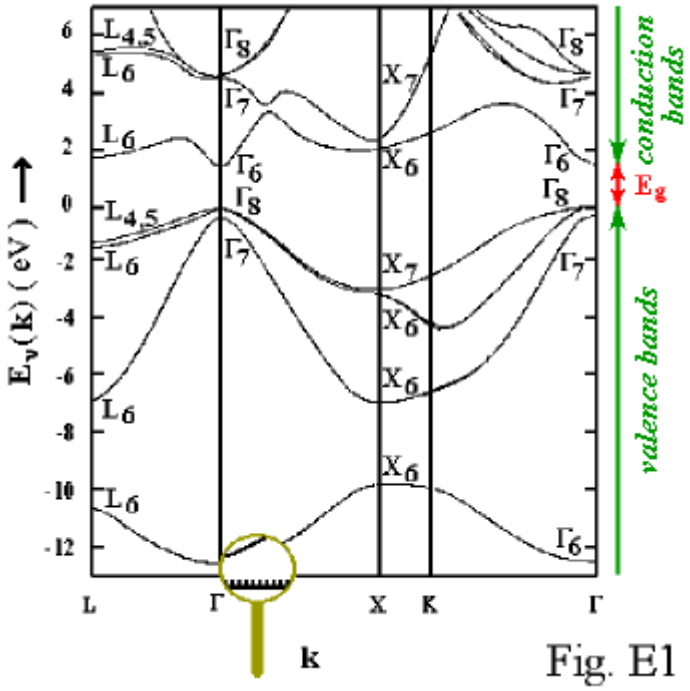

Fig. E1

In most discussions one can ignore the discrete structure of **k**. However, this structure is significant when dealing with the occupation of the states with electrons. According to our earlier remarks, a maximum number of 2 N_c electrons can be accommodated in each band (ν) . The factor 2 results from the two possible directions of spin.

Imagine that the electrons which are supplied by the atoms constituting the crystal are inserted in states with energies as low as possible. Following this procedure one finally arrives at a maximum energy (E_M) of occupied states. E_M approximately corresponds to the Fermi energy [3]. The position of this energy in the $E_\nu(\mathbf{k})$ diagram determines the basic properties of the material in question. The most important cases that can occur are

1. E_M is located within a band
2. E_M is located at the upper edge of a band, which is joined, without a gap, by further band states (contact or overlap of bands)
3. E_M is located at the upper edge of a band, which is followed by a gap

In cases 1. and 2. we are dealing with ***metals***, in case 3. with ***non-metals***. The non-metals are usually subdivided, depending on the magnitude of E_g into ***semiconductors*** ($E_g < 3$ eV) and ***insulators***($E_g > 3$ eV), the dividing line being, of course, arbitrary from the physical point of view. In this sense, GaAs (with E_M above the valence bands) is a non-metal or semicondoctor.

One of the most significant differences between metals and non-metals is the magnitude of the electric conductivity: In the case of metals, an applied electric field can supply minimal portions of energy to the electrons near E_M, and thus directly generate an electric current. In the non-metal case, such an energy transfer can occur only to a very limited extent, due to the existence of a forbidden gap.

Supplement 2. Derivation of the k-Selection Rule

In order to derive the **k**-selection rule Equ. (2.5) , we write the transition matrix element between Bloch states from Equ.. (2.4) in integral form, thereby omitting constant factors and taking into account that **p** is given by (ħ/i) grad in the position vector representation:

$$(E2.1)\quad \langle \mathbf{k}'v' | W_0 | \mathbf{k}v \rangle \sim \int_{\Omega} e^{-i\mathbf{k}'\mathbf{r}}\, u_{\mathbf{k}'v'}(\mathbf{r})^*\, e^{i\mathbf{s}\mathbf{r}}\, \mathrm{grad}\left(e^{i\mathbf{k}\mathbf{r}}\, u_{\mathbf{k}v}(\mathbf{r})\right) d\mathbf{r}$$

$$= \int_{\Omega} e^{i(-\mathbf{k}'+\mathbf{s}+\mathbf{k})\mathbf{r}}\, u_{\mathbf{k}'v'}(\mathbf{r})^*\, (i\,\mathbf{k} + \mathrm{grad}\, u_{\mathbf{k}v}(\mathbf{r}))\, d\mathbf{r}$$

We extend this integral over a ***model crystal*** of macroscopic size, which, as indicated in Fig. E2 is thought to be cut from an infinite crystal and to contain only complete unit cells (range **Ω**).

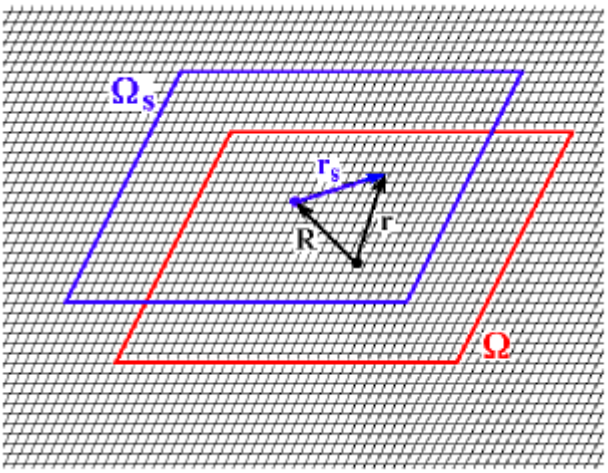

Fig. E2

(The integral has the character of a three-dimensional vector; note that in Equ. (2.2) one has a scalar product with the vector $\mathbf{A}_0$, whose direction is determined by the polarization direction of the radation.)

Now we introduce by means of

$$(E2.2)\quad \mathbf{r} = \mathbf{r}_s + \mathbf{R}$$

a new integration variable $\mathbf{r}_s$ (see Fig. E2). **R** is a lattice vector; the index n has been omitted. We see from Fig. E2 that in Equ. (E2.2) we are simply concerned with a shift of the origin of coordinates from ● to ●. Taking into account the lattice periodicity of the u's and denoting the integrand in Equ. (E2.1) with I(**r**), we get

$$(E2.3)\quad \int_{\Omega} I(\mathbf{r})\, d\mathbf{r} = e^{i(-\mathbf{k}'+\mathbf{s}+\mathbf{k})\mathbf{R}} \int_{\Omega_s} I(\mathbf{r}_s)\, d\mathbf{r}_s$$

The integral over $\mathbf{r}_s$ has the same integrand as the originat integral. However, now the integration refers to a model crystal $\mathbf{\Omega}_s$ (Fig. E2), which is displaced relative to the original model crystal **Ω** by **R** . Owing to the translation symmetry this displacement cannot affect the value of the integral. It follows that

$$e^{i(-\mathbf{k}'+\mathbf{s}+\mathbf{k})\mathbf{R}} = 1,$$

and this leads to the conditions

$$(E2.4)\quad (-\mathbf{k}'+\mathbf{s}+\mathbf{k})\,\mathbf{R} = 2\pi \times \text{integer}.$$

Since this must be true for all **R**, this relation can be fulfilled only if $-\mathbf{k}'+\mathbf{s}+\mathbf{k} = 0$. This corresponds to the selection rule Equ. (2.5). For other combinations of **k'**, **s** and **k**, Equ. (E2.3) is valid only when the integrals are zero; in these cases the interband transition is forbidden. *The crucial condition for getting this result is the translation symmetry of the system.*

Strictly speaking, the direct conclusion from Equ. (E2.4) is that $\mathbf{k}'+\mathbf{s}+\mathbf{k}$ is equal to a vector of the reciprocal lattice. However, this vector can be chosen to be zero, because Bloch states, in particular $\psi_{\mathbf{k}'v'}$, are periodic with respect to the reciprocal lattice. Since s is small, this also ensures that, together with **k**, **k'** lies in the Brillouin zone, as postulated (possibly except for a small **k** range near the zone boundary).

For a more rigorous derivation of the selection rule, see, e. g. [1].

Supplement 3. Phonon Dispersion Curves of Materials with fcc Lattice

In the following we compile some properties of the functions $\omega_j(\mathbf{q})$ (***phonon dispersion curves***) for the materials with indirect band structure, mentioned in Section 2.3. A systematic treatment of the problems related to phonons will be given in Chapter 7.

In discussions of the **q** dependence we can restrict ourselves, as in the case of the **k** dependence, to the Brillouin zone for the corresponding type of lattice . Si and Ge crystallize in the diamond structure, GaP in the zincblende structure. In all cases we are concerned with the Brillouin zone shown in Fig. 1.3.

Representing the phonon dispersion curves for a substance with zincblende structure along a straight line in the Brillouin zone which passes $\mathbf{q} = 0$, we qualitativelyget the diagram shown in Fig. E3. There are six phonon bands (j = 1, . . , 6) ; three of them are so-called acoustic bands (two transverse (TA) and one longitudinal (LA)) and three so-called optical bands (also two transverse (TO) and one longitudinal (LO)). This picture refers to a high-symmetry direction (e. g. Γ - L). In such directions the TA and TO bands coincide to give one band of each type.

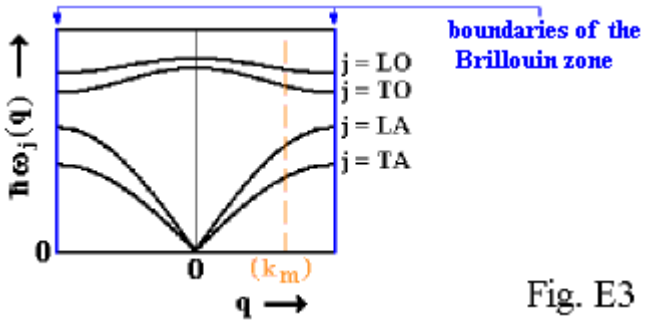

Fig. E3

The phonon energies relevant for the indirect transitions are obtained by checking the corresponding values at $\mathbf{q} = \pm \mathbf{k}_m$.

Supplement 4. Development of Conduction-Band, Valence - Band and Core States

Let us describe - in an idealizing consideration - the qualitative changes in the wavefunctions which occur when atoms are put together to form a crystalline solid. For simplicity we refer to system with a single type of atoms, using a one-dimensional picture. In Fig. E4a we first represent the situation for an isolated atom:

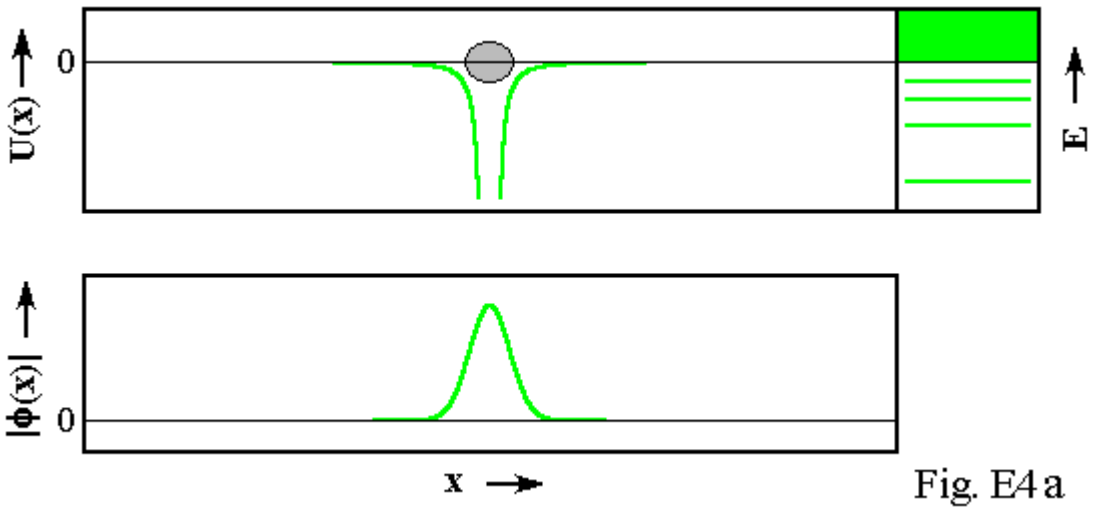

Fig. E4 a

We are dealing with an attractive potential U(x) (funnel-shaped in the simplest case) and - in the negative energy-range - with bound states having discrete energy-levels and localized wavefunctions ϕ(x), which is also illustrated in Fig. E4a (one-electron picture).

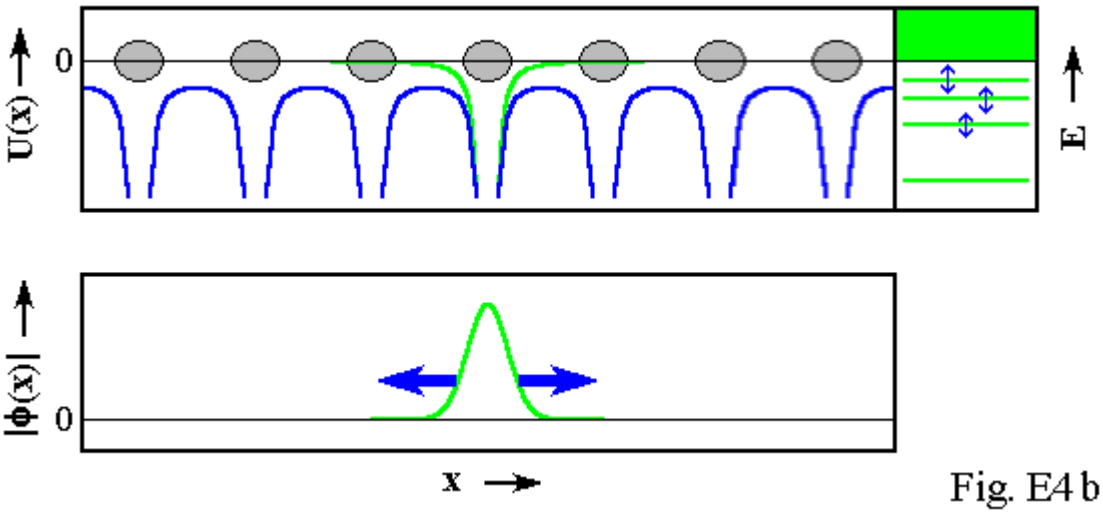

Fig. E4 b

Now we show in Fig. E4b , how , when assembling the atoms, the individual potentials are superposed to give the total potential U(x). Due to the changes in the potential, the electrons, which were originally bound to separate atoms, are now able to tunnel from atom to atom (⟷). In this process, the localized states develop into delocalized states (Bloch states, see Fig. 1.2) . This delocalization process is accompanied by the broadening of the (originally discrete) energy levels E (↕), i. e. by the formation of bands.

Qualitatively these broadening effects can be explained by the familiar energy-time uncertainty relation

(E4.1) $\Delta E\, \Delta t \gtrsim \hbar$

Accordingly, the broadening (ΔE) increases with decreasing time (Δt) of dwelling in a given funnel. The dwelling time decreases with growing probability of tunnelling, i. e. when the potential barrier for the initial energy-level becomes lower and thinner. Consequently, broadening particularly occurs for higher atomic levels.

Here we are mainly concerned with levels of valence electrons and non-occupied levels; these develop into valence bands and conduction bands, respectively. Deep atomic levels (core levels) continue to be sharp. In the latter case Δt is so large that delocalization does not occur during the interaction with the radiation field. Hence the wavefunctions of the core states determining the oscillator strengths (transition probabilities) may be regarded as atomic wavefunctions (see Equ. (3.6)).

Supplement 5. Exziton Wavefunctions

The "correct" wavefunctions, which we will refer to as $\Psi(\mathbf{r}_e, \mathbf{r}_h)$, can be described by expressions containing Bloch functions. The $\Psi(\mathbf{r}_e, \mathbf{r}_h)$ include the spatial variations *inside* the unit cells, which is not the case for the functions $\Phi(\mathbf{r}_e, \mathbf{r}_h)$ and $\phi(\mathbf{r}_e - \mathbf{r}_h)$ used in the text (compare Equ. (5.7), (5.8) and (5.12)) .

Let us illustrate this for the special case $\mathbf{K} = 0$ (exciton at rest). In this case Ψ is given, to a good approximation, by the product of Φ with the Bloch functions corresponding to the edges of the respective bands:

(E5.1) $$\Psi(\mathbf{r}_e, \mathbf{r}_h)_{\mathbf{K}=0} = \Phi(\mathbf{r}_e, \mathbf{r}_h)_{\mathbf{K}=0}\, \Psi_{\mathbf{k}=0,\,c}(\mathbf{r}_e)\, \Psi_{\mathbf{k}=0,\,v}(\mathbf{r}_h) = V^{-1/2}\, \phi(\mathbf{r}_e - \mathbf{r}_h)\, \Psi_{\mathbf{k}=0,\,c}(\mathbf{r}_e)\, \Psi_{\mathbf{k}=0,\,v}(\mathbf{r}_h).$$

Here we have taken into account Equ. (5.7) and (5.8). We illustrate this in Fig.E5, where we present, in the lower part, the dependence on the electron coordinates $\mathbf{r}_e$ *for a fixed position of the hole* $\mathbf{r}_h = 0$, along a straight line passing through atoms of the same type. Here we have been guided, with respect to ϕ, by Equ. (5.12). For comparison we show, in the upper part of Fig. E5, the Bloch function $\Psi_{\mathbf{k}=0,\,c}(\mathbf{r}_e)$ (being equal to the corresponding Bloch factor, see Fig. 1.2). Evidently, in Ψ the oscillation amplitudes, appearing in the atomic regions, diminish more and more, as the distance from the hole increases, which is due to the factor ϕ. Because of the magnitude of a_{exz} (Fig. 5.2), this decrease is a relatively slow process: The probability of finding the electron (proportional to $|\Psi|^2$) is still significant for large distances from the hole.

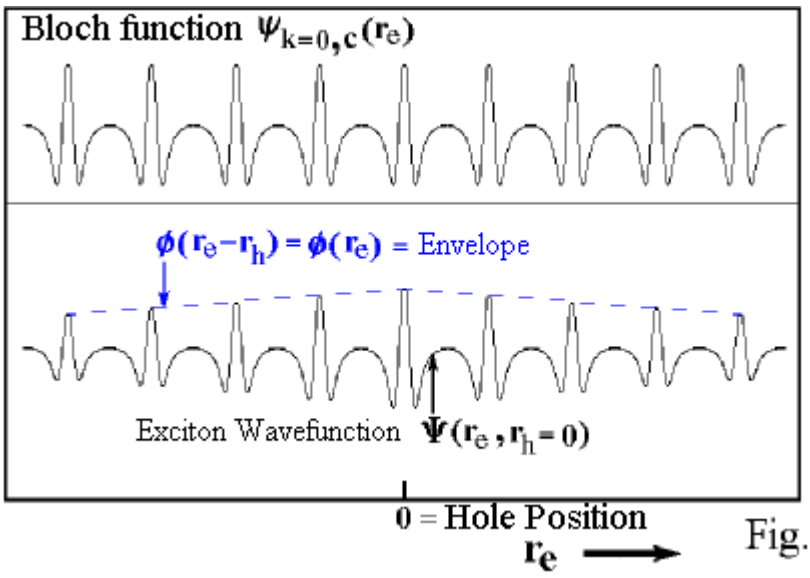

Fig. E5

$\phi(\mathbf{r}_e - \mathbf{r}_h)$ is often referred to as ***envelope function***; this is suggested by Fig. E5.

Of course, an analogous situation is found for the $\mathbf{r}_h$ dependence in the case of fixed $\mathbf{r}_e$.

Supplement 6. Relation Between the K- and the k-Selection Rule

In the case of optical transitions involving the creation or annihilation of electron-hole pairs, Equ. (5.16) is equivalent with the **k** selection rule in the simple way of consideration . In this case **K** should be composed additively of contributions of the electron and the hole:

(E6.1) $\mathbf{K} = \mathbf{k}_e + \mathbf{k}_h$

If the hole concept is defined correctly [1, 3], $\mathbf{k}_h$ is equal to the negative **k** vector of the electron missing in the valence band ($\mathbf{k}_v$). Renaming $\mathbf{k}_e = \mathbf{k}_c$, we get from $\mathbf{K} = 0$ and Equ. (E6.1) the old selection rule

(E6.2) $\mathbf{k}_c = \mathbf{k}_v$.

Supplement 7. Molecular Beam Epitaxy (MBE)

This is a method for producing layers or layer systems with crystalline structure.

We explain the principle of this technique in Fig. E6, for the example of the elementary components Ga, Al, and As. We are dealing with an ultrahigh-vacuum system containing so-called ***effusion cells*** (***Knudsen cells***) for the evaporation of the components, and the so-called substrate, on which the layers are to be grown. Usually a massive crystalline material of similar composition and crystal structure is chosen as substrate material, in our example normally massive GaAs.

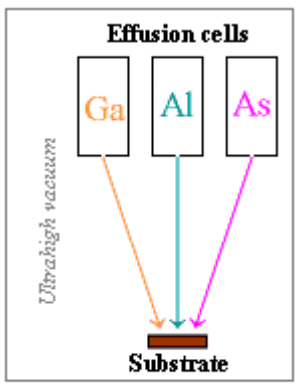

Fig. E6

The effusion cells are containers which are closed except for a very small hole opposite the substrate. On heating the cell,

a fine vapour beam ("molecular beam") of the corresponding element, which is directed toward the the substrate with the help of diaphragms, is emitted. The elementary material is condensed on the substrate, thereby reacting with the elements emerging from the other cells, thus forming the desired types of compound.

By choosing the temperatures of the effusion cells one can adjust the evaporation rates (and, consequently, condensation rates) as desired, and, in particular, realize a slow, controlled kind of crystal growth. The establishment of low growth rates is very important for getting high crystallographic perfection (i. e. small concentrations of defects).

The properties of the resultant layers are also dependent on the substrate temperature, which is usually about some hundred ^{o}C. The low growth-temperature, together with the ultra-high vacuum conditions, result in a degree of purity which is much better than that of crystals grown by classical techniques (usually occurring at temperatures about one thousand ^{o}C or higher).

The composition of the layer material, in the present case the Ga-As mixing ratio (x-value), is generally controlled by varying the temperatures of the effusion cells. (For producing the GaAs (x = 0) layer, the Al cell is blocked with a shutter.)

Finally, the materials can be *doped* with impurity atoms by adding further effusion cells. This is frequently done to generate certain kinds and concentrations of current carriers, by incorporating donor or acceptor impurities (see e. g. the systems discussed in Sections 6.3 und 6.4).

Supplement 8. States of Quantum Wells in the Case of Infinite Band-Offset

In the case of an infinitely large offset U_0, the function $U_c(z)$ (see Fig. 6.3) represents a square well potential with infinitely high walls. In this case we are concerned only with discrete energy levels. Consequently, the whole ε spectrum (Equ. (6.3) und (6.4)) is discrete. For these levels (ε_N) and the corresponding wavefunctions ($\chi_N(z)$) one is then dealing with simple explicit expressions:

(E8.1) $\varepsilon_N = (\hbar^2/2m_c^*(A))\,(\pi / d)^2\, N^2$ N = 1,2,....

(E8.2) $\chi_N(z) = C \cos(N\pi z / d)$ for N = 1,3,5,....

$\chi_N(z) = C \sin(N\pi z / d)$ for N = 2,4,6,....

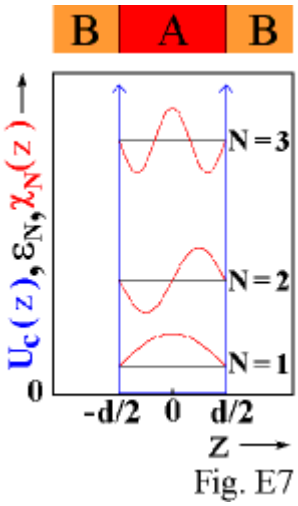

Fig. E7

C is a normalization constant. The two Equ. (E8.2) refer to the A region ($|z| \leq d/2$). In the B region ($|z| > d/2$) $\chi_N(z)$ is zero, because the walls of the well are infinitely high (compare Fig. E7); as a consequence, ε_N (Equ. (E8.1)) is determined only by the effective mass of the A region $m_c^*(A)$ (rather than by an average of the masses in the regions A and B as in the general case). The confinement energy is given by

(E8.3) $\varepsilon_1 = (\hbar^2/2m_c^*(A))\,(\pi / d)^2$

For not too small U_0 values, Equ. (E8.3) is frequently used as an approximation. The same is true for Equ. (E8.1) and (E8.2) in the case of the lowest ε_N levels.

Supplement 9. Dynamical Matrix

In the following we show that the expression

$$(M_k M_{k'})^{-1/2} \sum_{n'} \phi_{n\,k\,\alpha\,n'\,k'\,\alpha'} \exp(i\,\mathbf{q}\,(\mathbf{R}_{n'}-\mathbf{R}_n))$$

appearing in Equ. (7.8) is independent of the cell index n.

First we will prove that the whole summand depends on the indexes n and n' only through the difference of the lattice vectors $\mathbf{R}_{n'} - \mathbf{R}_n$. For the exponential factor this corresponds to the dependence which appears explicitly.

For the first factor in the sum this result is obtained taking into account the fact that the ϕ's are forces (in the case of unit displacements) (see Equ. (7.3)).

We consider in Fig. E8 two pairs of atoms, A / B und C / D, having the same combination of the indexes k and k' and the same difference of lattice vectors $\mathbf{R}_n - \mathbf{R}_{n'}$. As a consequence of translation symmetry the force acting on atom A due to a displacement of atom B must be equal to the force acting on atom C *for the same displacement* of atom D. That means that the ϕ's also depend on n and n' only via the difference of lattice vectors quoted earlier.

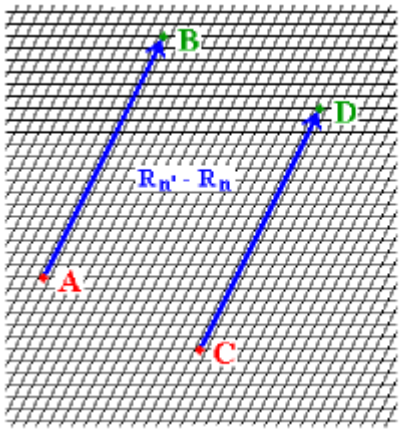

Fig. E8

The n' summation is performed over the positions of all unit cells relative to a certain unit cell n. Because of translation symmetry (and the finite action range of the forces) , it is not important, for a sufficiently large crystal, how the reference vector $\mathbf{R}_n$ is chosen.

Consequently, the dynamical matrix defined in Equ. (7.8) is, in fact, only dependent on the indexes k, α, k', and α'.

Supplement 10. Limitation of the Phonon Lifetime by Anharmonic Interaction

In the harmonic approximation (Equ. (7.1)) used in the previous chapters terms of higher than second order in the atomic displacements are omitted. As a consequence, the system of vibrating atoms is characterized by fixed phonon-numbers $l_{\mathbf{q}j}$ (see Section 7.3). Hence, this discussion leads to an infinitely large lifetime of the phonons. Finite lifetimes are obtained, only if allowance is made for higher-order tems in the potential energy Φ, so-called ***anharmonic terms***. Here we restrict ourselves to additional third-order terms, assuming as earlier Φ(0) = 0:

(E10.1) $\quad \Phi = \{ u\,u' \} + \{ u\,u'\,u'' \}$

Making use of the linear coordinate-transformations described in Sections 7.2 and 7.3, one then obtains additional third-order terms in the Hamilton operator (see Equ. (7.21)) :

(E10.2) $$H = \sum_{\mathbf{q}j} \hbar\,\omega_j(\mathbf{q})\, b_{\mathbf{q}j}^{+}\, b_{\mathbf{q}j} + H_{anh}$$

$$H_{anh} = \{ b_{\mathbf{q}j}^{+}\, b_{\mathbf{q}'j'}^{+}\, b_{\mathbf{q}''j''} \} + \{ b_{\mathbf{q}j}^{+}\, b_{\mathbf{q}'j'}\, b_{\mathbf{q}''j''} \} + \text{further three-b combinations}$$

(The { } symbols have an analogous meaning as those used in Section 8.1). Assuming that the system is initially in an eigenstate |....., $l_{\mathbf{q}\,j}$,.....> and that then H_{anh} is "switched on", processes due to the two H_{anh} terms explicitly given in Equ. (E10.2) occur, in which

(a) one phonon decays into two (smaller) phonons:  , or

(b) two phonons combine into a new (larger) phonon:  .

The terms that are not explicitly given in Equ. (E10.2) (combinations of three creation and three destruction operators) do not result in such processes, because in these cases the energy balance would be violated.

The lifetime broadening of the one-phonon absorption line mainly originates from the fact that the TO phonon generated optically is subject to type (a) and (b) processes:

(a) 

(b) 

(Here we have represented the photon in each case by →.) Obviously, the frequency of type (b) processes grows with increasing supply of partner phonons (↗), i. e. with increasing temperature. This leads to a growth of linewidth occurring in this direction.

> By the way, the anharmonic contributions to the potential energy of atoms are also important for fundamental properties of solids, such as thermal expansion and thermal conductivity.

List of References

[1] J. M. Ziman: Principles of the Theory of Solids, Cambridge University Press 1972

[2] M. L. Cohen and J. R. Chelikowsky: Electronic Structure and Optical Properties of Semiconductors, Springer 1988 (Springer Series of Solid-State Sciences, Vol. 75)

[3] W. A. Harrison: Solid State Theory, McGraw-Hill 1970

[4] J. Pehek and H. Levinstein, Phys. Rev. **140**, A576 (1965)

[5] M. Gershenzon, D. G. Thomas and R. E. Dietz, Proc. Intern. Conf. Semicond. Phys., Exeter 1962, page 752, Inst. Phys. und Phys. Soc. (London) 1962

[6] D. E. Aspnes and A. A. Studna, Phys. Rev. B **27**, 985 (1983)

[7] R. M. A. Azzam and N. M. Bashara: Ellipsometry and Polarized Light, North Holland 1986

[8] H. B. Briggs and R. C. Fletcher, Phys. Rev. **87**, 1130 (1952)

[9] S. Nakai and T. Sagawa, J. Phys. Soc. Japan **26**, 1427 (1969)

[10] J. R. Dixon, Proc. Intern. Conf. Semicond. Phys., Prague 1960, page 366, Academic Press 1961

[11] W. G. Spitzer and H. Y. Fan, Phys. Rev. **106**, 882 (1957)

[12] J. O. Dimmock, Semiconductors and Semimetals **3** (Editors R. K. Willardson and A. C. Beer), page 259, Academic Press 1967

[13] L. I. Schiff: Quantum Mechanics, McGraw-Hill 1968

[14] D. D. Sell, Phys. Rev. B **6**, 3750 (1972)

[15] M. D. Sturge, Phys. Rev. **127**, 768 (1962)

[16] B. Segall and D. T. F. Marple, Physics and Chemistry of II-VI Compounds (Editors M. Aven and J. S. Prener), page 319, North Holland 1967

[17] U. Heim and P. Hiesinger, phys. stat. sol. (b) **66**, 461 (1974)

[18] C. Weisbuch and B. Vinter: Quantum Semiconductor Structures, Academic Press 1991

[19] D. Bimberg, M. Grundmann, and N. N. Ledentsov: Quantum Dot Heterostructures, Wiley 1999

[20] R. Dingle, W. Wiegmann and C. H. Henry, Phys. Rev. Letters **33**, 827 (1974)

[21] Y. C. Chang and J. N. Schulman, Phys. Rev. B **31**, 2069 (1985)

[22] S. Schmitt-Rink, D. S. Chemla, and D. A. B. Miller, Advances in Physics **38**, 89 (1989)

[23] L. C. West and S. J. Eglash, Appl. Phys. Letters **46**, 1156 (1985)

[23a] B. F. Levine, J. Appl. Phys. **78**, R1(1993)

[24] W. A. Harrison: Electronic Structure and the Properties of Solids, Dover Publications (New York) 1989

[25] A. Mitsuishi, J. Phys. Soc. Japan **16**, 533 (1961)

[26] M. Hass and B. W. Henvis, J. Phys. Chem. Solids **23**, 1099 (1962)

[27] F. A. Johnson, Proc. Phys. Soc. **73**, 265 (1959)

[28] R. Becker: Theorie der Elektrizität, Volume 2, Teubner 1949 (in German)

Index